

Developing a hydrogen impurity enrichment device for measuring impurities in fuel-grade hydrogen

Marc Plunkett

June 22, 2020

Declaration of Originality

I hereby declare that the work reported in this thesis was composed and originated entirely by me. Information derived from published and unpublished results of others has been acknowledged in the text and in the relevant references included within the thesis.

Marc Plunkett

A handwritten signature in black ink, appearing to read "M. Plunkett", followed by a thin horizontal line.

Imperial College London

The copyright of this thesis rests with the author and is made available under a 'Creative Commons Attribution Non-Commercial No Derivatives' licence. Researchers are free to copy, distribute or transmit the thesis on the condition that they attribute it, that they do not use it for commercial purposes and that they do not alter, transform or build upon it. For any reuse or redistribution, researchers must make clear to others the licence terms of this work.

Executive summary

The copyright of this thesis rests with the author and is made available under a 'Creative Commons Attribution Non-Commercial No Derivatives' licence. Researchers are free to copy, distribute or transmit the thesis on the condition that they attribute it, that they do not use it for commercial purposes and that they do not alter, transform or build upon it. For any reuse or redistribution, researchers must make clear to others the licence terms of this work.

The copyright of this thesis rests with the author and is made available under a 'Creative Commons Attribution Non-Commercial No Derivatives' licence. Researchers are free to copy, distribute or transmit the thesis on the condition that they attribute it, that they do not use it for commercial purposes and that they do not alter, transform or build upon it. For any reuse or redistribution, researchers must make clear to others the licence terms of this work.

The copyright of this thesis rests with the author and is made available under a 'Creative Commons Attribution Non-Commercial No Derivatives' licence. Researchers are free to copy, distribute or transmit the thesis on the condition that they attribute it, that they do not use it for commercial purposes and that they do not alter, transform or build upon it. For any reuse or redistribution, researchers must make clear to others the licence terms of this work.

The copyright of this thesis rests with the author and is made available under a 'Creative Commons Attribution Non-Commercial No Derivatives' licence. Researchers are free to copy, distribute or transmit the thesis on the condition that they attribute it, that they do not use it for commercial purposes and that they do not alter, transform or build upon it. For any reuse or redistribution, researchers must make clear to others the licence terms of this work.

The copyright of this thesis rests with the author and is made available under a 'Creative Commons Attribution Non-Commercial No Derivatives' licence. Researchers are free to copy, distribute or transmit the thesis on the condition that they attribute it, that they do not use it for commercial purposes and that they do not alter, transform or build upon it. For any reuse or redistribution, researchers must make clear to others the licence terms of this work.

The copyright of this thesis rests with the author and is made available under a 'Creative Commons Attribution Non-Commercial No Derivatives' licence. Researchers are free to copy, distribute or.

Acknowledgements

Throughout the writing of this dissertation I have received a great deal of support and assistance. I would first like to thank my supervisor, Dr. M. Gellar, whose expertise was invaluable in the formulating of the research topic and methodology in particular.

I would like to acknowledge my colleagues from my internship at Central P. for their wonderful collaboration. You supported me greatly and were always willing to help me. I would particularly like to single out my supervisor at Central P., Ms. P. Buffay. Phoebe, I want to thank you for your excellent cooperation and for all of the opportunities I was given to conduct my research and further my dissertation at Central P.

I would also like to thank my tutors, Messrs. R. Geller and C. Bing, for their valuable guidance. You provided me with the tools that I needed to choose the right direction and successfully complete my dissertation.

In addition, I would like to thank my parents for their wise counsel and sympathetic ear. You are always there for me. Finally, there are my friends, who were of great support in deliberating over our problems and findings, as well as providing happy distraction to rest my mind outside of my research.

List of Publications and Presentations

Publications

1. **M. Plunkett**, K.Li, A. Murugan; Review of membrane technologies for hydrogen impurity enrichment; International Journal of Hydrogen Energy, 163 (2016), pp. F3119-F3124, 10.1149/2.0141611jes
2. **M. Plunkett**, K.Li, A. Murugan; Review of membrane technologies for hydrogen impurity enrichment; International Journal of Hydrogen Energy, 163 (2016), pp. F3119-F3124, 10.1149/2.0141611jes
3. **M. Plunkett**, K.Li, A. Murugan; Review of membrane technologies for hydrogen impurity enrichment; International Journal of Hydrogen Energy, 163 (2016), pp. F3119-F3124, 10.1149/2.0141611jes

Oral Presentations

1. **M. Plunkett**, A. Murugan, K. Li; A hydrogen impurity enrichment device using Pd-Alloy membranes to support the hydrogen economy. Presented at International Conference for Membrane and Electromembrane Processes 2018, 13th – 16th May 2018, Prague, Czech Republic.
2. **M. Plunkett**, A. Murugan, K. Li; A hydrogen impurity enrichment device using Pd-Alloy membranes to support the hydrogen economy. Presented at 15th International Conference on Inorganic Membranes, 18th – 22nd June 2018, Dresden, Germany.
3. **M. Plunkett**; The use of hydrogen selective materials for quality assurance of fuel grade hydrogen to ISO 14687-2 . Presented at 2nd bi-annual Gas and Particle Metrology symposium, 14th August, 2018, Teddington, United Kingdom

List of Figures

1.1	Schematic presentation of the thesis structure	15
2.1	Schematic of a PEMFC cell [1]	18
2.2	Classification of MEA materials [3]	19
2.3	Schematic of a PEMFC stack [4]	19
2.4	Simplified block diagram of a typical modern SMR plant. WGS is a water gas shift reactor. CO ₂ concentrations are in mol.%. [8]	20
2.5	Illustration of the five membrane separation mechanisms (i) Poiseuille Flow/Knudsen diffusion, (ii) Molecular Sieving, (iii) Surface diffusion (iV) Capillary condensation (V) Solution diffusion (Vi) Facilitated transport	30
3.1	Schematic representation of the fabrication process of SZ hollow fibre.	71
3.2	Schematic representation of the sequential baths for sensitisation/activation process.	72
3.3	Example of ELP procedure when manufacturing a PdCu membrane on YSZ substrate	73
5.1	SEM images of fabricated membranes (a) PdCu (fcc) (Sputtering) (b) PdAg (ELP) (c)PdAu (ELP) (d) PdCuZr (Sputtering) (e) PdAgAu (ELP) (f) PdCuAg (ELP) (g) PdCu (bcc) (Sputtering) (h) typical cross section	85
5.2	Permeability data for pure hydrogen, non-sulphur, and sulphur permeation tests	90

List of Tables

1.1	Concentration limits for ISO-14687 impurities	13
2.1	Summary of ISO 14687-2 impurities in the supply chain and their effects on fuel cell operation adapted from [13]	23
2.2	Types of hydrogen separation membrane	33
2.3	Metals which show the ability for hydrogen permeation [31]	35
2.4	Review of palladium alloys and their interactions with impurities	41
2.5	Hydrogen permeable non-palladium metallic membranes	48
2.6	Hydrogen permeable ceramic and cermet membranes which show resistance to common hydrogen impurities	52
3.1	Compositions used for preparation of palladium based membranes on YSZ substrate through electroless plating and immersion plating	72
3.2	Conditions used during magnetron sputtering of palladium membranes on YSZ tubular substrate	74
3.3	Gas mixture composition of the non-sulphur sample used during impurity tests	75
3.4	Gas mixture composition of the sulphur sample used during impurity tests	75
4.1	Simulated total energy values of ISO 14687-2 impurities	79
4.2	Simulated total energy values of alloy slabs	80
5.1	Membrane compositions analysed by EDS and their thickness measured using FIB-SEM	84
5.2	Pure hydrogen permeability of studied alloy membranes under pure hydrogen at 300°C and 1 bar pressure differential	87
5.3	Permeability results for all membranes under both impurity conditions	87
5.4	XPS composition analysis of the palladium alloy membrane surfaces after impurity tests	89

List of Acronyms, Abbreviations and Symbols

AHF Asymmetric Hollow Fibre

ASTM American Society for Testing and Materials

BCC Body Centered Cubic

CRDS Cavity Ring Down Spectroscopy

CTE Coefficient of thermal expansion

DFT Density Functional Theory

ELP Electroless Plating

EU European Union

EDS Energy-dispersive X-ray spectroscopy

FCC Face-centred cubic

FTIR Fourier-transform infrared spectroscopy

HF Hollow Fibre

ISO International Standards Organisation

GC Gas Chromatography

NPL National Physical Laboratory

NPT National Pipe Thread

MS Mass Spectrometry

PDHID Pulsed discharge helium ionization detector

PEMFC Proton Exchange Membrane Fuel Cell

PID Proportional–integral–derivative

PPB Parts-Per-Billion

PPM Parts-Per-Million

PSA Pressure Swing Adsorption

SMR Steam Methane Reforming

WGS Water Gas Shift

XRD X-ray diffraction

XPS X-ray photoelectron spectroscopy

YSZ Yttrium stabilized zirconium

Ag Silver

Ar Argon

Au Gold

CH₄ Methane

Cu Copper

CO Carbon Monoxide

CO₂ Carbon Dioxide

He Helium

H₂ Hydrogen

HCHO Formaldehyde

HCOOH Formic Acid

H₂O Water

N₂H₄ Hydrazine

HCl Hydrochloric Acid

H₂S Hydrogen Sulphide

NaOH Ammonium hydroxide

Pd Palladium

PdNH₃4Cl₂H₂O Tetra- amminepalladium (II) chloride monohydrate

SnCl₂ Tin(ii)Chloride

Zn Zinc

Contents

1	Introduction	12
1.1	Problem statement	12
1.2	Research Objectives	14
1.3	Thesis structure and presentation	15
2	Literature review	17
2.1	Fuel cell electric vehicles	17
2.2	Hydrogen Production	20
2.2.1	Hydrogen from fossil fuels and hydrocarbons	20
2.2.2	Hydrogen from water	21
2.3	Hydrogen impurities in the supply chain	22
2.4	Hydrogen impurity enrichment	27
2.4.1	Other enrichment methods	28
2.5	Review of hydrogen selective membranes	29
2.5.1	Criteria for a hydrogen impurity enrichment material	32
2.5.2	Membrane manufacture	54
2.6	Density functional theory for screening of membrane alloy compositions .	55
2.7	Conclusion	55
3	Experimental methods	69
3.1	Simulations	69
3.2	Membrane manufacture	69
3.2.1	Materials used	69
3.2.2	Support fabrication	69
3.2.3	Membrane deposition	70
3.2.4	Materials testing	74
3.3	Membrane testing	74
3.3.1	Preparation of gas standards	74
3.3.2	Membrane testing rig	76
3.4	Hydrogen impurity enrichment	76
3.4.1	Device design	76

4 Density functional theory as a screening method for dense metal membranes	78
4.1 Abstract	78
4.2 Introduction	78
4.3 Results and discussion	79
4.3.1 Stability of palladium alloy compositions	80
4.3.2 Hydrogen and Impurity adsorption on palladium alloy membranes	80
4.4 Conclusion	80
5 Impurity resistance of dense metal membranes under hydrogen impurities	82
5.1 Abstract	82
5.2 Introduction	82
5.3 Results and Discussion	84
5.3.1 Membrane characterisation	84
5.3.2 Hydrogen permeation	86
5.3.3 Impurity reactivity	87
5.4 Conclusion	90
6 A hydrogen impurity measurement device for measuring ISO 14687 impurities	93
6.1 Abstract	93
6.2 Introduction	93
6.3 Results and discussion	93
6.4 Conclusion	93
7 Conclusion and future work	94
7.1 Impurity enrichment devices	94
7.1.1 Further research	94
7.1.2 Additional use cases	94
7.1.3 Commercialisation	94
7.2 Closing remarks	94

Chapter 1

Introduction

1.1 Problem statement

Due to the damaging environmental effects of using fossil fuels in the transport sector, national and international targets have been set in order to reduce global CO₂ emissions. In the UK for example, there is a plan to completely ban the sale of new conventional petroleum vehicles by as early as 2040. [1] One proposed solution is further adoption of fuel cells and other energy generation methods which utilize hydrogen as a carbon free energy source.

Despite the fact that the technology for hydrogen powered fuel vehicles has existed since the early 1960's, their application has been limited to providing power for space missions and other niche applications. It wasn't until the late 90's when developments in lowering the platinum catalyst loading and breakthroughs in the production of thin film electrodes drove the cost of fuel cells down to a level where they were a commercially viable option. As of 2017, a number of auto mobile manufacturers including Toyota,[2] Hyundai, [3] Honda [4] and Daimler [5] now offer hydrogen vehicles commercially. It is also possible to retrofit a petroleum vehicle to run off hydrogen.[6] Many countries both in the EU, and globally have ambitious hydrogen infrastructure plans over the next 10 years. This is in an effort to become less reliant on importing fossil fuels, increase their energy security, and transition to a carbon free energy system.

The development of the hydrogen economy is still in its infancy, however several countries are aiming to deploy sizable hydrogen fuelling infrastructures over the next few decades. National reports state that Europe's position in 2030 will be: UK - 1,100 hydrogen refuelling stations and 1.6 million fuel cell vehicles [7] France – 600 hydrogen refuelling stations and 0.8 million fuel cell vehicles [8], Germany – 1,180 hydrogen refuelling stations [9] and 1.8 million fuel cell vehicles and the Netherlands – 200 hydrogen refuelling stations and 0.2 million fuel cell vehicles. [9] The fuel cell system in a hydrogen vehicle can easily degrade if even parts-per-billion to parts-per-million level of some impurities are present in the hydrogen. Therefore, it is imperative that hydrogen purity, and techniques for verifying purity, are adequate to ensure customers vehicles are not inadvertently damaged by fluctuations in hydrogen composition.

Table 1.1: Concentration limits for ISO-14687 impurities

Characteristics	Regulation
Minimum mole fraction of hydrogen	99.97%
Total non-hydrogen gases	300 $\mu\text{mol mol}^{-1}$
Maximum concentration of individual components	
Total Hydrocarbons (Methane basis)	5 $\mu\text{mol mol}^{-1}$
Water	2 $\mu\text{mol mol}^{-1}$
Oxygen	5 $\mu\text{mol mol}^{-1}$
Helium	300 $\mu\text{mol mol}^{-1}$
Carbon dioxide	2 $\mu\text{mol mol}^{-1}$
Carbon monoxide	0.2 $\mu\text{mol mol}^{-1}$
Total sulphur compounds (H_2S basis)	0.004 $\mu\text{mol mol}^{-1}$
Formaldehyde	0.01 $\mu\text{mol mol}^{-1}$
Formic acid	0.2 $\mu\text{mol mol}^{-1}$
Ammonia	0.1 $\mu\text{mol mol}^{-1}$
Total halogenated compounds	0.05 $\mu\text{mol mol}^{-1}$
Maximum particulate concentration	1 mg/kg

International standards advise that all hydrogen suppliers should prove that their product is pure enough to prevent degradation of fuel cell components. ISO 14687-2:2012 [10], shown in Table 1.1 specifies the maximum impurity levels of 13 impurities that are permissible in fuel cell hydrogen. ISO 14687-2:2012 includes some challenging hydrogen purity specifications mainly due to the impurity limits being below the limits of detection of the standard techniques commonly used to measure the concentration of these compounds.

Existing hydrogen purity laboratories are unable to perform traceable analysis to ISO 14687 specifications because appropriate methods and standards have not been developed. The consequence of this is that hydrogen suppliers cannot provide evidence that their fuel meets these specifications and therefore are not permitted to supply hydrogen. Of the 13 gaseous impurities listed in ISO 14687-2, there is no single method for measuring all impurities. Laboratories must therefore use several instruments to perform such an analysis. In 2015 Murugan et al published a review of methods for analysing the purity of fuel grade hydrogen [11]. They concluded that in order for a single laboratory to provide full hydrogen analysis to ISO 14687-2 specifications it would require a number of instruments including GCs, FTIR and CRDS. The capital cost of purchasing the gas analysers to perform analysis on the measurable impurities in a hydrogen sample can amount to $\text{\textsterling}500,000$ [11] and hence performing analysis would be out of reach for many of the smaller laboratories.

While the impurities listed in ISO 14687-2 are specified at extremely low amount fractions, many can be analysed at higher amount fractions through the use of cheap and routine gas analysers such as a GC-MS. Therefore a solution is to increase the

concentration of impurities above the limit of detection of a cheaper, more widespread analyser. These techniques are referred to as enrichment or pre-concentration. The most commonly used technique for pre-concentration of hydrogen fuel samples is referred to as ‘Hydrogen Impurity Enrichment’. This method involves passing the sample through a semi permeable membrane material, such as palladium, which only allows the passage of hydrogen.[12] As hydrogen leaves the system, the impurities remain, increasing in concentration with time as more hydrogen permeates through the membrane. This increase in concentration is referred to as the enrichment factor and once the enrichment is complete the sample can then be analysed at these higher concentrations, and using the enrichment factor, the original composition of the sample can be found.

The accuracy, cost and time taken for a hydrogen enrichment device is highly dependent on the membrane material. Different materials will allow hydrogen to permeate at different rates and will interact differently with impurities that may be present in hydrogen.[12] While hydrogen enrichment is a promising technology for hydrogen impurity measurement, more research must be done to properly understand how different membrane materials interact with common hydrogen impurities, and therefore identify the most appropriate material.

1.2 Research Objectives

This thesis will focus on developing hydrogen impurity enrichment as a low-cost technique for measuring the impurities in fuel grade hydrogen to ISO 14687-2 specification. This study will revolve around the membrane materials used to concentrate the impurities in hydrogen samples and will aim to determine the best material, and conditions for the hydrogen impurity enrichment device. The thesis aims are as follows:

- Identify the best material for enriching impurities based on the degree of interaction and reactivity with the impurities shown in Table 1
- Finalise a protocol for national measurement institutions to follow when enriching a hydrogen sample.
- Convert the experimental set up in to a commercially viable prototype which could be used in analytical laboratories
- Perform full enrichment using these three conclusions on a real sample taken from a hydrogen refuelling station

In order to determine suitable enrichment material ‘Density Functional Theory (DFT) will be used to screen a number of materials for their suitability as an impurity enrichment membrane on their simulated interaction strength with ISO 14687 impurities.

The best performing membrane materials simulated in Chapter 3 will then be synthesised in Chapter 4. The hydrogen permeability of each material under a number of ISO 14687-2 impurities will be measured to validate the simulation results and further narrow down the most suitable membrane composition. Following from this the best

membrane will be used in Chapter 5 which will describe the design and commercialisation of the final hydrogen impurity enrichment device. The design of the enrichment device will include an uncertainty budget of the technique, automation of the device, and compliance to European standards.

Finally the new device, featuring the most suitable membrane, redesigned process, and protocols for tracer enrichment will be tested using a real sample taken from a hydrogen refuelling station.

1.3 Thesis structure and presentation

This thesis consists of 7 chapters, which includes the ‘Introduction’, ‘Literature Review’, experimental chapters and ‘Conclusion’. The thesis structure is visualised in figure 1.1. The experimental chapters address different aspects of development of hydrogen metrology techniques as described above.

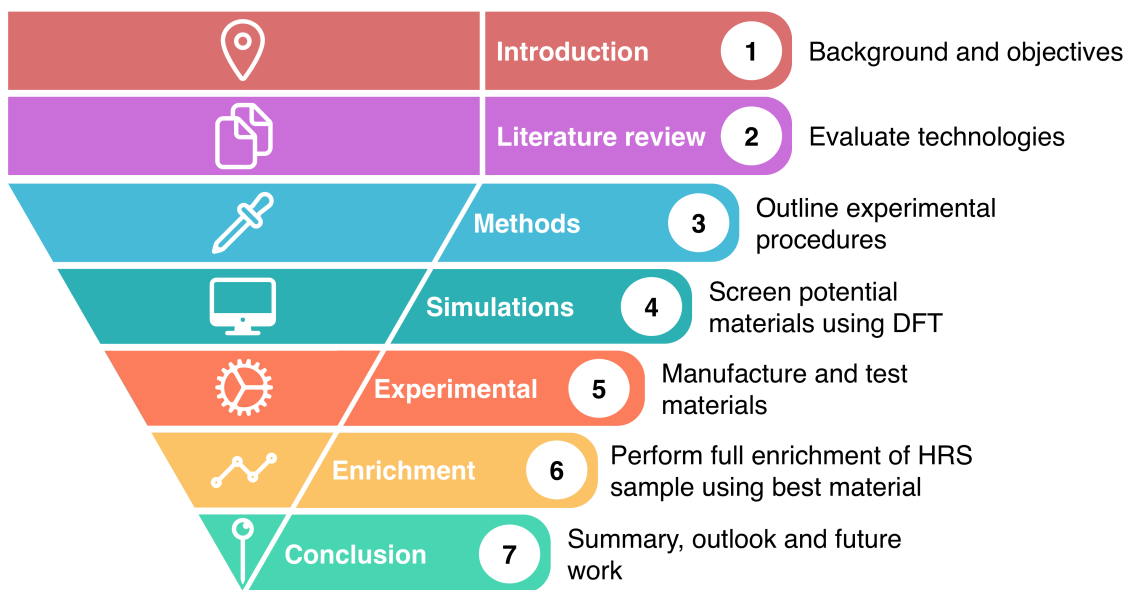


Figure 1.1: Schematic presentation of the thesis structure

References

- [1] Food & Rural Affairs Department for Environment and Department for Transport. Air quality plan for nitrogen dioxide (NO₂) in UK, 2017.
- [2] Toyota. The Toyota Mirai, 2015. URL <https://www.toyota.co.uk/new-cars/new-mirai/landing.json>.
- [3] Hyundai. Hyundai ix35 Hydrogen Fuel Cell Vehicle, 2015. URL <https://www.hyundai.co.uk/about-us/environment/hydrogen-fuel-cell>.
- [4] Honda. Honda Clarity Fuel Cell. URL <http://www.honda.co.uk/cars/new/coming-soon/clarity-fuel-cell/overview.html>.
- [5] C Mohrdieck. Daimler's road to FCEV market introduction. In *7th Stakeholder Forum of the FCH JU*, Brussels, 2014.
- [6] Symbio FCell. Zero emission mobility solutions, 2016. URL <https://www.symbio.one/en/>.
- [7] UK H2 Mobility. UK H2 Mobility: Phase 1 Results. Technical report, 2013.
- [8] Phil Summerton, Sophie Billington, Alex Stewart, Element Energy, Pierre Bidet, and Nathalie Faure. Fuelling France. Technical report, 2015.
- [9] Dennis Hayter and Intelligent Energy. Global H2Mobility initiatives – what they mean for FCEV introduction. Technical Report September, 2014.
- [10] International Standard ISO 14687-2: 2012. Hydrogen Fuel - Product Specification, 2012.
- [11] Arul Murugan and Andrew S Brown. Review of purity analysis methods for performing quality assurance of fuel cell hydrogen. *International Journal of Hydrogen Energy*, 40(11):4219–4233, 2015. doi: 10.1016/j.ijhydene.2015.01.041.
- [12] Tina M Nenoff Nathan W. Ockwig. Membranes for Hydrogen Separation. *Chemical Reviews*, 107:4078–4110, 2007.

Chapter 2

Literature review

2.1 Fuel cell electric vehicles

A Fuel cell electric vehicle (FCEV) refers to a vehicle which uses a solid state electrochemical device to convert chemical energy into electrical energy for motor power. The most common fuel source for FCEV's is hydrogen, where energy is produced using oxygen from air and compressed hydrogen stored on board.

A fuel cell is made up from an electrolyte and two electrocatalysts at both the anode and cathode sides of the cell. The electrolyte separates the two electrodes and usually defines the type of fuel cell. At the anode side the fuel is oxidised as shown in equation 2.1, creating a positivley charged ion and an electron. The electrolyte is designed to only allow the passage of ions, and prevents the passage of electrons. The freed electron travels through a circuit, creating an electric current to provide power for it's desired use. The ions travel through the electrolyte to the cathode side of the fuel cell where they are reunited with the freed electrons, and oxygen to produce water as shown in equation 2.2. The overall process for a hydrogen fuel cell is shown in equation 2.3 and visualised in figure 2.1

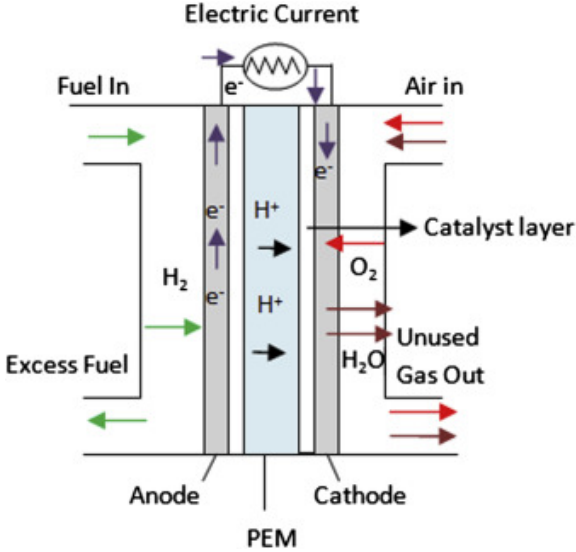
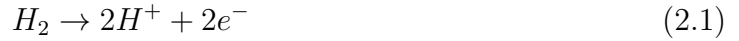


Figure 2.1: Schematic of a PEMFC cell [1]



While a number of fuel cell technologies can use hydrogen as a fuel source, the most suitable for FCEV's, and in particular mass production of affordable vehicles, are proton exchange membrane fuel cells (PEMFC). This is due to their high power density, low start up time, and low operating temperatures. [2]

A PEMFC uses a proton conducting polymer membrane as an electrolyte material, typically nafion. A PEMFC cell consists of two metal bipolar plates which act to distribute the fuel and oxidant within the cell, aid water management within the cell, separate individual cells in a fuel cell stack, and carry current away from the cell. [2] A Membrane electrode assembly (MEA) which consists of the polymer membrane, two dispersed noble metal catalyst layers to enable the anode and cathode reactions, and two gas diffusion layers to ensure uniform access of fuel and oxidant to the catalyst layer. Common materials for the MEA are shown in figure 2.2[3]. The components are wedged between two rubber seals to ensure the cell is gas tight. Individual cells are combined in series to form a fuel cell stack which can provide the desired power as shown in 2.3

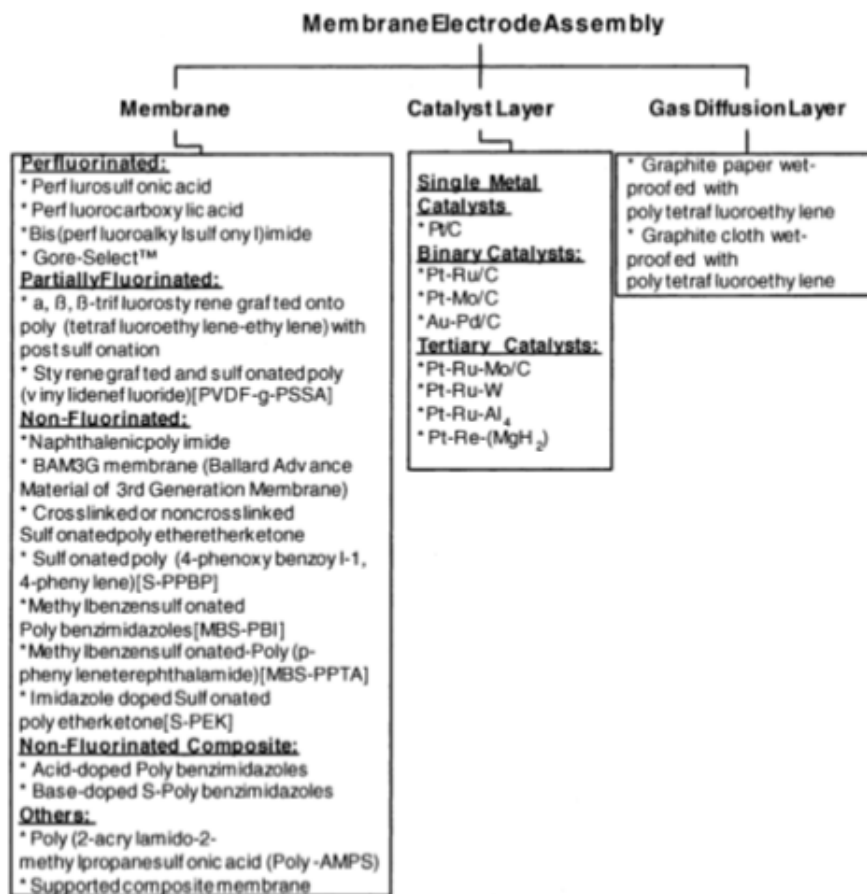


Figure 2.2: Classification of MEA materials [3]

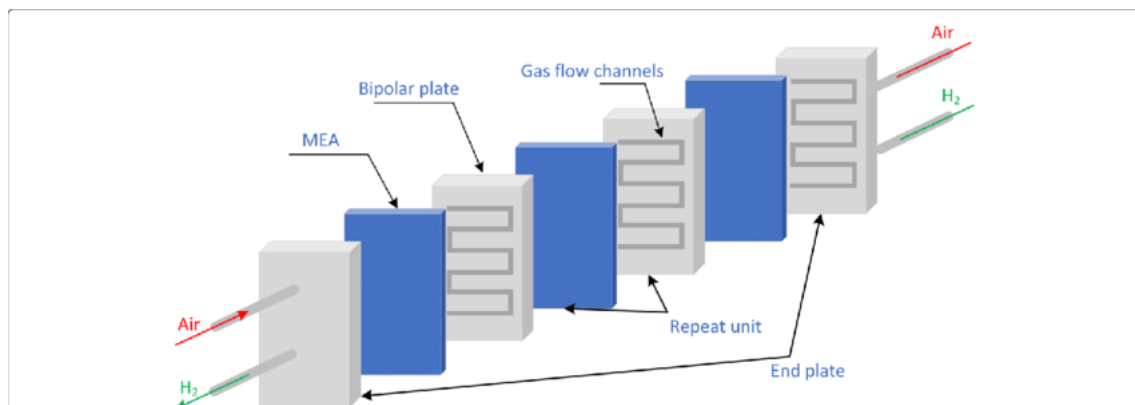


Figure 2.3: Schematic of a PEMFC stack [4]

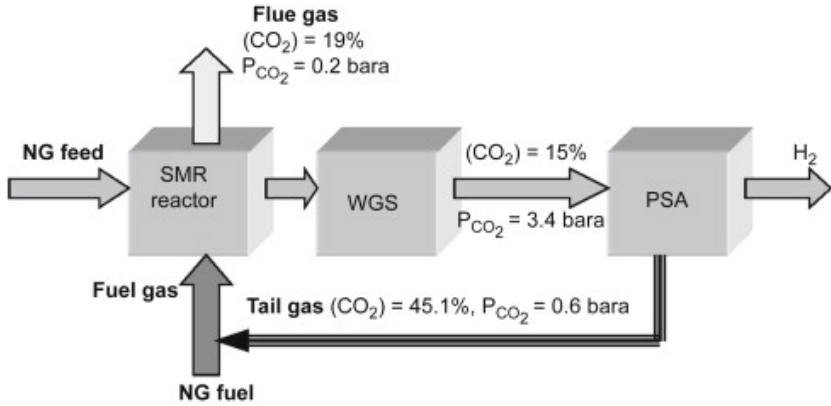


Figure 2.4: Simplified block diagram of a typical modern SMR plant. WGS is a water gas shift reactor. CO₂ concentrations are in mol.%. [8]

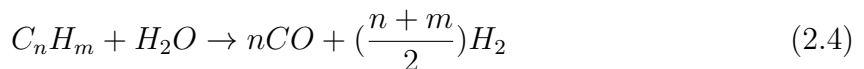
2.2 Hydrogen Production

Hydrogen production refers to a range of industrial processes for generating hydrogen. Since there are no natural reserves of hydrogen, it must be obtained through one of these methods. The most important factor for determining the feasibility of a hydrogen production process is the primary source of energy that is used. Currently the options for this are nuclear energy in the form of heat, renewable energy in the form of heat, electricity, light, or fossil fuels. Currently the primary sources of hydrogen are from fossil fuels: steam reforming of methane accounts for 48% and other hydrocarbons account for 30% of global hydrogen production; gasification of coal accounts for 18%; and electrolysis of water accounting for the remaining 4%. [5] Electrolysis and SMR will be discussed since these are expected to be the most dominant production methods in the future. [6]

2.2.1 Hydrogen from fossil fuels and hydrocarbons

Fossil fuels are the most dominant source of hydrogen production [5] and there are a number of processes which are commonly utilized in industry. The most popular and therefore the ones which will be discussed are steam methane reforming and hydrocarbon decomposition.

Steam Methane Reforming is the conventional and most economical method for producing hydrogen, and it has been predicated by the IEA that this trend will continue despite the emergence of other hydrogen production methods. [7] Steam methane reforming occurs through a two-step chemical process. If another hydrocarbon other than methane is being used it must first be pre-reformed into methane as shown in equation 2.4. A schematic representation of the process can be seen in figure 2.4

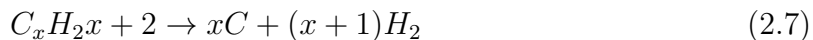




Equation 2.5 takes place in a reactor operating at 700-850°C, at pressures of 3-25 bar, and in the presence of a nickel based catalyst. [8] The result of this step is a mixture of CO and H₂, commonly referred to as syngas. This syngas is further used as a feedstock for the reaction shown in equation 2.6 known as water gas shift in order to produce greater hydrogen yields. This step is carried out in a two-step reaction. An initial high temperature stage at 350°C which converts majority of the syngas to CO₂ and hydrogen, and a final low-temperature step which operates at 250°C which utilizes a catalyst with higher activity to minimise the remaining CO₂. [8] The final product will be a mixture of CO₂ and H₂.

A number of separation steps are used in order to prevent impurities from contaminating the resulting gas mixture. The traditional separation step is pressure swing adsorption (PSA) which takes advantage of adsorption of gaseous molecules onto a molecular sieve at high pressures. Hydrogen purities of ~99.9% are achievable using this method however the cost is high and typically contributes to around 20-30% of the total production cost. [8] The other main separation step is desulphurization which uses a combination of CoMo and ZnO catalysts in series at 450-550°C to remove sulphur. [8] This step is essential to ensure sulphur is not present in the gas exit stream and also to ensure catalyst poisoning does not occur at any point in the process.

Hydrocarbon decomposition is a process by which hydrocarbon molecules are converted into solid carbon and hydrogen. [9] This reaction is typically operated either thermally or by creating a plasma. A metallic catalyst such as nickel or iron is required. The reaction is shown in equation 2.7 [10]

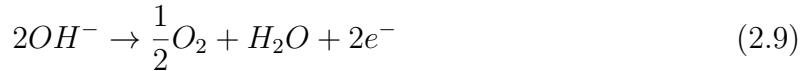


An advantage of this process is that the only feedstock is the hydrocarbon, so presuming that the feedstock is sufficiently pure this method of hydrogen production should remove the needs for further downstream processing. [9] The main disadvantage of this method is the since solid carbon is the main by-product the catalyst will be easily deactivated and will require regular maintenance to ensure carbon build up is managed. [9]

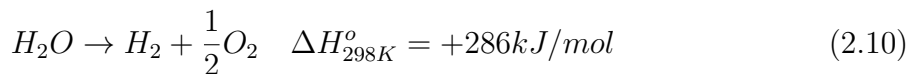
2.2.2 Hydrogen from water

Electrolysis uses an electric current to split water into hydrogen and oxygen using separate anode and cathode chambers isolated using an ion exchange membrane. The anode and cathode reactions are shown in equations 2.8 and 2.9. The main competitive advantage of electrolysis is that reactors are modular and highly scalable, allowing hydrogen to be produced in a distributed manner. [11] The main input to the process is electricity and if this electricity is produced using renewable sources then the process can be considered carbon neutral. However if a non-renewable source of energy is used the net carbon produced per mole of hydrogen would be higher than that produced by

SMR. [12] Electrolysis is incentivised by the increasing price of natural gas and the decreasing price of electricity, which some predict will result in electrolysis becoming more economically feasible than SMR in the future. [11]



Thermal decomposition of water is the process of splitting water into hydrogen and oxygen at temperatures of 2000°C as shown in equation 2.10. [6] The operating temperature of the reaction can be lowered under the presence of a nickel or iron based catalyst. [6] Due to the high energy demand for this production method water splitting is not a feasible method of commercial hydrogen production.



Chloro alkali hydrogen production

2.3 Hydrogen impurities in the supply chain

The method used to manufacture hydrogen will affect which potential impurities can be present in the final product. While steps are taken in both electrolysis and SMR to ensure a pure product is produced, there is still the chance of impurities reaching the customers fuel cell. This section will explore how ISO 14687-2 impurities can enter the supply chain, and their effect on the operation of a PEMFC. A summary is shown in table 2.1

Water

Water can be present from both SMR and electrolysis due to it being a main by-product of SMR reactions, and the main reactant in electrolysis.

The PSA process used in SMR is an appropriate barrier to prevent water contaminating the end product. This is due to the molecular sieves commonly used having a high selectivity for water. [8] When a PSA system is designed to produce an output of CO below 0.2 µmol/mol, the concentration of water will be less than 0.1 µmol/mol. [13] This makes it unlikely for H₂O to be present in hydrogen produced using this method.

There are three potential pathways for water to contaminate hydrogen through electrolysis. These are:

- Electro-osmosis through the proton exchange membrane
- Hydrogen water saturated at 60°C
- Drier malfunction

Table 2.1: Summary of ISO 14687-2 impurities in the supply chain and their effects on fuel cell operation adapted from [13]

Impurity	Production sources	Contamination source	Contamination barriers	Effect on fuel cell operation
N ₂	SMR	Raw material PSA malfunction Maintenance Leakage	PSA Maintenance PEM membrane	Reduced energy density of fuel
	Electrolysis	Air intake into water tank	H ₂ pressure > N ₂ pressure supply PSA	
Ar He	SMR	Raw materials	-	Potential damage to hydrogen storage
	-	Generation at the anode	TSA operating condition Oxygen sensor	
O ₂	Electrolysis	Membrane cross over TSA malfunction By-product	PSA CO sensor on line	Temporary electrocatalyst poisoning
CO	SMR	Raw materials By-product	PSA	Damage to hydrogen storage medium Could cause formation of CO
CO ₂	SMR	Raw materials	PSA CO ₂ filter	Reduced energy density of fuel Ice formation during refilling K ⁺ and Na ⁺ contamination reducing cathode side conductivity
	Electrolysis	Water at anodic side Air into the pure water tank	Anodic separator tank Ion exchange resin in closed water loop PEM membrane	
CH ₄	SMR	Raw material	PSA	Reduced energy density of fuel
H ₂ O	SMR	Raw material Reactant	Methane sensor on line PSA	Ice formation during refilling K ⁺ and Na ⁺ contamination reducing cathode side conductivity
	Electrolysis	Through PEM membrane Hydrogen output water saturated TSA malfunction	TSA dryer Dew point monitor Operating procedure	
Total sulphur compounds	SMR	Raw material	Desulfuration unit Sulphur trap in reforming system PSA	Permanent electrocatalyst poisoning
NH ₃	SMR	Raw material	Stainless steel pipe and vessel PSA	Reduced ion exchange capacity
	Electrolysis	Water at anodic side	Reverse osmosis PEM membrane	
Formaldehyde	SMR	Raw material	PSA	Temporary electrocatalyst poisoning
Formic acid	SMR	Raw material	PSA	Temporary electrocatalyst poisoning
Halogenated compounds	SMR	Raw material	Desulfuration unit Chlorinated trap in reforming system PSA Stainless steel pipe and vessel	Permanent electrocatalyst poisoning
Monitoring Cl ₂ concentration	Electrolysis	Raw material contamination	Reverse osmosis	

Modern electrolysers are fitted with a drier, which is the main barrier for water vapour exiting the process with hydrogen. [13] In the event of drier failure, most systems are fit with a dew point analyser that will trip, shutting off production until the issue can be fixed. [13]

Water generally does not affect the function of a fuel cell, however; it provides a transport mechanism for water-soluble contaminants such as K⁺ and Na⁺ [14] to pass through the electrolyte and have a negative long-term effect on the conductivity of the cathode side of the membrane. In addition, water may increase the risk of ice formation within vehicle fuel storage and hydrogen dispensing systems under certain conditions.

Total hydrocarbon content

The presence of hydrocarbons are most likely to result from the SMR process. Hydrocarbons are not expected to be present at all in electrolysis. Similar to water contamination through SMR, the most likely reason for hydrocarbon contamination is due to malfunction of the PSA system used to purify the product hydrogen.

A PSA system designed to deliver hydrogen with a CO concentration $\geq 0.2 \mu\text{mol/mol}$ should be sufficient to reduce the amount fraction of hydrocarbons to below the 5 $\mu\text{mol/mol}$ required by ISO 14687. [13]

Different hydrocarbons have different effects on fuel cell performance. Generally aromatic hydrocarbons adsorb more strongly on the catalyst surface than other hydrocarbons, inhibiting access to hydrogen.[14] Methane (CH₄) is generally considered an inert constituent and it's main effect on fuel cell performance is diluting the hydrogen fuel stream. [14]

Oxygen

In SMR processes oxygen is not used as a raw material, nor is it stable during the process conditions, readily reacting with hydrogen to produce water. In addition to this the oxygen content of the feedstock to the PSA separation stage must be below a certain level for safety reasons. Therefore oxygen contamination from hydrogen produced from SMR is unlikely.

Oxygen is a main by-product of electrolysis, although is generated at the anode side of the electrolysis stack. Likely methods of contamination are through cross over through the PEM membrane. Due to the danger of high oxygen levels in hydrogen streams, most electrolysis systems are fit with an oxygen sensor that trips the system if the concentration of oxygen in the hydrogen stream surpasses 5 umol/mol. [13]

Oxygen in low concentrations does not adversely affect the function of the fuel cell system; however, it may be a concern for some on-board vehicle storage systems, for example, by reaction with metal hydride storage materials. [14]

Helium, nitrogen and argon

Helium is not present as a feed material in any of the discussed processes, however there is also no barrier to Helium in the exit stream and therefore any helium that enters a SMR or electrolysis process will not be removed. Despite this it is unlikely that helium will be present in a hydrocarbon feedstock, or water.

Argon is similar to helium, however it is more likely for Argon to be present in the natural gas feedstock for SMR. Unlike helium, the PSA step in SMR can act as a barrier for Argon, however this will depend on the specific molecular sieve used in the system. [13]

Nitrogen is the most likely inert impurity to be present in fuel cell hydrogen, this is due to the abundance of nitrogen in the air which the system could be exposed to, and the frequency at which nitrogen is used as a functional gas in processes for purging chambers, actuating valves etc.

Inert constituents, such as helium (He), nitrogen (N_2) and argon (Ar) do not adversely affect the function of fuel cell components or a fuel cell system. However, they dilute the hydrogen gas. N_2 and Ar especially can affect system operation and efficiency and can also affect the accuracy of mass metering instruments used for hydrogen dispensing. [14]

Carbon dioxide

Like most other impurities which are present in SMR, CO_2 is likely to be removed from the SMR process at the PSA step, with most commonly used molecular sieves being able to remove carbon dioxide during normal operation. [8]

CO_2 can be present in the water used for electrolysis although there are several interlocks to prevent it reaching the exit stream. Most electrolysis systems have a CO_2 filter on the inlet and a reverse osmosis unit to ensure the purity of the inlet water. An anodic separation tank which features an ion exchange resin in a closed water loop also acts as an additional barrier, and finally CO_2 has a low crossover potential through the PEM membrane and therefore is unlikely to cross into the cathode side of the system.[13]

CO_2 does not typically affect the function of fuel cells. However, CO_2 may adversely effect on board hydrogen storage systems using metal hydride alloys. With CO_2 , at levels higher than the specification, a reverse water gas shift reaction can occur under certain conditions in fuel cell systems to create carbon monoxide. [14]

Carbon monoxide

Carbon monoxide is a main byproduct of SMR which is separated from the exit gas stream through PSA. [8] If this fails SMR processes are fitted with a CO sensor to ensure the concentration in the product does not pass a certain threshold. [13] It is unlikely for CO to be present from electrolysis.

Carbon monoxide (CO) is a severe catalyst poison that adversely effects fuel cell performance by inducing a competitive adsorption effect between itself and hydrogen on

the electrocatalyst surface. The result is a temporary reduction in operating efficiency. [14] Although its effect can be reversed through mitigating strategies, such as material selection of membrane electrode assembly (MEA), system design, and operating conditions, its effect on operation is still a concern. Lower catalyst loadings are particularly susceptible to catalyst poisoning contaminants.

Total sulfur compounds

Sulphur contamination is most likely to come from hydrogen produced from hydrocarbon sources. Since the SMR process also uses catalysts that are susceptible to poisoning from sulphur compounds all plants are fit with a desulphurisation unit upstream from the main process. [8] This is designed to reduce the concentration of sulphurous compounds to ≤ 50 nmol/mol. [13]

Should the desulphurisation unit fail the catalysts used in both reforming steps will be deactivated, preventing the process from operating and will likely result in shut down of the plant. PSA also acts as a final barrier, since H_2S will adsorb onto the molecular sieves more strongly than CO . [13]

The other potential source of sulphur contamination is the potential release from any gasket materials used in the process. This can be easily prevented by ensuring only materials that do not contain sulphur are used. [14]. It is unlikely that sulphur contamination will arise from electrolysis.

Sulfur containing compounds are severe catalyst poisons that at even very low levels can cause irreversible degradation of fuel cell performance due to a permanent reaction taking place between sulphur and the platinum catalyst. The specific sulfur compounds addressed in particular are: hydrogen sulfide (H_2S), carbonyl sulfide (COS), carbon disulfide(CS_2), methyl mercaptan (CH_3SH). [14]

Formaldehyde and formic acid

Formaldehyde ($HCHO$) and formic acid ($HCOOH$) is produced through a side reaction in SMR depending on the specific operating conditions of the process.[8] PSA is the main barrier for preventing contamination of the product. [13]

Formaldehyde and formic acid have a similar effect on fuel cell performance as CO and are thus considered as reversible contaminants. The effect of $HCHO$ and $HCOOH$ on fuel cell performance can be more severe than that of CO due to slower recovery kinetics and their specifications are lower than that for CO . [14] Lower catalyst loadings are particularly susceptible to catalyst poisoning contaminants.

Ammonia

Hydrogen could be contaminated with ammonia through either SMR or electrolysis. Ammonia is a by-product of the reforming steps and PSA should be sufficient to remove ammonia from the exit stream of SMR. Ammonia can also be present in water used in

electrolysis however the reverse osmosis step used to purify the water before the process is normally sufficient in removing all ammonia before it is used in the process. [13]

Ammonia (NH_3) causes some irreversible fuel cell performance degradation by affecting the ion exchange capacity of the ionomer of the proton exchange membrane. [14]

Total halogenated compounds

Halogenated compounds can contaminate hydrogen by entering either SMR or electrolysis through the process input, or leaking into the process at other points where they are used. Potential sources include chlor-alkali production processes, refrigerants used in processing, and cleaning agents. [13]

Halogenated compounds cause irreversible performance degradation similar to sulphur, reacting with the platinum electrocatalysts to form platinum-halides such as PtCl_4 . [15] However the concentrations required to cause this damage has not been well documented in literature.

2.4 Hydrogen impurity enrichment

'Hydrogen impurity enrichment' is a term for any technique which involves increasing the concentration of impurities within a hydrogen sample by means of removing the hydrogen matrix gas. There are two previous reports of impurity enrichment being used as a technique for hydrogen impurity analysis. The first report by Papadis et al at Argonne National Laboratory used a Pd/Cu [16] coated Pd/Ag membrane for non-sulphur containing hydrogen samples and a Pd/Au coated Pd/Ag membrane for sulphur containing hydrogen samples to enrich impurities in a 50 bar sample. The analyte gas used contained N_2 , CH_4 and CO_2 at $100\mu\text{mol/mol}$ and an additional $2\mu\text{mol/mol}$ of H_2S during sulphur tests sulphur. The enrichment was calculated by using measured values of temperature and pressure along with the non-ideal gas law, this was represented through a 'calculated enrichment factor' as shown in equations 3.1 and 2.12.

$$CEF_{NI} = \frac{\frac{P_{1,a}V_1}{Z_{1,a}RT_{1,a}} \frac{P_{2,a}V_2}{Z_{2,a}RT_{2,a}} - \frac{P_{1,b}V_1}{Z_{1,b}RT_{1,b}}}{\frac{P_{2,b}V_2}{Z_{2,b}RT_{2,b}}} \quad (2.11)$$

$$y_{i,a} = \frac{y_{i,b}}{CEF} \quad (2.12)$$

The set-up was able to reach enrichment factors of around 32 for non-sulphur tests and 15 for sulphur tests. The non-sulphur tests closely matched with the actual component concentrations, however in the second set of tests there was some loss of sulphur observed, most likely due to the formation of palladium sulphide on the surface of the membrane, or through wall catalysed reactions.

A similar experiment was performed by National Physical Laboratory with the aim of decreasing the uncertainty of using such a device. [17] The non-ideal gas law method

used in the previous paper [16] was compared to a novel tracer enrichment method developed by NPL. [17] The tracer enrichment method involves spiking the hydrogen sample with a known quantity of krypton prior to enrichment. The enrichment factor is then calculated using the change in concentration of the krypton as shown in equation 2.13.

$$CEF_{Tracer} = \frac{y_{Krb}}{y_{Kra}} = \frac{1}{y_{Kra}} \frac{A_{Krb}}{A_{Kra}} y_{Krst} \quad (2.13)$$

The set-up was similar to the one used by Papadias et al [16] and was used to enrich a 50 bar 10L hydrogen sample containing 1.5-2 $\mu\text{mol/mol}$ of CO, Kr, CH_4 and N_2 . Use of the tracer enrichment method reduced the associated uncertainty from 2.6% to 1%. Two tests were performed, with the second test resulting in membrane failure.

When operating the hydrogen impurity enrichment device it was found that both methods should be used to calculate the CEF.[17, 18] While the tracer enrichment method has a lower uncertainty due to it being dependant on fewer variables, it is impossible to tell if a leak has occurred in the device due to the covariance phenomena. [17] Leaks in the enrichment device could occur due to thermal expansion of components due to heating to the required operating temperature or cracks forming in the membrane. The stability of membranes used in such a device will be discussed in the following section. During a leak it will be expected that the ratio of krypton, along with other impurities which are not naturally present in air, will remain constant, resulting in no change in the CEF. A leak will allow oxygen and nitrogen to enter the system and throw off the measurement of these two impurities. While the tracer enrichment method could still be used to calculate the amount fraction of other impurities, the non-ideal gas law method would have to be used to provide an accurate measurement for Oxygen and Nitrogen.

A device similar to the HIED is the Hydrogen Elimination Mass Spectrometer (HEMS) designed by Power + Energy USA. [19] The principle behind the HEMS is the same as the HIED, where a palladium membrane is used to selectively remove the hydrogen matrix gas and thus concentrate the impurities within the hydrogen sample. The output is directly fed into a mass spectrometer which allows in-situ measurements to be performed. The limit of detection specified by the manufacturer claims to be in the range of pmol/mol however there is no published information regarding the accuracy or uncertainty associated with the device. As of 2016 the device was discontinued by the manufacturer.

2.4.1 Other enrichment methods

Sorbent tubes

The use of traps and sorbent tubes to pre-concentrate impurities in gases is very common in gas analysis, but only two hydrogen purity analysis standards have incorporated this technique to facilitate purity analysis. A method for concentrating the impurities in a sample of hydrogen using a zeolite- packed chromatographic column has been described

in a paper by Hille [20]. The method involves flowing the gas sample into the column using a pump and cooling the column to a temperature that allows the impurities to remain trapped whilst the matrix gas passes through. The sample is then transferred to GC-MS for analysis. The enrichment factor for this method is determined by the flowrate and amount of time that the gas is sampled into the column. The method was validated by analysing gas mixtures of hydrogen containing 8.7 mmol/mol of silane. By enriching the sample, the signal- to-noise for the same measurement was increased by a factor of 2000 indicating that levels in the range of 4 nmol/mol of silane would easily be measured using this method whereas the usual limit of detection (without pre-concentration) would have been 1 μ mol/mol.

Cryo-focusing

A method for performing pre-concentration by cryo-focusing has been detailed in ASTM WK34574 where the device is used to concentrate the impurities in a sample of hydrogen before introducing the gas to a GC-MS [18]. The pre-concentration method involves trapping the impurities onto a glass bead trap at -150°C. By increasing the temperature of the trap all of the impurities apart from water are transferred to a separate Tenax trap which is cooled to -170°C. Upon heating once again the enriched sample is introduced to the analyser. Very high enrichment factors can be achieved using this method by flowing a high volume of the sample gas through the pre-concentration device to allow capture of the impurities whilst the hydrogen is removed. No information was provided in the standard to indicate the accuracy or limitations of this method.

2.5 Review of hydrogen selective membranes

The term membrane is used to describe a semipermeable barrier which selectively allows certain species to pass through it, while preventing or inhibiting the passage of others. The driving force for gas separation through a membrane is the pressure and component concentration gradients across the chosen material. In the context of hydrogen separation, the trans-membrane pressure and hydrogen concentration gradient across the feed and permeate, combined with the unique properties of the chosen separation material, will allow hydrogen to pass through the membrane, while preventing or inhibiting the transport of impurities which the membrane is not selective or less selective towards. A large number of materials have been studied for hydrogen separation. For the purpose of this review they will be split into four broad categories based on their material type and separation mechanism which is related to their pore structure (dense or porous); these categories are shown in Table 2.2 and visualized in Figure 5.1.

The material, its structure with regards to pore size and pore size distribution, and surface chemistry, all contribute to the separation mechanism for removing hydrogen from its constituent gas mixture. The six main membrane separation mechanisms are visualised in Figure 5.1, with (i) – (iv) showing the four separation mechanisms for gases in porous media, and (V)- (Vi) showing gas separation through dense media. For porous

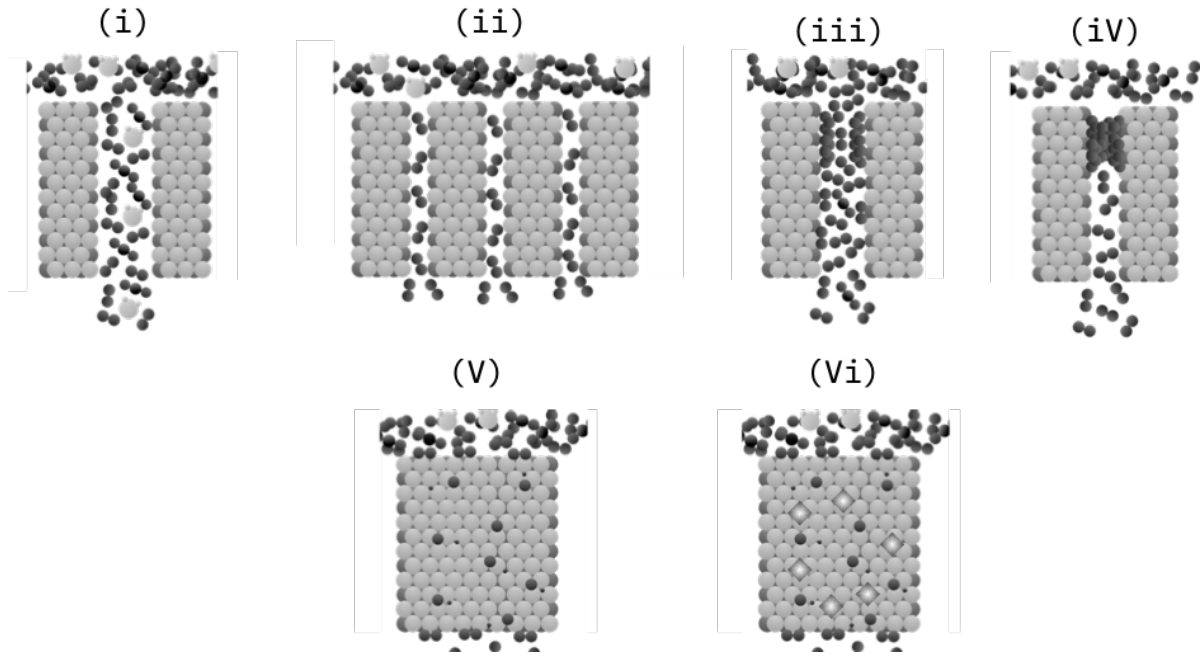


Figure 2.5: Illustration of the five membrane separation mechanisms (i) Poiseuille Flow/Knudsen diffusion, (ii) Molecular Sieving, (iii) Surface diffusion (iV) Capillary condensation (V) Solution diffusion (Vi) Facilitated transport

materials typically a combination of these mechanisms dictates the overall separation performance due to imperfections in the membranes structure. All dense membranes should be dictated by the solution diffusion mechanism and the presence of any other mechanisms are evidence of imperfections in the membrane.

For most porous media, the separation mechanism is dominated by Poiseuille flow or Knudsen Diffusion. The precise separation mechanism can be determined by calculating the ratio between the mean free path of the gas molecules (λ) and the pore radius (r) as shown in Equation 2.14 where η is the viscosity of the gas, P is the pressure, T is the temperature, M_w is the molecular weight of the gas, and R is the universal gas constant.

$$\frac{r}{\lambda} = \frac{2P}{3\eta} \sqrt{\left(\frac{2M_w}{\pi RT}\right)} \quad (2.14)$$

This ratio determines the contribution of Knudsen and Poiseuille flow. If $r/\lambda \gg 1$ it would indicate that the main gas transport rate limiting step is due to molecule-molecule collisions indicating that Poiseuille flow is the dominant transport mechanism. Likewise if $r/\lambda \ll 1$ it indicates that molecule-wall collisions govern the rate limiting step showing that Knudsen diffusion is the dominant mechanism. If the transport is purely Knudsen diffusion the H_2/CO_2 selectivity of the membrane will be equal to around 4.7. Since this value is relatively low, it has pushed researchers into fabricating membranes with smaller pore structures, and to modify their membranes to take advantage of specific surface interactions. Both of these developments allow researchers to surpass the selectivity

achievable with purely Knudsen diffusion.

Molecular sieve materials can be classed as macroporous ($\geq 50\text{nm}$), mesoporous (2– 50nm) and microporous ($\leq 2\text{nm}$) with microporous materials being the most relevant for hydrogen separation processes. These membranes are fabricated in such a way that the passageways are small enough that the entrance of molecules with large kinetic diameters is not possible. This results in higher permeation of smaller components in a gas mixture such as H_2 or He while slowing, or completely preventing the passage of bulkier molecules. This mechanism, while effective for some gas mixtures, may not be feasible when looking to perform separation on similar sized gas pairs; selectivity is often hindered by competitive adsorption between the species due to the surface chemistry of the material. Fabrication of these membranes can also be difficult and manufacturing large scale membranes with a tight enough pore size distribution to ensure molecular sieving still proves to be a difficult task. Common microporous materials which are able to be fabricated into molecular sieving membranes are zeolites, metal organic frameworks, activated carbon, and amorphous silica.

Surface diffusion and capillary condensation are similar in that the surface chemistry of the pores in the membrane has a large effect on the separation efficiency. Surface diffusion occurs when the walls of the pore either intrinsically, or following modification, provides adsorption sites for the desired gas molecule. The gas molecule will adsorb onto the walls resulting in faster diffusion through the pore structure than other gases in the mixture. Similarly, capillary condensation typically follows on from surface diffusion and involves the gas species condensing within the pore of the membrane, either due to stronger molecule-wall interactions, or a smaller pore radius. The condensation of the molecule results in further selectivity improvements towards this component by providing an added transport barrier to other gas species.

Gas transport in dense media is typically harder to categorise due to the unique material chemistry present in each material, however all dense membranes perform separation through some variation of the solution diffusion mechanism. Typically, the following steps are always present in some form:

1. Adsorption of gas species onto the surface of the membrane
2. Diffusion of gas species through the bulk of the membrane
3. Desorption and diffusion of the gas species in the downstream.

More details will be provided on the precise features of solution diffusion in each material in the following sections. Facilitated transport is a sub section of solution diffusion and occurs in dense membranes which have a selected chemical species added into the bulk of the membrane. These materials are chosen based on the presence of a particular interaction with components of a gas species. These interactions are typically reversible reactions between the added species and the gas intended for separation and is intended to enhance the diffusion of the selected gas, this additive could either be fixed species (solid) or mobile (liquid).

The most commonly reported metrics for membrane performance is the flux or permeability coefficient and selectivity. The flux (J) of a membrane is a measure of the

amount of gas the membrane is allowing to pass per unit time per unit surface area and is typically used as a measure for how effective the fabricated membrane performs. The permeability coefficient (P) can be derived from the flux and is a quantitative expression which gives a specific measure of the separation properties of a material independent of operational and manufacturing constraints such as operating pressure and membrane thickness. While flux and permeability are similar and tied to each other they are both useful in their own way. The permeability coefficient is typically tied to the material and is useful for comparing different materials to each other, while the flux offers a measure on how effective a specific membrane is.

The selectivity ($\alpha_{i/j}$) represents the separating ability of the membrane for a specific gas species (i) with respect to another gas species (j). This is common notation for porous membranes and membranes which are not completely selective towards one component. For membranes which are only selective towards one component such as dense metal and dense ceramic, the selectivity is not reported since any presence of another component in the exit stream is generally an indication of a manufacturing defect.

While these values are reported for all membranes in order to allow for a direct comparison of performance, this is where the similarities end. The fundamental separation mechanism, manufacturing techniques, and unique material chemistry are often different for each material. In addition to this there are other important metrics for the usefulness of a membrane such as mechanical stability, lifespan, and chemical resistance which are more difficult to quantify.

2.5.1 Criteria for a hydrogen impurity enrichment material

In order for a membrane to be suitable for hydrogen impurity enrichment material it must be able to increase the concentration of low-level impurities in a hydrogen sample. Although all past examples of hydrogen impurity enrichment have used dense membranes with an infinite selectivity towards hydrogen, it is theoretically possible to use a membrane which has a lower selectivity to perform enrichment. This would have the advantage of allowing membranes with faster flux to be used, greatly reducing the amount of time required for an enrichment run, while allowing cheaper materials to be used in place of the palladium membranes used in past studies. In order to perform this calculation, the following must be known:

- Selectivity of the membrane must be known to a high accuracy
- Total number of moles leaving the system
- Concentration of enriched impurities

Since the selectivity shows the ratio of substances passing through the membrane (i.e. H_2/N_2 selectivity of 2 represents 2 moles of hydrogen for every 1 mole of nitrogen passing through the membrane) if both quantities are known the number of moles of impurity leaving the system through permeation could be easily estimated.

$$n_{i_{exit}} = n_{exit_{total}} / \alpha^{H_2/i} \quad (2.15)$$

Table 2.2: Types of hydrogen separation membrane

Material	Separation mechanism	Mechanical stability	Chemical Stability	Operating temperature	Selectivity
Polymer (Dense)	Solution diffusion, Facilitated transport	Susceptible to Compaction [21] and Swelling [22]	Low chemical stability, Degrades under H ₂ S, HCl, CO ₂ , SO _x [23]	A	A
Polymer (Porous)	Knudsen diffusion, Molecular sieving, Surface diffusion, Capillary condensation, Poiseuille flow	Susceptible to Compaction [21] and Swelling [22]	Low chemical stability, Degrades under H ₂ S, HCl, CO ₂ , SO _x [23]	>100°C	2.5 9 -960 [24] (H ₂ /N ₂ selectivity)
Nano-porous	Knudsen diffusion, Poiseuille flow, Capillary condensation, Surface diffusion, Molecular sieving	Brittle	Good[25]	Ambient -500°C	2.4 [26] - 1000 ref for this (H ₂ /N ₂ selectivity)
Dense Metal	Solution Diffusion	Phase transition [27] Dependant on support [27] Surface segregation[27]	Negative interaction with CO, CH ₄ , and H ₂ O. Reacts with H ₂ S and SO _x [27]	300-600 [28]	∞
Dense Ceramic	Solution Diffusion	Brittle	Difficult to seal due to high operating temperature	Degrades under CO ₂ [29]	500-1000 [29]

The concentration, and therefore the number of moles of impurity on the retentate side of the membrane could then be analysed using suitable instrumentation. These values could then be added together and divided by the enrichment factor in order to give the original number of moles that would be in the vessel.

$$y_i = \frac{(n_{i_{ret}} + n_{i_{exit}})/n_{totret}}{CEF} \quad (2.16)$$

In practice however this may not be feasible due to the low concentrations of impurities expected to be present in these hydrogen samples. In order for an enrichment calculation to work there must be an analysable concentration of impurity remaining in order to back calculate. Since the level of expected impurities in a hydrogen sample is so low, and the selectivity of many membranes also low, there is a high risk of either all impurities simply leaving the sample during the enrichment run, or only achieving a lower enrichment factor. Take the example of enriching a sample containing 0.2 $\mu\text{mol/mol}$ of CO by 100 in order to analyse its composition on a GC-MS. If the sample is a standard 10L cylinder containing 100 bar a H₂/CO selectivity of ~4950000 is required to simply prevent all of the CO leaving the enrichment device, which is effectively the same as the selectivity's seen in dense metal membranes. However, for the same sample containing 0.3 $\mu\text{mol/mol}$ of Helium a H₂/He selectivity of 330 is the minimum required which is more feasible. However, both these values are the exact values required by the standard, in reality they would be much lower. The highest reported selectivity of a non-infinitely selective membrane was Liquid crystalline polyester which had a H₂/N₂ selectivity of 2632 [30] which indicates that this method may be suitable for enriching some of the higher concentration impurities in hydrogen samples, it is not a solution for lower concentration. It is also unlikely that the selectivity of a membrane material will stay constant throughout its lifespan. Any drift in selectivity would throw off the calculation and either require regular changing of the membrane, driving up cost, or regular calibration to recalculate the selectivity of the membrane at a given time, which would be time consuming. It is however likely that infinitely selective membranes are the only feasible enrichment material due to their ability to enrich every impurity in hydrogen, whereas non-infinitely selective membranes may be applied to analysis of individual impurities, it is unlikely such a scenario would occur in reality which makes them a non-ideal solution.

The common thread with all the micro-porous materials discussed here is that they are currently difficult and expensive to synthesise on a large scale, particularly in membrane form. Due to the separation mechanism of micro-porous materials they are not suitable for use in hydrogen impurity enrichment as their selectivity will not produce a viable enrichment medium. However, due to their high surface areas and ability to be modified to promote integration with specific gas species, they may find use in sensor applications for detecting the ISO-14687 impurities. There is a wealth of work on the use of many of these materials as chemical sensors however much of this work has been performed using the gases in non-hydrogen matrix gases and therefore much work is required before their true potential in this area can be realised.

Polymer membranes have a similar issue to micro porous materials in that their

selectivity is too low to be effective at enriching impurities in hydrogen samples. The mechanical strength and impurity resistance of polymer membranes also limits their use as hydrogen impurity enrichment mediums. While again there are some successful applications of polymers as sensor materials, the same issues as micro porous materials regarding lack of information of their effectiveness in a hydrogen matrix crops up again. It is likely that polymer membranes will continue to be most effective in industrial separation and will be limited in their use as an analytical material.

Therefore this section will only concern itself with membranes which show permselectivity towards hydrogen therefore making them viable as hydrogen impurity enrichment materials. This section will discuss the performance of dense metallic and dense ceramic membranes, and by comparing their reported metrics, their suitability for hydrogen impurity enrichment will be determined.

Dense metallic

Metallic membranes are comprised of dense metal or alloy sheets which allow the permeation of hydrogen through its constituent electrons and protons. While this is the same separation mechanism seen in dense polymer membranes the hydrogen selectivity is typically a lot higher in these systems since molecules which are not hydrogen are unable to dissociate and permeate through the membrane surface, giving a theoretically infinite selectivity towards hydrogen. The minimum requirement for a dense metal membrane for hydrogen separation is the ability to dissociate and permeate hydrogen. There are a number of metals which have shown varying degrees of suitability for hydrogen separation and these are shown in Table 2.3.

Table 2.3: Metals which show the ability for hydrogen permeation [31]

Structure	Metal	Activation energy for hydrogen permeation (kJ/mol)	Heat of hydride formation (kJ/mol)	Hydrogen permeability at 500°C (mol/ m s pa ^{1/2})
fcc	Ni	40.0	-6	7.8 × 10 ⁻¹¹
	Cu	38.9	-	4.9 × 10 ⁻¹²
	Pd	24.0	20	1.9 × 10 ⁻⁸
	Pt	24.7	26	2.0 × 10 ⁻¹²
bcc	V	5.6	-54	1.9 × 10 ⁻⁷
	Fe	44.8	14	1.8 × 10 ⁻¹⁰
	Nb	10.2	-60	1.6 × 10 ⁻⁶
	Ta	14.5	-78	1.3 × 10 ⁻⁷

The flux of a dense metal membrane is given by Eqn 2.17 and is a function of the metals permeability to hydrogen, the concentration and pressure gradient across the membrane, and the thickness of the dense layer.

$$J = \frac{\phi}{l} (P_{H,ret}^{0.5} - P_{H,perm}^{0.5}) \quad (2.17)$$

From the metals shown in Table 2.3 palladium and its alloys are by far the most popular choice due to a combination of high hydrogen permeability, favourable catalytic

activity towards hydrogen dissociation and re-association, and aversion towards hydride formation compared to other metals.[31, 32, 33]

For other metals there is often a trade-off, V, Nb and Ta exhibit higher permeability than palladium but are limited by their low catalytic activity for hydrogen dissociation and typically must be combined with another metal to compensate for this. A common strategy is to deposit palladium particles on both sides of membranes made from these metals to provide this catalytic activity. Embrittlement of pure metal membranes is also an issue, even for metals with a high heat of hydride formation. Embrittlement is a side effect of hydrogen passing through the crystal lattice. During transport a H-M phase will form which has a higher lattice parameter than the original crystal lattice. This change in lattice parameter can cause stress in the overall structure of the dense membrane layer and cause the formation of pin holes, cracks, and eventually membrane failure. Metals with a low heat of hydride formation in Table 2.3 will readily embrittle within hydrogen containing atmospheres.

This section will discuss developments in both palladium and non-palladium membranes and the issues still surrounding the technology.

As previously mentioned palladium is typically the material of choice for dense metallic membranes due to its combination of high stability, permeability, and catalytic activity. Palladium based membranes have been successfully used to provide ultrapure hydrogen for a number of applications including electronics, industrial gas, and fuel cell industries for a number of years. The main downside to the use of palladium is its high cost of around \$25 per gram. [34] This high cost has pushed researchers into focusing on reducing the amount of palladium used in the membrane in order to find a more economical solution. This is done either by using a traditional membrane approach, whereby the thickness of the membrane layer is reduced as much as possible to maximise the flux while decreasing the overall amount of palladium used, or by alloying palladium with a cheaper metal to reduce the amount of bulk palladium in the manufacturing process.

During operation of a pure palladium membrane at temperatures lower than 300°C, hydrogen embrittlement can occur due to the aforementioned phase transition between interstitial hydrogen within palladium (α phase) and palladium hydride (β phase). The β phase (0.4025 nm) has a lattice parameter bigger than the α phase (0.389nm). [35] The formation of this α - β phase will cause the membrane to distort, become brittle, and eventually results in membrane failure when a leak occurs. [36] Aside from this pure palladium has poor chemical stability, it can be poisoned by a number of impurities which are commonly found in hydrogen. Some of these impurities simply inhibit permeation of hydrogen but do not have a permanent interaction and thus their effects can be mitigated by optimising the operating conditions. Others such as H₂S and CH₄ are known to interact with the membrane through chemisorption and permanently damage the membrane through the formation of compounds with palladium, breaking the crystalline lattice resulting in membrane failure.

From the impurities listed in ISO 14687-2 CO, H₂O, Hydrocarbons and sulphur containing compounds are known to have a physisorption interaction with palladium. Physisorption based poisoning occurs by the impurity inducing a competitive adsorption with hydrogen, blocking active sites for hydrogen dissociation, and hence reducing the

active area available for hydrogen permeation.[27] The ultimate effect of this is a temporary flux reduction which has no long lasting damage on the membrane. Compounds such as H₂S, and CH₄ have a more extreme effect on the membrane as adsorption leads to a reaction between palladium and the metal permanently changing the membrane composition and structure. The most commonly studied interaction is the interaction between palladium and H₂S to form palladium sulphide. Palladium sulphide, while still permeable to hydrogen, has an extremely low permeability, drastically reducing the efficiency of the membrane. Palladium sulphide also has a larger lattice constant than that of pure palladium which can lead to membrane failure by creating gaps in the crystal lattice resulting in pinholes. Some of these impurities, in particular those which only exhibit physisorption, can be mitigated by altering the operating conditions. It has been reported that the effects of CO and H₂O poisoning can be completely eliminated by operating at temperatures above 300°C. Another example where this is shown is with H₂S related poisoning. Since the reaction between palladium and H₂S is exothermic, and produces hydrogen as a side product, it can be inhibited by increasing the H₂:H₂S ratio and increasing the temperature.

A combination of cost, easy formation of phase transitions [35, 36] and its low tolerance for common impurities found in hydrogen processes limits pure palladium's use as a hydrogen separation material. Many of these effects however, can be completely mitigated through alloying palladium with another metal. By forming an alloy with a metal which has a lattice parameter similar to that of the β -phase the average difference between the sizes of the two phases is effectively decreased and thus the hydrogen embrittlement effect can be effectively mitigated. The effect of impurities on palladium membranes can also be partially mitigated by alloying with another metal and oftentimes an increase in permeability is reported with certain alloy compositions.

Both binary and ternary alloys of palladium have been reported and is a mature topic in literature. By far the three most popular alloying compounds with palladium are silver, copper and gold. The current literature landscape of palladium alloy membranes are summarised in **BIG METAL TABLE** and for the purpose of this review studies which looked at the impurity resistance, which is currently the most pressing issue in the field, were focused on.

Silver is the most popular dopant for palladium membranes and forms a stable alloy with palladium at concentrations greater than 20wt %, with the optimal composition occurring at 23%. On top of mitigating the effects of hydrogen embrittlement, a 60% increase in permeability is observed when compared to pure Pd membranes. Despite having enhanced permeation properties, PdAg is still susceptible to poisoning, in particular from sulphurous compounds which can form both Pd₄S and Ag₅Pd₁₀S₅. Several studies exposing PdAg membranes to sulphurous compounds have been performed and in most cases the membranes suffer a large decrease in flux, and are permanently damaged as shown by a permanent decrease in flux when sulphide is removed from the inlet. [37] It has been observed that exposure to 5 $\mu\text{mol mol}^{-1}$ H₂S in the feed stream is enough to induce Pd₄S formation [37] and therefore this composition is only suitable for atmospheres and applications which do not contain any sulphur.

Copper is another widely studied binary alloy which is known to suppress hydrogen

embrittlement. Alloying with copper also has the advantage that it reduces the cost of the membrane by a larger amount than most other metals and through improving the membranes sulphur resistance. The maximum permeability of a palladium copper membrane occurs at the composition $Pd_{60}Cu_{40}$ and this is due to the formation of a bcc lattice rather than the fcc lattice commonly seen in pure palladium and most binary alloys. [38] Temperature cycling has been performed on this alloy composition and it has been found that the bcc crystalline configuration has a higher permeability than the fcc phase. [39] This behaviour is due to the increased number of hcp adsorption sites which hydrogen has a slight preference for.[40] Conversely the fcc structure has a higher impurity resistance than the bcc structure, particularly for H_2S . This has been theorised to be because adsorption of H_2S on a palladium membranes surface is largely controlled by electronic factors.[41] There have been several studies reporting an increased resistance to sulphur poisoning by alloying palladium with copper. A $Pd_{80}Cu_{20}$ membrane exposed to $20 \mu\text{mol mol}^{-1}$ of H_2S for 90 hours results in a 22% drop in flux, performing much better than $Pd_{75}Ag_{25}$ reported in the same paper which became impermeable after 65 hours of exposure in the same conditions.[37] In a similar study, the performance of bcc and fcc alloys in response to H_2S $Pd_{20}Cu_{80}$, $Pd_{40}Cu_{60}$ and $Pd_{53}Cu_{47}$ foils at varying temperatures was tested in hydrogen containing $1000 \mu\text{mol mol}^{-1} H_2S$.[42] It was found that when the alloys were in the fcc phase the reduction in flux was only round 10%, while in the bcc phase the membrane loses around 99% of its permeance. The H_2S concentration required to make a $Pd_{60}Cu_{40}$ membrane completely impermeable was found to be around $300 \mu\text{mol mol}^{-1}$ [43].

PdAu alloys see a slight increase in permeability, up to 30% more than pure Pd, with gold additions up to 20%, after which the permeability rapidly decreases. While alloying with gold does not improve the permeability much compared to silver or copper, gold alloys show greatly improved sulphur resistance. Several studies have been performed which show that PdAu membranes show no permanent permeability loss after exposed to ppm levels of sulphurous compounds implying that permeability decline is only due to H_2S adsorption. It has been reported that a $Pd_{92}Au_8$ membrane exposed to $54.8 \mu\text{mol mol}^{-1}$ of H_2S was able to resist reaction with H_2S and its permeability was completely recoverable. [44]. When tested higher temperatures it was also found that the adsorption effect of H_2S was reduced which is evidence that dissociative adsorption of H_2S on metals is exothermic. [44] In the original patent for palladium membranes by McKinley [45] in 1964 $Pd_{60}Au_{40}$ was found to be the composition which performed best under sulphur containing atmospheres, losing only 9.44% of its flux compared to the 99% and 95% lost by PdAg and PdCu membranes respectively.[45] However under recovery the flux increased to 120% of its original value while the PdCu membrane was fully recovered under the same conditions. This may be evidence that the $Pd_{60}Au_{40}$ membrane used is not completely stable. [45] When comparing the performance of PdCu and PdAu membranes under a number of gases which commonly result from the water gas shift reaction it was found that the PdAu resisted . [46] It was found that from the four membranes tested, the PdAu membranes show no permeability loss under an atmosphere containing CO , CO_2 and H_2O while the PdCu membranes showed considerable permeability loss. [46] The biggest downside to alloying with gold is that due to its high

price in recent years alloying palladium with gold drives up the price higher than that of a pure palladium membrane and is one of the less economic options. [47]

Other metals have been alloyed with palladium although outside of these three metals, studies evaluating the impurity resistance of other binary alloys are rare. The adsorption of CO on Pd₉₂Y₈ membranes under various concentrations has been studied using TDS and XPS and found that CO can react with the Pd-Y allow at 623K, forming YO and solid carbon. [48] Bryden et al studied the poisoning resistance of nanostructured palladium-iron alloys compared to polycrystalline membranes of the same composition. [49] They found that nanostructured membranes not only display higher fluxes, but also exhibit a higher resistance to hydrogen sulphide poisoning. When exposed to $\sim 60 \mu\text{mol mol}^{-1}$ of H₂S for 2.2 hours there was no permanent reduction in flux. Howard et al studied the performance of PdPt₂₀ membranes under 1000 $\mu\text{mol mol}^{-1}$ H₂S at temperatures between 350°C and 450 °C. [50] The alloy had decent performance on the lower end of the temperature, only losing about 5% of permanent permeability. At higher temperatures the membrane lost around 25% of its permeability, much of this attributed to platinum segregation to the surface of the membrane.[50] The impurity resistance of PdPt membranes has also been studied under common WGS compositions which concluded that small additions of Pt (Between 5-9%) can decrease the flux decline caused by WGS mixtures from 39% for pure Pd, to anywhere between 7%-22%. [50] Platinum however does not appear to be as effective at mitigating the effects of WGS mixtures as alloying with Au which can completely mitigate the flux decline. [51] The use of Pd₉₅Ru₅ membranes in syngas mixtures has been tested in WGS conditions and also showed good resistance to adsorbing compounds, losing only 6% of their flux compared to the 11% lost by a pure Pd membrane under the same conditions.[52]

Ternary alloys are a newly emerging field which aims at utilizing the strengths of a binary alloy while mitigating its weaknesses with another component. Research in this area has mainly focused on ternary alloys based on copper, gold and silver however there are theoretically infinite combinations possible. A Pd₈₀Au₁₀Pt₁₀ membrane manufactured through magnetron sputtering was found to be completely resistant to H₂S poisoning, recovering 100% of its flux prior to exposure to impurity containing gas streams. [53] However after long term testing, the purity of the permeate decreased which implies that pinholes had started to form on the membrane surface. [53] This is most likely due to segregation of the individual components, destabilising the structure. This was not confirmed in the papers analysis however. [53] The most in depth study of PdAgAu membranes under H₂S was performed by Braun et al, who studied the performance of Pd, Pd₉₀Ag₁₀, Pd₇₈Ag₉Au₁₃, Pd₇₅Ag₁₆Au₉, and Pd₉₁Au₉. While all the tested membranes saw a permanent permeability loss under 100 $\mu\text{mol mol}^{-1}$ of H₂S the Pd₉₁Au₉, Pd₇₈Ag₉Au₁₃, and Pd₇₅Ag₁₆Au₉ all resisted bulk corrosion as proven by Energy-dispersive X-ray spectroscopy (EDS), with the Pd₉₁Au₉ sample having the highest resistance to H₂S atmospheres. [54, 55] While this study shows that ternary alloys do offer an increase in impurity resistance over pure Pd and PdAg membranes, the original flux values are not provided so it is difficult to see if there are any inherent advantages over simply using a PdAu alloy. [54, 55] The Materials and Chemistry group at SINTEF have performed the most extensive study into ternary alloys, [56, 57]

testing by far the widest range of alloys and using a combination of X-ray Diffraction (XRD) and X-ray photoelectron spectroscopy to analyse the segregation behaviour of the ternary alloys. [56, 57] Through alloying PdCu alloys with a third transition metal they found that the addition of 1% of a transition metal component always resulted in an increase in permeability, likely due to a phenomenon where the activation energy for hydrogen permeation decreases with increasing fcc lattice constant. [58] In particular the addition of 1% Ta, 1% Y and 14% Ag resulted in an increase in permeability of 10, 45 and 65% respectively when compared with Pd₇₃Cu₂₇ membranes for Y and Ta, and Pd₆₅Cu₃₅ membranes for Ag additions. [58] In the follow up paper Pd₇₅Ag₂₂Au₃, Pd₇₆Ag₂₁Mo₃ and Pd₆₉Ag₂₇Y₄ membranes were exposed to 20 $\mu\text{mol mol}^{-1}$ of H₂S for 500 hours. The Pd₇₅Ag₂₂Au₃ membrane was the only membrane which showed no bulk sulphur formation, with the other two membrane compositions showing large levels of oxidation and segregation when analysed using XPS. [59] The PdAgAu composition has been further studied by Braun et al, [55] who backed up that small additions of Au to PdAg membranes can reduce the membranes reactivity with sulphides and would be suitable for application in a hydrogen impurity enrichment device. Tarditi et al, have done a similar study on the impurity resistance of PdCuAu membranes. [60] While XRD and EDS of this alloy showed no formation of bulk sulphides, the XPS depth profile showed low, but measurable levels of sulphur showing that this composition has some reactivity with impurities. [60]

Table 2.4: Review of palladium alloys and their interactions with impurities

Membrane composition	Support	Susceptability to poisoning compounds				Pressure (bar)	Permeability $molm^{-1}s^{-1}pa^{-\frac{1}{2}}$	Temperature °C	Fabrication technique	Membrane thickness (μm)	Ref	
		Compound concentration	Exposure time	Percentage flux drop	Flux Recovery							
PdAg ₂₃	PSS/Al ₂ O ₃	19.2% CO ₂ , 15.4% H ₂ O, 4% CO, 1.2% CH ₄ 40.5% CO ₂ ,	500h	88.36%	-	990 $cm^3cm^{-2}min^{-1}$	26	2.42×10^{-9}	400	Magnetron Sputtering	2.2	[61]
PdAg ₂₃	PSS/Al ₂ O ₃	25% H ₂ O, 2% CO, 2.5% CH ₄ 60% CO ₂ ,	500h	94.65%	-	990 $cm^3cm^{-2}min^{-1}$	26	2.42×10^{-9}	400	Magnetron Sputtering	2.2	[61]
PdAg ₂₃	PSS/Al ₂ O ₃	25.5% H ₂ O, 2% CO, 2.5% CH ₄	500h	94.65%	-	990 $cm^3cm^{-2}min^{-1}$	26	2.42×10^{-9}	400	Magnetron Sputtering	2.2	[61]
Pd	Self-supported	1000 ppm H ₂ S	6h	90%	-	14 $cm^3cm^{-2}min^{-1}$	3.1	1.2×10^{-8}	350	-	25	[42]
PdCu ₅₃	Self-supported	1000 ppm H ₂ S	6h	90%	-	14 $cm^3cm^{-2}min^{-1}$	3.1	1.3×10^{-8}	350	-	25	[42]
Pd	PSS/Al ₂ O ₃	54.8 ppm H ₂ S	24h	93%	0%	-	2.02	-	400	ELP	10.3	[44]
PdAu ₈	PSS/Al ₂ O ₃	54.8 ppm H ₂ S	24h	85%	54%	-	2.02	-	400	ELP/Electroplating	16	[44]
PdAg ₂₃	PSS	2 ppm H ₂ S	10 minutes	7%	100%	66.7 $cm^3cm^{-2}min^{-1}$	-	1.9×10^{-8}	450	Magnetron Sputtering	10	[62]
PdAg ₂₃	PSS	5 ppm H ₂ S	10 minutes	29%	100%	66.7 $cm^3cm^{-2}min^{-1}$	-	1.9×10^{-8}	450	Magnetron Sputtering	10	[62]
PdAg ₂₃	PSS	2-5-2 ppm H ₂ S	10 minutes at 5ppm	25%	99.4%	51.5 $cm^3cm^{-2}min^{-1}$	-	1.9×10^{-8}	450	Magnetron Sputtering	10	[62]
PdAg ₂₃	PSS	2-6.6-2 ppm H ₂ S	10 minutes at 6.6ppm	25%	36%	51.2 $cm^3cm^{-2}min^{-1}$	-	1.9×10^{-8}	450	Magnetron Sputtering	10	[62]
PdAg ₂₃	PSS	2-10-2 ppm H ₂ S	10 minutes at 10ppm	83%	99.6%	51.2 $cm^3cm^{-2}min^{-1}$	-	1.9×10^{-8}	450	Magnetron Sputtering	10	[62]
PdAg ₂₃	PSS	2-20-2 ppm H ₂ S	10 minutes at 20ppm	85%	100%	51.0 $cm^3cm^{-2}min^{-1}$	-	1.9×10^{-8}	450	Magnetron Sputtering	10	[62]
PdAg ₂₃	PSS	5-20-5 ppm H ₂ S	10 minutes at 6.6ppm	71%	17.99%	18.9 $cm^3cm^{-2}min^{-1}$	-	1.9×10^{-8}	450	Magnetron Sputtering	10	[62]
Pd	PSS/Al ₂ O ₃	111.8% CO ₂ , 5.3% H ₂ O, 14.2% CO, 1.7% CH ₄ 51% N ₂	48h	11%	-	-	0.1	-	350	ELP	6.5	[63]

Pd	PSS/Al ₂ O ₃	11.8% CO ₂ , 5.3% H ₂ O, 14.2% CO, 1.7% CH ₄ 51% N ₂ 120 mg/m ³ tar	24h	66.7%	-	-	0.1	-	350	ELP	6.5	[63]
Pd	PSS/Al ₂ O ₃	11.8% CO ₂ , 5.3% H ₂ O, 14.2% CO, 1.7% CH ₄ 51% N ₂ 240 mg/m ³ tar	24h	100%	-	-	0.1	-	350	ELP	6.5	[63]
PdRu ₅	PSS	11.8% CO ₂ , 5.3% H ₂ O, 14.2% CO, 1.7% CH ₄ 51% N ₂	48h	6%	-	-	0.1	-	350	ELP	7.3	[63]
PdRu ₅	PSS	11.8% CO ₂ , 5.3% H ₂ O, 14.2% CO, 1.7% CH ₄ 51% N ₂ 120 mg/m ³ tar	24h	66.7%	-	-	0.1	-	350	ELP	7.3	[63]
PdRu ₅	PSS	11.8% CO ₂ , 5.3% H ₂ O, 14.2% CO, 1.7% CH ₄ 51% N ₂ 240 mg/m ³ tar	24h	93%	-	-	0.1	-	350	ELP	7.3	[63]
Pd	YSZ	50% NH ₃	75h	0%	-	0.056.0 mol m ⁻² s ⁻¹	2-7	-	400	ELP	1.6	[64]
PdAg ₂₅	PSS	0.5%CO	Until stable	80%	-	-	-	-	400	-	100	[65]
PdAg ₂₅	PSS	0.5%CO	Until stable	4%	-	-	-	-	573	-	100	[65]
PdAg ₂₅	PSS	0.5%CO	Until stable	0%	-	-	-	-	773	-	100	[65]
PdAg ₂₅	PSS	1.5%CO	Until stable	91%	-	-	-	-	400	-	100	[65]
PdAg ₂₅	PSS	1.5%CO	Until stable	7%	-	-	-	-	573	-	100	[65]
PdAg ₂₅	PSS	1.5%CO	Until stable	0%	-	-	-	-	773	-	100	[65]
PdAg ₂₅	PSS	10%CO	Until stable	98%	-	-	-	-	400	-	100	[65]
PdAg ₂₅	PSS	10%CO	Until stable	50%	-	-	-	-	573	-	100	[65]
PdAg ₂₅	PSS	10%CO	Until stable	0%	-	-	-	-	773	-	100	[65]
PdAg ₂₅	PSS	20%CO	Until stable	99.8%	-	-	-	-	400	-	100	[65]
PdAg ₂₅	PSS	20%CO	Until stable	50.5%	-	-	-	-	573	-	100	[65]
PdAg ₂₅	PSS	20%CO	Until stable	0%	-	-	-	-	773	-	100	[65]
Pd	PSS	0.1%H ₂ S	120h	75%	-	8.5cm ³ cm ⁻² min ⁻¹	-	4 × 10 ⁻⁸	350	-	100	[66]
Pd	PSS	0.1%H ₂ S	120h	82%	-	13.5cm ³ cm ⁻² min ⁻¹	-	4 × 10 ⁻⁸	450	-	100	[66]

Pd	PSS	0.1% H ₂ S 12% CO, 12% N ₂	120h	81%	-	27.5 cm ³ cm ⁻² min ⁻¹	-	4 × 10 ⁻⁸	550	-	100	[66]
Pd	PSS	1.6% Steam, 1.6% N ₂	Until stable	22%	-	8.5 cm ³ cm ⁻² min ⁻¹	3	-	380	ELP	10	[67]
Pd	PSS	20 ppm H ₂ S, 40% N ₂	Until stable	17%	-	12.87 cm ³ cm ⁻² min ⁻¹	3	-	380	ELP	10	[67]
Pd	-	10 ppm H ₂ S, 20% N ₂	115h	71.88%	-	-	31	1.5 × 10 ⁻⁸	320	-	100	[37]
PdAg ₂₅	-	20 ppm H ₂ S, 40% N ₂	65h	100%	-	27.5 cm ³ cm ⁻² min ⁻¹	31	1.4 × 10 ⁻⁸	320	-	130	[37]
PdCu ₂₀	-	20 ppm H ₂ S, 40% N ₂	90h	22%	-	-	31	-	320	-	130	[37]
PdCu ₈	PSS	42.7 ppm H ₂ S	2.5h	82%	86.67%	-	2	-	450	ELP	14	[68]
PdAg ₂₇	-	4.4 ppm H ₂ S	48h	99%	67%	3.7 cm ³ cm ⁻² min ⁻¹	5.17	-	350	-	920	[45]
PdCu ₄₀	-	4.5 ppm H ₂ S	72h	95%	100%	2.9 cm ³ cm ⁻² min ⁻¹	5.17	-	350	-	1030	[45]
PdAu ₄₀	-	4.7 ppm H ₂ S	72h	9.4%	120%	0.99 cm ³ cm ⁻² min ⁻¹	5.17	-	350	-	820	[45]
Pd	-	4.7 ppm H ₂ S	96h	70.1%	10%	1.8 cm ³ cm ⁻² min ⁻¹	5.17	-	350	-	900	[45]
PdAu ₄₀	-	20.6 ppm H ₂ S	168h	56.6%	120%	0.99 cm ³ cm ⁻² min ⁻¹	5.17	-	350	-	790	[45]
PdAu ₄₀	-	6.6% H ₂ S	6h	99%	120%	0.99 cm ³ cm ⁻² min ⁻¹	5.17	-	350	-	810	[45]
PdFe ₆	PSS	59.1 ppm H ₂ S	2.2h	75%	100%	8.8 cm ³ cm ⁻² min ⁻¹	1	-	200	Electroplating	10	[49]
PdFe ₆	PSS	59.1 ppm H ₂ S	2.2h	95%	100%	6.4 cm ³ cm ⁻² min ⁻¹	1	-	200	Electroplating	10	[49]
PdFe ₅	PSS	1% CO	4.2h	83.3%	-	5.5 cm ³ cm ⁻² min ⁻¹	1	-	200	Electroplating	18	[49]
PdFe ₅	PSS	1% CO	4.2h	79%	-	3.9 cm ³ cm ⁻² min ⁻¹	1	-	200	Electroplating	18	[49]
PdCu ₄	Accusep	20% CO ₂ , 8% CO	2h	17%	-	5.85 cm ³ cm ⁻² min ⁻¹	1.38	-	350	-	7	[46]
PdAu ₁₃	Accusep	26% CO ₂ , 21% H ₂ O, 2% CO	13h	0%	-	35.56 cm ³ cm ⁻² min ⁻¹	4.96	-	350	-	7	[46]
PdCu ₄	Accusep	50 ppm H ₂ S 26% CO ₂ , 21% H ₂ O, 2% CO	2h	70%	100%	5.85 cm ³ cm ⁻² min ⁻¹	4.96	-	350	-	7	[46]
PdAu ₁₃	Accusep	50 ppm H ₂ S 26% CO ₂ , 21% H ₂ O, 2% CO	2h	0%	-	35.56 cm ³ cm ⁻² min ⁻¹	4.96	-	350	-	7	[46]
PdAu ₁₀	Self-supported	30% CO ₂ , 19% H ₂ O, 1% CO	43h	32%	-	0.28 molm ⁻² s ⁻¹	12.7	-	400	Magnetron Sputtering	-	[53]
PdAu ₁₀	Self-supported	30% CO ₂ , 19% H ₂ O, 1% CO 20ppm H ₂ S	100h	70%	-	0.28 molm ⁻² s ⁻¹	12.7	-	400	Magnetron Sputtering	-	[53]

PdAu ₂₀ Pt ₁₀	Self-supported	30% CO ₂ , 19% H ₂ O, 1% CO	43h	30%	-	0.212 mol m ⁻² s ⁻¹	12.7	-	400	Magnetron Sputtering	-	[53]
PdAu ₂₀ Pt ₁₀	Self-supported	30% CO ₂ , 19% H ₂ O, 1% CO 20 ppm H ₂ S	100h	100%	-	0.28 mol m ⁻² s ⁻¹	12.7	-	400		33	[53]
PdAu _{10.2}	PSS	30% CO ₂ , 19% H ₂ O, 1% CO	350h	36%	-	0.21 mol m ⁻² s ⁻¹	6.27	-	400	Cold working	25	[51]
PdAu _{10.2}	PSS	30% CO ₂ , 19% H ₂ O, 1% CO 20 ppm H ₂ S	350h	72%	-	0.21 mol m ⁻² s ⁻¹	6.27	-	400	Cold working	25	[51]
PdAu ₁₉	PSS	30% CO ₂ , 19% H ₂ O, 1% CO	350h	0%	-	0.25 mol m ⁻² s ⁻¹	6.27	-	400	Cold working	25	[51]
PdAu ₁₉	PSS	30% CO ₂ , 19% H ₂ O, 1% CO 20 ppm H ₂ S	350h	0%	-	0.25 mol m ⁻² s ⁻¹	6.27	-	400	Cold working	25	[51]
PdAu ₇	PSS	30% CO ₂ , 19% H ₂ O, 1% CO	350h	32%	-	0.47 mol m ⁻² s ⁻¹	6.27	-	400	Cold working	11	[51]
PdAu ₇	PSS	30% CO ₂ , 19% H ₂ O, 1% CO 20 ppm H ₂ S	350h	68%	-	0.47 mol m ⁻² s ⁻¹	6.27	-	400	Cold working	11	[51]
PdAu _{10.1}	PSS	30% CO ₂ , 19% H ₂ O, 1% CO	350h	24%	-	0.36 mol m ⁻² s ⁻¹	6.27	-	400	Cold working	31	[51]
PdAu _{10.1}	PSS	30% CO ₂ , 19% H ₂ O, 1% CO 20 ppm H ₂ S	350h	62%	-	0.36 mol m ⁻² s ⁻¹	6.27	-	400	Cold working	31	[51]
PdAg ₁₀	ZrO ₃ /PSS	100 ppm H ₂ S	24h	85%	16%	-	-	1.21×10 ⁻⁸	400	ELP	-	[55]
PdAg ₁₆ Au ₉	ZrO ₃ /PSS	100 ppm H ₂ S	24h	75.7%	33%	-	-	1.65×10 ⁻⁸	400	ELP	-	[55]
PdAg ₉ Au ₁₃	ZrO ₃ /PSS	100 ppm H ₂ S	24h	73%	64.5%	-	-	1.18×10 ⁻⁸	400	ELP	-	[55]
PdAu ₉	ZrO ₃ /PSS	100 ppm H ₂ S	24h	66.67%	81%	-	-	1.34×10 ⁻⁸	400	ELP	-	[55]
PdAg ₂₃	Micro channel stainless steel	10% N ₂ , 20 ppm H ₂ S	1h	97.5%	67.5%	170 cm ³ cm ⁻² min ⁻¹	-	1.3×10 ⁻⁸	450	Magnetron Sputtering	2.2	[57]
PdAg ₂₂ Au ₃	Micro channel stainless steel	10% N ₂ , 20 ppm H ₂ S	1h	87.5%	80%	145 cm ³ cm ⁻² min ⁻¹	-	9.3×10 ⁻⁹	450	Magnetron Sputtering	1.9	[57]

PdAg ₂₇ Y ₄	Micro channel stainless steel	10% N ₂ , 20 ppm H ₂ S	1h	92.5%	65%	140 cm ³ cm ⁻² min ⁻¹	-	1.3×10 ⁻⁸	450	Magnetron Sputtering	2.4	[57]
PdAg ₂₁ Mo ₃	Micro channel stainless steel	10% N ₂ , 20 ppm H ₂ S	1h	97.5%	98%	75 cm ³ cm ⁻² min ⁻¹	-	5.8×10 ⁻⁸	450	Magnetron Sputtering	2.3	[57]
PdAg ₁₁ Mo ₄	Micro channel stainless steel	10% N ₂ , 20 ppm H ₂ S	1h	97.5%	96%	125 cm ³ cm ⁻² min ⁻¹	-	8.8×10 ⁻⁸	450	Magnetron Sputtering	2.2	[57]
PdAg ₂ Au ₁₅	Al ₂ O ₃ /PSS	1000 ppm H ₂ S	30h	-	-	-	-	1.3×10 ⁻⁸	350	ELP	-	[54]
PdAg ₁₄ Au ₁₂	Al ₂ O ₃ /PSS Pd PSS	1000 ppm H ₂ S	30h	-	-	-	-	-	350	ELP	-	[54]
PdCu ₆₅	ZrO ₂ /PSS	Varying	Varying	-	-	-	-	-	450	ELP	10	[43]
PdCu ₇₃	ZrO ₂ /PSS	Varying	Varying	-	-	-	-	-	450	ELP	8	[43]
Pd	ZrO ₂ /PSS	Varying	Varying	-	-	-	-	-	450	ELP	4	[43]
Pd	ZrO ₂ /PSS	Varying	Varying	-	-	-	-	-	450	ELP	3	[43]
PdCu ₃₂	ZrO ₂ /PSS	Varying	Varying	-	-	-	-	-	450	ELP	2	[43]
PdCu ₂₀	ZrO ₂ /PSS	Varying	Varying	-	-	-	-	-	450	ELP	3	[43]
PdCu ₄₀	ZrO ₂ /PSS	Varying	Varying	-	-	-	-	-	450	ELP	15	[43]
PdCu ₄₀	ZrO ₂ /PSS	Varying	Varying	-	-	-	-	-	450	Cast rolled	25	[43]
PdPt ₂₀	Self-supported	1000 ppm H ₂ S	150h	50%	95%	1.85 mLcm ⁻² min ⁻¹	6.2	-	350	Metalurgical	100	[50]
PdPt ₂₀	Self-supported	1000 ppm H ₂ S	125h	80%	75%	2.95 mLcm ⁻² min ⁻¹	6.2	-	400	Metalurgical	100	[50]
PdPt ₂₀	Self-supported	1000 ppm H ₂ S	125h	25%	75%	3.55 mLcm ⁻² min ⁻¹	6.2	-	450	Metalurgical	100	[50]
PdY ₈	-	2-26% CO SO ₂	-	-	-	-	0.06	-	Varying	-	-	[48]
Pd	-	CS ₂ H ₂ S	-	-	-	-	0.07 mBar	-	Varying	-	-	[69]
PdCu ₂₀	Inconel	1000 ppm H ₂ S	-	-	-	-	-	-	Varying	Vacuum arc welding	100	[70]
PdCu ₄₀	Inconel	1000 ppm H ₂ S	-	-	-	-	-	-	Varying	Vacuum arc welding	100	[70]
PdCu ₄₇	Inconel	1000 ppm H ₂ S	-	-	-	-	-	-	Varying	Vacuum arc welding	100	[70]
Pd	PSS	100 ppm H ₂ S	24h	36%	80%	0.0475 molm ⁻² s ⁻¹	0.5	1.2 × 10 ⁻⁸	400	ELP	4	[71]
PdAu ₉	PSS	100 ppm H ₂ S	24h	59%	75%	0.05 molm ⁻² s ⁻¹	0.5	9.9 × 10 ⁻⁹	400	ELP	4	[71]
PdCu ₂₅ Au ₅	PSS	100 ppm H ₂ S	24h	50%	74%	0.01 molm ⁻² s ⁻¹	0.5	1.9 × 10 ⁻⁹	400	ELP	4	[71]
PdCu ₃₇ Au ₃	PSS	100 ppm H ₂ S	24h	54%	70%	0.015 molm ⁻² s ⁻¹	0.5	2.9 × 10 ⁻⁹	400	ELP	4	[71]
PdAu ₂₃	Accusep	20 ppm H ₂ S	96h	29%	97%	1.4 molm ⁻² s ⁻¹	11	1.55 × 10 ⁻⁸	500	ELP	4.8	[72]
PdAu ₂₀ Ag ₁₃	Accusep	20 ppm H ₂ S	96h	50%	89%	0.9 molm ⁻² s ⁻¹	11	1.65 × 10 ⁻⁸	500	ELP	9.3	[72]

Non-palladium

Due to the high cost of palladium there is a particular interest to use alternative materials which still give the high selectivity intrinsic to dense metallic membranes, while reducing the cost, for example, by switching to a cheaper, non-platinum group metal. Non-palladium alloy membranes in the form of amorphous, or crystalline structures generally attract the most research interest.

Crystalline non-palladium membranes are generally based on Group IV based alloys and follow a similar philosophy to the previously discussed palladium membranes. Group IV metals are alloyed with other metals in order to improve their physical properties while maintaining the bcc structure essential for the material to transport hydrogen. Crystalline metals typically have the same advantages and disadvantages as palladium membranes. Recent research activity has focused mainly on studying how the size of the grain boundary affects the permeability of such a membrane, an area which has been mostly neglected in palladium research. [25] This is likely due to the fact that many of these alloys are manufactured through cold work where the grain size can be more easily tailored than in the traditional electroless and sputtering methods used to manufacture palladium membranes. A key aspect of crystalline alloy research is the effect of nano-crystalline structures. Most research in this area has revolved around the addition of small amounts of elements to alloys based on either Zr or Hf to tailor these nano-crystalline structures and study their effects on permeability. Similarly to palladium alloys, dopants are generally chosen based on their effectiveness at suppressing hydride formation, with Zr, Mo, Ru and Rh being popular choices. [73, 74, 75, 76, 77] Alloying in this context would also likely be useful in reducing the membranes interaction with impurities through surface contamination. However this has not been touched upon much in research outside of palladium. The largest drawback to this technology is that crystalline alloys often do not show the catalytic activity necessary for dissociation of hydrogen. This requires an additional coating of palladium to be applied to the surface in order for the material to be viable for hydrogen separation. Interestingly when this was done with some commonly used industrial alloys [78] it was found that they showed reasonable hydrogen permeability which further highlights the importance of catalytic dissociation of hydrogen. Crystalline membranes are also mechanically weak and still susceptible to hydrogen embrittlement through hydride formation in a similar manner to palladium membranes. [25]

On the other hand amorphous metal membranes are generally seen as more attractive than crystalline membranes and are often reported to have greater mechanical strength and hydrogen solubility properties than crystalline structures due to their amorphous structure giving them a more open lattice. Unlike crystalline structures, amorphous metallic membranes can also have high catalytic activity towards hydrogen dissociation which reduces the need for an additional layer to induce this catalytic activity. This property is highly composition dependent and is typically shown by Nickel containing alloys. [79] For example $Zr_{36}Ni_{64}$ in its pure form due to the presence of nickel which is catalytically active for hydrogen dissociation, however when researchers started to dope the material with Ti or Hf, the catalytic properties of the material was drastically

reduced and required a layer of palladium in order to induce permeability.

Amorphous membranes still show some tendency towards hydrogen embrittlement however this is less prevalent than the crystalline alloys previously discussed. This is due to the differences in mechanisms of hydrogen embrittlement between the two classes of materials. Amorphous alloys do not show the α - β phase transition which is the main suspect of embrittlement in crystalline structures [79] and the embrittlement effect is instead due to the filling of free volume within the amorphous structure.

The main disadvantage of amorphous alloys is that given sufficient energy amorphous metallic membranes may crystallise, drastically changing their structure. This has been reported when the material is heated to high temperatures above 500°C. [79] This limits the application of amorphous alloys to low-temperatures however if the material is intended to be used at 300°C, like most palladium membranes, and the material shows a high enough permeability, then this would likely not be an issue.

Judging from the current research landscape on non-palladium membranes, the technology is still in its infancy, with most studies focusing on the fundamental properties of these alloys and with little focus on the practical applications of the technology. Non-palladium dense metal membranes are promising due to the drastic reduction in material cost with, in many cases, an increase in permeability. Of these technologies amorphous membranes appear to be the most appealing, in particular compositions such as Zr₃₆Ni₆₄ which require no precious metals to induce catalytic activity. This has the great advantage of reducing cost of the module and bringing dense metallic membranes, and their high associated selectivity, to a wider market by taking advantage of already established industrial production of amorphous alloys. Further practical research must be performed on these membrane compositions, in particular impurity interactions, thermal stability, and long-term stability to bring this technology to market.

Table 2.5: Hydrogen permeable non-palladium metallic membranes

Membrane composition	Structure	Catalytic coating	Feed pressure	Permeability mol m ² m s	temperature OC	Membrane thickness (um)	Ref
(Ni _{0.6} Nb _{0.4}) ₇₀ Zr ₃₀	Amorphous	Pd	7	1.8×10 ⁻⁸	400	40	[80]
(Ni _{0.6} Nb _{0.4}) ₆₀ Zr ₄₀	Amorphous	Pd	7	6×10 ⁻⁹	400	40	[80]
Ni ₆₅ Nb ₂₅ Zr ₁₀	Amorphous	Pd	7	5 ×10 ⁻⁹	400	40	[80]
Ni ₄₅ Nb ₄₅ Zr ₁₀	Amorphous	Pd	7	3 ×10 ⁻⁹	400	40	[80]
Ni ₆₀ Nb ₄₀	Amorphous	Pd	7	2 ×10 ⁻⁹	400	40	[80]
Ni ₄₄ Nb ₄₃ Zr ₁₀ Pd ₃	Amorphous	Pd	7	1×10 ⁻⁹	400	40	[80]
Zr ₃₆ Ni ₆₄	Amorphous	None	1	1.2×10 ⁻⁹	350	30	[81]
(Ni _{0.6} Nb _{0.4}) ₄₅ Zr ₅₀ Al ₅	Amorphous	Pd	3	1.9 ×10 ⁻⁸	400	50	[82]
(Ni _{0.6} Nb _{0.4}) ₄₅ Zr ₅₀ Co ₅	Amorphous	Pd	3	2.46 ×10 ⁻⁸	400	50	[82]
(Ni _{0.6} Nb _{0.4}) ₄₅ Zr ₅₀ Cu ₅	Amorphous	Pd	3	2.34 ×10 ⁻⁸	400	50	[82]
(Ni _{0.6} Nb _{0.4}) ₄₅ Zr ₅₀ Pd ₅	Amorphous	Pd	3	1.36 ×10 ⁻⁸	400	50	[82]
V ₈₅ Ni ₁₅	Crystalline	Pd	0.8	5 ×10 ⁻⁸	300	300-400	[83]
V ₉₅ Ni ₁₅	Crystalline	Pd	0.1-2.0	4 ×10 ⁻⁷	400	2000	[84]
V ₈₅ Ni _{14.91} Al _{0.09}	Crystalline	Pd	0.1-2.0	4.5 ×10 ⁻⁷	400	2000	[84]
V ₈₅ Ni _{14.1} Al _{0.9}	Crystalline	Pd	0.1-2.0	4.5 ×10 ⁻⁷	400	2000	[84]
V ₈₅ Ni _{12.4} Al _{2.6}	Crystalline	Pd	0.1-2.0	6 ×10 ⁻⁷	400	2000	[84]
V ₈₅ Ni _{10.5} Al _{4.5}	Crystalline	Pd	0.1-2.0	7 ×10 ⁻⁷	400	2000	[84]
V ₉₀ Al ₁₀	Crystalline	Pd	0.2 – 2.0	2 ×10 ⁻⁷	900	800-2300	[85]
V ₇₀ Al ₃₀	Crystalline	Pd	0.2 – 2.0	1.8 ×10 ⁻⁹	700	800-2300	[85]
INCOLOY903	Crystalline	Pd	1	1.33 ×10 ⁻⁷	430	200	[78]

WASPALOY	Crystalline	Pd	1	2.99×10^{-7}	430	200	[78]
JBK-75	Crystalline	Pd	1	4.36×10^{-7}	430	200	[78]
GH85A	Crystalline	Pd	1	2.73×10^{-7}	430	200	[78]
INCOLOY907	Crystalline	Pd	1	9.67×10^{-8}	430	200	[78]
INCONEL718	Crystalline	Pd	1	2.22×10^{-7}	430	200	[78]
GH761	Crystalline	Pd	1	1.5×10^{-7}	430	200	[78]
<i>Nb₂₀Zr₃₅Ni₃₅</i>	Crystalline	Pd	1	2.73×10^{-8}	400	500-700	[86]
<i>Nb₁₀Zr₄₅Ni₄₅</i>	Crystalline	Pd	1	2.5×10^{-8}	400	500-700	[86]
<i>Nb₂₉Ti₃₁Ni₄₀</i>	Crystalline	Pd	2	7×10^{-9}	400	550-750	[87]
Nb17Ti42Ni41	Crystalline	Pd	2	0.6×10^{-8}	400	550-750	[87]
Nb10Ti50Ni40	Crystalline	Pd	2	4.5×10^{-9}	400	550-750	[87]
Nb39Ti31Ni30	Crystalline	Pd	2	2.0×10^{-8}	400	550-750	[87]
Nb28Ti42Ni30	Crystalline	Pd	2	1×10^{-8}	400	550-750	[87]
Nb21Ti50Ni29	Crystalline	Pd	2	1×10^{-8}	400	550-750	[87]
<i>Ta₉₅W₅</i>	Crystalline	None	1.4	$52 \text{ mol m}^{-2} \text{s}^{-1}$	500	650	[88]

Dense Ceramic

Dense ceramic membranes operate in a similar manner to metallic membranes, with the key difference being that they are made from ion conducting ceramics rather than metals. Dense ceramic membranes have a selectivity comparable to dense metal membranes since they only allow hydrogen to permeate, however at a lower cost than Pd-based membranes. Unlike dense metallic membranes, most ion conducting materials claim to be intrinsically inert to common hydrogen impurities and hence are stable in CO, CO₂ and H₂S containing atmospheres. [25] The major drawback to ion conducting ceramic membranes is that generally high temperatures are required to achieve any form of H₂ flux. While palladium membranes can achieve a high flux at temperatures between 300-400°C, most Perovskite membranes require temperatures between 700-900°C and generally only achieve a hydrogen permeability $\pm 10\%$ compared to a palladium membrane of the same thickness.

The hydrogen separation process in a dense ceramic membrane is near identical to that which occurs in a dense metal membrane with the main driving forces being the pressure and concentration gradients. This is primarily controlled by the catalytic surface effects and bulk diffusion rather than thickness due to ceramic materials intrinsically low catalytic activity for such a process. For practical purposes both sides of the membrane should have sufficient catalytic activity to dissociate hydrogen atoms and the bulk should have high enough proton and electron conductivities to ensure a reasonably high flux can be achieved. More information on the precise mechanism behind proton conducting membranes can be found in the following reviews [89, 90]. The bulk diffusion of a dense ceramic membrane can be described through the Wagner equation written as Eq 2.18

$$J_{H_2} = \frac{RT}{4F^2L} \frac{\theta_H \theta_e}{\theta_H + \theta_e} \ln \left(\frac{P'_{H_2}}{P''_{H_2}} \right) \quad (2.18)$$

Dense ceramic membranes can be split into two broad categories; single phase ceramic membranes are composed of a single material which has the ability to conduct both protons and electrons, and multi-phase ceramic membranes which are normally composed of two or more phases which when combined show proton and electron conductivity. The most common type of multi-phase ceramic membranes is known as ‘cermet’ which combines a proton conducting ceramic and a metal, such as palladium or nickel, as the electron conducting phase.

Single phase ceramic membranes must be given proton conductivity by doping a single phase ceramic material (typically perovskite) in order to create a proton hole within the material. This combined with catalytic dissociation of hydrogen on the surface allows uptake of a certain number of protons, which then diffuse through the material using the proton holes within the material. [89, 90]

Extensive efforts have been placed into developing proton-electron conducting ceramic materials for hydrogen separation however there are still many technical hurdles which must be overcome before the technology can be applied on a useful scale. The

main problem holding back the technology is the incredibly low flux values reported despite operating at such high temperatures. Until this is solved there will be no point in using the technology over faster porous materials, or even dense metal membranes which offer the same selectivity's, at much faster permeation rates. This stems back to a lack of understanding behind the surface kinetics of hydrogen dissociation (which is also an issue for non-palladium dense membranes). Despite claims that ceramic membranes are inert to impurities there is contradictory evidence showing that the materials cannot withstand acidic conditions and degrade under atmospheres containing CO₂ and H²S. Finally, since such high temperatures are required there will be difficulties forming a hermetic seal with ceramic membranes which can withstand the high temperature environments. This is already an issue with ceramic supported metallic membranes which operate at much more mild conditions.

From this it can be concluded that dense ceramic membranes for hydrogen separation are still at a research level and a better understanding of the material science behind the surface interactions with hydrogen and other gases, along with research into new classes of ceramics which can either permeate hydrogen at faster rates, at lower temperatures, or both are key to bringing this technology to market.

Table 2.6: Hydrogen permeable ceramic and cermet membranes which show resistance to common hydrogen impurities

Material	Class	Feed	Temperature °C	Flux	Thickness (um)	Stability	Notes	Ref
$SrCe_{0.75}Zr_{0.2}Tm_{0.05}O_{3-\alpha}$	Perovskite	100 mLmin ⁻¹ 50% H ₂ + He	900	0.042 mLcm ⁻² min ⁻¹	1200	-	-	[91]
$Nd_{5.5}WO_{12-\alpha}$	Lanthanide tungstate	80% He + 20 % H ₂	1000	0	900	Stable under 115 ppm H ₂ S, 4.43% CO ₂ , 2.12% CO	No flux due to dry conditions	[92]
$La_{5.5}WO_{11.25}$	Lanthanide tungstate	80% He + 20 % H ₂	1000	< 0.005 mLmin ⁻¹ cm ⁻²	900	Stable in 15% CO ₂ for 3 days	Requires humidification for faster permeation	[93]
Nd_6Wo_{12}	Lanthanide tungstate	He + H ₂	1000	0.012 mLmin ⁻¹ cm ⁻²	510	Stable in CO ₂ and CH ₄ after 3 days	Humidified atmosphere	[94]
$La_{5.5}W_{0.8}Re_{0.2}O_{11.25-\alpha}$	Lanthanide tungstate	2.5% H ₂ , 2.5% H ₂ O, H ₂ balance	1000	0.095 mLmin ⁻¹ cm ⁻²	760	Stable in 5% CO ₂ 1000 ppm COS 100 ppm HCN 46% CO 46% H ₂ at 35 bar	Humidified atmosphere	[95]
$(La_{5/6}Nd_{1/6})_{5.5}WO_{12-\alpha}$	Lanthanide tungstate	80% He + 20 %H ₂	1000	0.005 mLmin ⁻¹ cm ⁻²	900	Stable in 15% CO ₂ for 3 days	Requires humidification	[96]
$La_{27}Mo_{1.5}W_{3.5}O_{55.5}$	Lanthanide tungstate	10% H ₂ 90% He	700	0.78×10^4 mLmin ⁻¹ cm ⁻²	650	-	-	[97]
$La_{27}Mo_{1.5}W_{3.5}O_{55.5}$	Lanthanide tungstate	10% H ₂ 90% He	700	0.78×10^4 mLmin ⁻¹ cm ⁻²	650	-	-	[97]
$Nd_{5.5}W_{0.5}Mo_{0.5}O_{11.25-\alpha}$	Lanthanide tungstate	50% H ₂ , 50% He	1000	0.235 mLcm ⁻² min ⁻¹	900	Stable in environments containing 330 ppm H ₂ S and 22% H ₂ in N ₂ . 480 ppm H ₂ S and 32% H ₂ in N ₂ . 705 ppm H ₂ S and 47% H ₂ in N ₂ 1500 ppm H ₂ S and H ₂ .	Values for humidified atmosphere. Stabilised flux value after 3 sets of tests Flux reduction due to Mo reduction	[98]
$Ni - Ba(Zr_{0.7}Pr_{0.1}Y0.2)O_{3-\alpha}$	Cermet	40% H ₂ , 57% N2, 3% H ₂ O	900	1.36×10^8 molcm ⁻² s ⁻¹	400	Stable under 30% CO ₂	Maximum value achieved for humid atmosphere	[99]
$Ni - Ba(Zr_{0.1}Ce_{0.7}Y_{0.2})O_{3-\alpha}$	Cermet	20% H ₂ , 77% N2, 3% H ₂ O	900	1.37×10^{-7} molcm ⁻² s ⁻¹	30	-	Maximum value achieved for humid atmosphere	[100]
$La_{27}W_5O_{55.5} - LaCrO_3$	Dual phase ceramic	50% H ₂ (humid)	700	0.384×10^{-3} mLcm ⁻² min ⁻¹	1210	-	Pt coating	[101]
$La_{5.5}WO_{11.25-\alpha} - La_{0.87}Sr_{0.13}CrO_{3-\alpha}$	Dual phase ceramic	50% H ₂ , 2.5%H ₂ O	700	0.15 mLcm ⁻² min ⁻¹	360	Stable in 15% CO ₂ after 24 hours.	No dry atmosphere testing	[102]
$Ni - La_{0.5}Ce_{0.5}O_{2-\alpha}$	Cermet	20% H ₂ , 80% N2	900	5.64×10^{-8} molcm ⁻² s ⁻¹	48	Stable in CO ₂	Flux increased in humidified conditions	[103]
$Ni - Ca_{0.0125}La_{0.4875}Ce_{0.5}O_{2-\alpha}$	Cermet	20% H ₂ , 77% N2, 3%H ₂ O	900	1.88×10^{-8} molcm ⁻² s ⁻¹	600	Stable in CO ₂	No dry atmosphere testing	[104]
$Ni - La_{0.5}Ce_{0.5}O_{2-\alpha}$	Cermet	20% H ₂ , 80% N2	900	1.57×10^{-8} molcm ⁻² s ⁻¹	600	Stable in CO ₂	No dry atmosphere testing	[104]

$Ni - La_{0.5}Ce_{0.5}O_{2-\alpha}$	Cermet	20% H ₂ , 80% N2	900	$2.87 \times 10^{-8} molcm^{-2}s^{-1}$	600	-	No dry atmosphere testing	[105]
$BaZr_{0.8}Y_{0.15}Mn_{0.05}O_{3-\alpha}$	Perovskite	50% H ₂ , 50% He	1000	$0.01 - 0.03 mLcm^{-2}min^{-1}$	900	-	No dry atmosphere, Pt coated	[96]
$SrCe_{0.75}Zr_{0.2}Tm_{0.05}O_{3-\alpha}$	Perovskite	10% H ₂ , 90% He	900	$0.025 mL(STP)cm^{-2}min^{-1}$	1600	Stable in 20% CO ₂ and 11.3% CO	-	[106]
$SrCe_{0.75}Zr_{0.2}Eu_{0.1}O_{3-\alpha}$	Perovskite	100% H ₂	900	$0.35 cm^3 cm^{-2}min^{-1}$	17	-	Flux improves in humid atmospheres	[107]
$Ni - BaCe_{0.7}Zr_{0.1}Y_{0.1}Yb_{0.1}O_{3-\alpha}$	Cermet	100% H ₂	700	$0.49 mLcm^{-2}min^{-1}$	44	-	-	[108]
$Ni - BaCe_{0.7}Zr_{0.1}Y_{0.1}Yb_{0.1}O_{3-\alpha}$	Cermet	100% H ₂	900	$1.12 mLcm^{-2}min^{-1}$	44	-	-	234
$BaCe_{0.7}Zr_{0.1}Y_{0.1}Yb_{0.1}O_{3-\alpha}$	Perovskite	50% H ₂ 50% He	1000	$0.422 molcm^{-2}s^{-1}$	-	-	Hollow fibre	[108]
$BaCe_{0.85}Tb_{0.05}Co_{0.1}O_{3-\alpha}$	Perovskite	50% H ₂ 50% He	1000	$0.385 mLcm^{-2}min^{-1}$	167	Unstable in H ₂	Hollow fibre. Also shows oxygen permeability	[109]
$Ni - BaCe_{0.7}Y_{0.1}Yb_{0.1}Zr_{0.1}O_{3-\alpha}$	Cermet	20% H ₂ , 20% CO ₂ , 60% N2	1000	$5.5 \times 10^{-8} molcm^{-2}s^{-1}$	44	Unstable in H ₂	Shows reverse WGS catalytic activity, Stable in 60% CO ₂ . CO causes Ni corrosion	[110, 111]
$BaCe_{0.8}Y_{0.2}O_{3-\alpha}$	Perovskite	25% H ₂ 75% He	1050	$0.38 mLcm^{-2}min^{-1}$	1000	Unstable in humid environments and CO ₂	Hollow Fibre	[112]
$La_{28-x}W_{4+x}O_{54+3x/2}(La = W \times 5.6)$	Lanthanum tungstate	10% H ₂ 90% Ar	925	$0.08 NmLcm^{-2}min^{-1}$	30	-	-	[113]
$La_{0.87}Sr_{0.13}CrO_{3-\alpha}$	Lanthanum tungstate	10% H ₂ , 2.5% H ₂ O 87.5% Ar	1000	$10 \times 10^{-4} mLcm^{-2}min^{-1}$	550	Chemically stable under tested conditions	-	[114]
$BaCe_{0.85}Tb_{0.05}Co_{0.1}O_{3-\alpha}$	Perovskite	50% H ₂ , 50% He	700-1000	$0.009 - 0.164 mL(STP)cm^{-2}min^{-1}$	132	-	Hollow fibre	[115]
$BaCe_{0.85}Tb_{0.05}Co_{0.1}O_{3-\alpha}$	Perovskite	50% H ₂ , 50% He	700-1000	$0.018 - 0.269 mL(STP)cm^{-2}min^{-1}$	132	-	Hollow fibre, Ni Coating	[115]
$BaCe_{0.85}Tb_{0.05}Co_{0.1}O_{3-\alpha}$	Perovskite	50% H ₂ , 50% He	700-1000	$0.1 - 0.42 mL(STP)cm^{-2}min^{-1}$	132	-	Hollow fibre, Pd Coating	[115]
$BaCe_{0.95}Tb_{0.05}O_{3-\alpha}$	Perovskite	50% H ₂ , 50% He	900	$0.272 mLcm^{-2}min^{-1}$	100	-	Hollow fibre, Pd Coating	[116]

Viable membrane materials and outlook

While ceramic membranes provide a viable alternative to metallic membranes as an impurity enrichment material, the technology is still in its infancy and the membranes do not show suitable permeabilities to perform impurity enrichment in a reasonable time frame. While many studies on these materials also claim that impurity resistance of these materials outclasses metallic membranes, there is little backing up these claims.

Of the membranes discussed, metallic membranes are the most suitable for hydrogen impurity enrichment. Palladium membranes are the only current material that has successfully been used for hydrogen impurity enrichment however there is still room for improvement which will be discussed in the following section. Non-palladium dense metallic membranes for hydrogen impurity enrichment are the next logical step in development of these membranes for analytical purposes due to their lower costs however more practical research on the materials must first be performed.

2.5.2 Membrane manufacture

Dense metal membranes can either be supported or unsupported. Unsupported membranes are free standing structures, which usually feature high wall thicknesses in order to achieve the required mechanical strength to withstand use in a process. As a result of this the flux seen through these membranes is typically low due to the high transport resistance of the membrane. Self-supported membranes are also typically expensive due to the large amount of materials required. [66]

A more efficient method is to use a support structure to allow a thinner membrane layer to be deposited, while achieving the mechanical strength required by use of another, cheaper material. This allows thinner membranes to be deposited, thereby increasing the achievable flux, and greatly reducing the cost of such a membrane.[56] Because of these clear advantages this thesis will explore the use of self-supported membranes.

Support selection

When selecting a support material there are a number of considerations which should be taken into account prior to deposition:

- Pore size distribution: the membrane performance can be affected by the pore structure and size distribution. If the membranes pore size distribution is too small then it will provide an added transfer resistance to permeation. On the opposite side however the minimum thickness of a membrane deposited on a porous support has been found to be 3x the size of the smallest pore, **Mardilovich et al.** [68] so there is a trade-off between these two values
- Support surface: Adhesion of the deposited membrane to the surface of the support is compromised if the support is too smooth
- Thermal stability: The thermal stability of a support material is defined by the melting temperature, coefficient of thermal expansion (CTE) and intermetallic

diffusion potential. If the CTE difference between the deposited membrane and the support is too large it will lead to a difference in the expansion rate which eventually leads to membrane failure. Intermetallic diffusion is defined as the migration of atoms between the membrane and the substrate which can negatively affect its permeability and lead to membrane failure in extreme cases

- Mechanical Stability
- Chemical stability

The thickness of the deposited membrane is largely a function of the morphological properties of the support. Of the materials available for use as a support; ceramics, porous stainless steel, and porous glass have been the most widely used.

2.6 Density functional theory for screening of membrane alloy compositions

2.7 Conclusion

References

- [1] Sangeetha Dharmalingam, Vaidhegi Kugarajah, and Moogambigai Sugumar. Chapter 1.7 - Membranes for Microbial Fuel Cells. In S Venkata Mohan, Sunita Varjani, and Ashok B T Microbial Electrochemical Technology Pandey, editors, *Biomass, Biofuels and Biochemicals*, pages 143–194. Elsevier, 2019. ISBN 978-0-444-64052-9. doi: <https://doi.org/10.1016/B978-0-444-64052-9.00007-8>. URL <http://www.sciencedirect.com/science/article/pii/B9780444640529000078>.
- [2] A Alaswad, A Palumbo, M Dassisti, A G B T Reference Module in Materials Science Olabi, and Materials Engineering. Fuel Cell Technologies, Applications, and State of the Art. A Reference Guide. Elsevier, 2016. ISBN 978-0-12-803581-8. doi: <https://doi.org/10.1016/B978-0-12-803581-8.04009-1>. URL <http://www.sciencedirect.com/science/article/pii/B9780128035818040091>.
- [3] Viral Mehta and Joyce Smith Cooper. Review and analysis of PEM fuel cell design and manufacturing. *Journal of Power Sources*, 114(1):32–53, 2003. ISSN 0378-7753. doi: [https://doi.org/10.1016/S0378-7753\(02\)00542-6](https://doi.org/10.1016/S0378-7753(02)00542-6). URL <http://www.sciencedirect.com/science/article/pii/S0378775302005426>.
- [4] Zhongliang Li, Zhixue Zheng, Liangfei Xu, and Xiaonan Lu. A review of the applications of fuel cells in microgrids: opportunities and challenges. *BMC Energy*, 1, dec 2019. doi: 10.1186/s42500-019-0008-3.
- [5] Klaus-Michael Mangold. Introduction to Hydrogen Technology. By Roman J. Press, K. S. V. Santhanam, Massoud J. Miri, Alla V. Bailey, and Gerald A. Takacs. *ChemSusChem*, 2(8):781, aug 2009. ISSN 1864-5631. doi: 10.1002/cssc.200900109. URL <https://doi.org/10.1002/cssc.200900109>.
- [6] J D Holladay, J Hu, D L King, and Y Wang. An overview of hydrogen production technologies. *Catalysis Today*, 139(4):244–260, 2009. ISSN 0920-5861. doi: <https://doi.org/10.1016/j.cattod.2008.08.039>. URL <http://www.sciencedirect.com/science/article/pii/S0920586108004100>.
- [7] International Energy Agency (IEA). Technology Roadmap Hydrogen and Fuel Cell. Technical report, IEA/OECD Paris., 2015.

- [8] N Muradov. 17 - Low-carbon production of hydrogen from fossil fuels. In Velu Subramani, Angelo Basile, and T Nejat B T Compendium of Hydrogen Energy Veziroğlu, editors, *Woodhead Publishing Series in Energy*, pages 489–522. Woodhead Publishing, Oxford, 2015. ISBN 978-1-78242-361-4. doi: <https://doi.org/10.1016/B978-1-78242-361-4.00017-0>. URL <http://www.sciencedirect.com/science/article/pii/B9781782423614000170>.
- [9] Shakeel Ahmed, Abdullah Aitani, Faizur Rahman, Ali Al-Dawood, and Fahad Al-Muhaish. Decomposition of hydrocarbons to hydrogen and carbon. *Applied Catalysis A: General*, 359(1):1–24, 2009. ISSN 0926-860X. doi: <https://doi.org/10.1016/j.apcata.2009.02.038>. URL <http://www.sciencedirect.com/science/article/pii/S0926860X09001719>.
- [10] Nazim Z Muradov and T Nejat Veziroğlu. “Green” path from fossil-based to hydrogen economy: An overview of carbon-neutral technologies. *International Journal of Hydrogen Energy*, 33(23):6804–6839, 2008. ISSN 0360-3199. doi: <https://doi.org/10.1016/j.ijhydene.2008.08.054>. URL <http://www.sciencedirect.com/science/article/pii/S036031990801118X>.
- [11] Canan Acar and Ibrahim Dincer. Comparative assessment of hydrogen production methods from renewable and non-renewable sources. *International Journal of Hydrogen Energy*, 39(1):1–12, 2014. ISSN 0360-3199. doi: <https://doi.org/10.1016/j.ijhydene.2013.10.060>. URL <http://www.sciencedirect.com/science/article/pii/S0360319913025330>.
- [12] C Koroneos, A Dompros, G Roumbas, and N Moussiopoulos. Life cycle assessment of hydrogen fuel production processes. *International Journal of Hydrogen Energy*, 29(14):1443–1450, 2004. ISSN 0360-3199. doi: <https://doi.org/10.1016/j.ijhydene.2004.01.016>. URL <http://www.sciencedirect.com/science/article/pii/S0360319904000655>.
- [13] Thomas Bacquart, Arul Murugan, Martine Carré, Bruno Gozlan, Fabien Auprêtre, Frédérique Haloua, and Thor A Aarhaug. Probability of occurrence of ISO 14687-2 contaminants in hydrogen: Principles and examples from steam methane reforming and electrolysis (water and chlor-alkali) production processes model. *International Journal of Hydrogen Energy*, 43(26):11872–11883, 2018. ISSN 0360-3199. doi: <https://doi.org/10.1016/j.ijhydene.2018.03.084>. URL <http://www.sciencedirect.com/science/article/pii/S0360319918308450>.
- [14] International Standard ISO 14687-2: 2012. Hydrogen Fuel - Product Specification, 2012.
- [15] Enrico Doná, Michael Cordin, Clemens Deisl, Erminald Bertel, Cesare Franchini, Rinaldo Zucca, and Josef Redinger. Halogen-Induced Corrosion of Platinum. *Journal of the American Chemical Society*, 131(8):2827–2829, mar 2009. ISSN 0002-7863. doi: 10.1021/ja809674n. URL <https://doi.org/10.1021/ja809674n>.

- [16] Shabbir Ahmed, Sheldon H D Lee, and Dionissios D Papadias. Analysis of trace impurities in hydrogen: Enrichment of impurities using a H₂ selective permeation membrane . *International Journal of Hydrogen Energy*, 35(22):12480–12490, 2010. doi: 10.1016/j.ijhydene.2010.08.042.
- [17] Arul Murugan and Andrew S Brown. Advancing the analysis of impurities in hydrogen by use of a novel tracer enrichment method. *Analytical Methods*, 6(15): 5472, 2014. doi: 10.1039/c3ay42174k.
- [18] Arul Murugan and Andrew S Brown. Review of purity analysis methods for performing quality assurance of fuel cell hydrogen. *International Journal of Hydrogen Energy*, 40(11):4219–4233, 2015. doi: 10.1016/j.ijhydene.2015.01.041.
- [19] Peter R Bossard, Jacques Mettes, Luis Breziner, and Emeritus Fred Gornick. New Sensor for Measuring Trace Impurities in Ultra Pure Hydrogen. *Power & Energy, USA*.
- [20] Jürgen Hille. Enrichment and mass spectrometric analysis of trace impurity concentrations in gases. *Journal of Chromatography A*, 502:265–274, 1990. ISSN 0021-9673. doi: [https://doi.org/10.1016/S0021-9673\(01\)89591-1](https://doi.org/10.1016/S0021-9673(01)89591-1). URL <http://www.sciencedirect.com/science/article/pii/S0021967301895911>.
- [21] A Volkov. Membrane Compaction. In Giorno L Drioli E., editor, *Encyclopædia of Membranes*. Springer, Berlin, Heidelberg, 2014.
- [22] A. Gugliuzza. Membrane Swelling. In Drioli E. and Giorno L., editors, *Encyclopædia of Membranes*. Springer, Berlin, Heidelberg, 2015.
- [23] R. Farrauto, S. Hwang, L. Shore, W. Ruettinger, J. Lampert, T. Giroux, Y. Liu, and O. Ilinich. New Material Needs for Hydrocarbon Fuel Processing: Generating Hydrogen for the PEM Fuel Cell. *Annual Review of Materials Research*, 33(1):1–27, 2003. ISSN 1531-7331. doi: 10.1146/annurev.matsci.33.022802.091348. URL <http://www.annualreviews.org/doi/10.1146/annurev.matsci.33.022802.091348>.
- [24] G. Polotskaya, M. Goikhman, I. Podeshvo, V. Kudryavtsev, Z. Pientka, L. Brozova, and M. Bleha. Gas transport properties of polybenzoxazinoneimides and their prepolymers. *Polymer*, 46(11):3730–3736, 2005. ISSN 00323861. doi: 10.1016/j.polymer.2005.02.111.
- [25] Tina M Nenoff Nathan W. Ockwig. Membranes for Hydrogen Separation. *Chemical Reviews*, 107:4078–4110, 2007.
- [26] Hong Joo Lee, Hiroyuki Suda, Kenji Haraya, and Seung Hyeon Moon. Gas permeation properties of carbon molecular sieving membranes derived from the polymer blend of polyphenylene oxide (PPO)/polyvinylpyrrolidone (PVP). *Journal of Membrane Science*, 296(1-2):139–146, 2007. ISSN 03767388. doi: 10.1016/j.memsci.2007.03.025.

- [27] Huiyuan Gao, Y S Lin, Yongdan Li, and Baoquan Zhang. Chemical Stability and Its Improvement of Palladium-Based Metallic Membranes. *Ind. Eng. Chem. Res.*, 43:6920–6930, 2004.
- [28] K Atsonios, K D Panopoulos, A Doukelis, A K Koumanakos, E Kakaras, T A Peters, and Y C van Delft. Introduction to palladium membrane technology. In A Doukelis, K Panopoulos, A Koumanakos, and E Kakaras, editors, *Palladium Membrane Technology for Hydrogen Production, Carbon Capture and Other Application*, pages 1–21. Woodhead Publishing, 2015. doi: 10.1533/9781782422419.1.
- [29] Truls Norby and Reidar Haugsrud. Dense Ceramic Membranes for Hydrogen Separation, in Membranes for Energy Conversion. *Nonporous inorganic membranes*, pages 169–216, 2008. URL http://books.google.com/books?hl=en&lr={\&}id=gCQjw-cyulAC{\&}oi=fnd{\&}pg=PA1{\&}dq=Dense+Ceramic+Membranes+for+Hydrogen+Separation{\&}ots=e-3oiNW5EW{\&}sig=Iv9bFzwJWBTYe7brB66{_}qQ5W{_}u8.
- [30] D.H. Weinkauf and D.R. Paul. Gas transport properties of thermotropic liquid-crystalline copolyesters. II. The effects of copolymer composition. *J. Polym. Sci.: Part B: Polym. Phys.*, 30:837, 1992.
- [31] Tina M Nenoff Nathan W. Ockwig. Membranes for Hydrogen Separation. *Chemical Reviews*, 107:4078–4110, 2007.
- [32] V. Gryaznov. Metal Containing Membranes for the Production of Ultrapure Hydrogen and the Recovery of Hydrogen Isotopes. *Separation & Purification Reviews*, 29(2):171–187, 2000. ISSN 1542-2119. doi: 10.1081/SPM-100100008.
- [33] N A Al-Mufachi, N V Rees, and R Steinberger-Wilkins. Hydrogen selective membranes: A review of palladium-based dense metal membranes. *Renewable and Sustainable Energy Reviews*, 47:540–551, 2015. doi: 10.1016/j.rser.2015.03.026.
- [34] Johnson Matthey Precious Metals Management. Price Tables, 2016.
- [35] Ted B Flanagan and W A Oates. The Palladium-Hydrogen System. *Annu. Rev. Mater. Sci.*, 21:269–304, 1991.
- [36] Hui Li, Hengyong Xu, and Wenzhao Li. Study of n value and α/β palladium hydride phase transition within the ultra-thin palladium composite membrane. *Journal of Membrane Science*, 324(1-2):44–49, 2008. doi: 10.1016/j.memsci.2008.06.053.
- [37] M V Mundschau, X Xie, C R Evenson Iv, and A F Sammells. Dense inorganic membranes for production of hydrogen from methane and coal with carbon dioxide sequestration. *Catalysis today*, 118:12–23, 2006. doi: 10.1016/j.cattod.2006.01.042.

- [38] Ying She, Sean C Emerson, Neal J Magdefrau, Susanne M Opalka, Catherine Thibaud-Erkey, and Thomas H Vanderspurt. Hydrogen permeability of sulfur tolerant Pd–Cu alloy membranes. *Journal of Membrane Science*, 452:203–211, 2014. doi: 10.1016/j.memsci.2013.09.025.
- [39] M D Dolan. Non-Pd BCC alloy membranes for industrial hydrogen separation. *Journal of Membrane Science*, 362(1-2):12–28, 2010. doi: 10.1016/j.memsci.2010.06.068.
- [40] Ekin Ozdogan Wilcox and Jennifer. Investigation of H₂ and H₂S Adsorption on Niobium- and Copper-Doped Palladium Surfaces. *J. Phys. Chem. B*, pages 12851–12585, 2010. doi: 10.1021/acs.energyfuels.5b01294.
- [41] I R Harris D.T. Hughes. A comparative study of hydrogen permeabilities and solubilities in some palladium solid solution alloys. *Journal of Less Common Metals*, 61:9–21, 1978.
- [42] Casey P O Brien, Bret H Howard, James B Miller, Bryan D Morreale, and Andrew J Gellman. Inhibition of hydrogen transport through Pd and Pd₄₇Cu₅₃ membranes by H₂S at 350C. *Journal of Membrane Science*, 349(1-2):380–384, 2010. doi: 10.1016/j.memsci.2009.11.070.
- [43] A Kulprathipanja, G Alptekin, J Falconer, and J Way. Pd and Pd–Cu membranes: inhibition of H₂ permeation by H₂S. *Journal of Membrane Science*, 254(1-2):49–62, 2005. doi: 10.1016/j.memsci.2004.11.031.
- [44] Chao-Huang Chen and Yi Hua Ma. The effect of H₂S on the performance of Pd and Pd/Au composite membrane. *Journal of Membrane Science*, 362(1-2):535–544, 2010. doi: 10.1016/j.memsci.2010.07.002.
- [45] David L. McKinley. Metal Alloy for Hydrogen Separation and Purification, 1964.
- [46] G. Roa, F., Thoen, P.M., Gade, S.K., Way, J.G., De Voss, S., and Alptekin. Palladium-Copper and Palladium-Gold alloy Composite membranes for hydrogen separations. In *Inorganic Membranes for Energy and Environmental Applications*, page 211. 2009.
- [47] APMEC. Silver Prices, 2016. URL <http://www.apmex.com/spotprices/silver-prices>.
- [48] Lixia Peng, Yongchu Rao, Lizhu Luo, and Chang'An Chen. The poisoning of Pd–Y alloy membranes by carbon monoxide. *Journal of Alloys and Compounds*, 486(1-2):74–77, 2009. doi: 10.1016/j.jallcom.2009.06.158.
- [49] Kenneth J. Bryden and Jackie Y. Ying. Nanostructured palladium-iron membranes for hydrogen separation and membrane hydrogenation reactions. *Journal of Membrane Science*, 203(1-2):29–42, 2002. ISSN 03767388. doi: 10.1016/S0376-7388(01)00736-0.

- [50] B. H. Howard and B. D. Morreale. Effect of H₂ on performance of Pd₄Pt alloy membranes. *Energy Materials*, 3(3):177–185, 2008. ISSN 1748-9237. doi: 10.1179/174892309X12519750237717. URL <http://www.tandfonline.com/doi/full/10.1179/174892309X12519750237717>.
- [51] Sabina K. Gade, Sarah J. DeVoss, Kent E. Coulter, Stephen N. Paglieri, Gökhan O. Alptekin, and J. Douglas Way. Palladium-gold membranes in mixed gas streams with hydrogen sulfide: Effect of alloy content and fabrication technique. *Journal of Membrane Science*, 378(1-2):35–41, 2011. ISSN 03767388. doi: 10.1016/j.memsci.2010.11.044. URL <http://dx.doi.org/10.1016/j.memsci.2010.11.044>.
- [52] Shin Kun Ryi, Anwu Li, C. Jim Lim, and John R. Grace. Novel non-alloy Ru/Pd composite membrane fabricated by electroless plating for hydrogen separation. *International Journal of Hydrogen Energy*, 36(15):9335–9340, 2011. ISSN 03603199. doi: 10.1016/j.ijhydene.2010.06.014. URL <http://dx.doi.org/10.1016/j.ijhydene.2010.06.014>.
- [53] Kent E. Coulter, J. Douglas Way, Sabina K. Gade, Saurabh Chaudhari, Gökhan O. Alptekin, Sarah J. DeVoss, Stephen N. Paglieri, and Bill Pledger. Sulfur tolerant PdAu and PdAuPt alloy hydrogen separation membranes. *Journal of Membrane Science*, 405-406:11–19, 2012. ISSN 03767388. doi: 10.1016/j.memsci.2012.02.018. URL <http://dx.doi.org/10.1016/j.memsci.2012.02.018>.
- [54] Fernando Braun, James B. Miller, Andrew J. Gellman, Ana M. Tarditi, Benoit Fleutot, Petro Kondratyuk, and Laura M. Cornaglia. PdAgAu alloy with high resistance to corrosion by H₂S. *International Journal of Hydrogen Energy*, 37(23):18547–18555, 2012. ISSN 03603199. doi: 10.1016/j.ijhydene.2012.09.040. URL <http://dx.doi.org/10.1016/j.ijhydene.2012.09.040>.
- [55] Fernando Braun, Ana M Tarditi, James B Miller, and Laura M Cornaglia. Pd-based binary and ternary alloy membranes: Morphological and perm-selective characterization in the presence of H₂S. *Journal of Membrane Science*, 450:299–307, 2014. doi: 10.1016/j.memsci.2013.09.026.
- [56] T. A. Peters, T. Kaleta, M. Stange, and R. Bredesen. Development of thin binary and ternary Pd-based alloy membranes for use in hydrogen production. *Journal of Membrane Science*, 383(1-2):124–134, 2011. ISSN 03767388. doi: 10.1016/j.memsci.2011.08.050. URL <http://dx.doi.org/10.1016/j.memsci.2011.08.050>.
- [57] T A Peters, T Kaleta, M Stange, and R Bredesen. Development of ternary Pd–Ag–TM alloy membranes with improved sulphur tolerance. *Journal of Membrane Science*, 429:448–458, 2013. doi: 10.1016/j.memsci.2012.11.062.
- [58] Xuezhong He and May Britt Hägg. Hollow fiber carbon membranes: From material to application. *Chemical Engineering Journal*, 215-216:440–448, 2013. ISSN

13858947. doi: 10.1016/j.cej.2012.10.051. URL <http://dx.doi.org/10.1016/j.cej.2012.10.051>.

- [59] T A Peters, M Stange, and R Bredesen. Fabrication of palladium-based membranes by magnetron sputtering. In A Doukelis, K Panopoulos, A Koumanakos, and E Kakaras, editors, *Palladium Membrane Technology for Hydrogen Production, Carbon Capture and Other Application*, pages 25–41. Woodhead Publishing, 2015. doi: 10.1533/9781782422419.1.25.
- [60] AM Tarditi, C Imhoff, and F Braun. PdCuAu ternary alloy membranes: Hydrogen permeation properties in the presence of H₂S. *Journal of Membrane ...*, 479: 246–255, 2014. URL <http://www.sciencedirect.com/science/article/pii/S0376738814009338>.
- [61] T A Peters, M Stange, H Klette, and R Bredesen. High pressure performance of thin Pd–23%Ag/stainless steel composite membranes in water gas shift gas mixtures; influence of dilution, mass transfer and surface effects on the hydrogen flux. *Journal of Membrane Science*, 316(1-2):119–127, 2008. doi: 10.1016/j.memsci.2007.08.056.
- [62] T A Peters, M Stange, P Veenstra, A Nijmeijer, and R Bredesen. The performance of Pd–Ag alloy membrane films under exposure to trace amounts of H₂S. *Journal of Membrane Science*, 499:105–115, 2016. doi: 10.1016/j.memsci.2015.10.031.
- [63] Nong Xu, Sung Su Kim, Anwu Li, John R Grace, C Jim Lim, and Tony Boyd. Investigation of the influence of tar-containing syngas from biomass gasification on dense Pd and Pd–Ru membranes. *Powder Technology*, 290:132–140, 2016. doi: 10.1016/j.powtec.2015.08.037.
- [64] Sean-Thomas B Lundin, Taichiro Yamaguchi, Colin A Wolden, S Ted Oyama, and J Douglas Way. The role (or lack thereof) of nitrogen or ammonia adsorption-induced hydrogen flux inhibition on palladium membrane performance. *Journal of Membrane Science*, 514:65–72, 2016. doi: 10.1016/j.memsci.2016.04.048.
- [65] Thu Hoai Nguyen, Shinsuke Mori, and Masaaki Suzuki. Hydrogen permeance and the effect of H₂O and CO on the permeability of Pd0.75Ag0.25 membranes under gas-driven permeation and plasma-driven permeation. *Chemical Engineering Journal*, 155(1-2):55–61, 2009. doi: 10.1016/j.cej.2009.06.024.
- [66] Bryan D Morreale, Bret H Howard, Osemwengie Iyoha, Robert M Enick, Chen Ling, and David S Sholl. Experimental and Computational Prediction of the Hydrogen Transport Properties of Pd 4 S. *Ind. Eng. Chem. Res.*, 46:6313–6319, 2007.
- [67] A Li, W Liang, and R Highes. The effect of carbon monoxide and steam on the hydrogen permeability of a Pd/stainless steel membrane. *Journal of Membrane Science*, 165:135–141, 2000.

- [68] Natalie Pomerantz and Ma Yi Hua. Effect of H₂S on the performance and long-term stability of Pd/Cu membranes. *Industrial and Engineering Chemistry Research*, 48(8):4030–4039, 2009. ISSN 08885885. doi: 10.1021/ie801947a.
- [69] M Saleh. Interaction of Sulphur Compounds with Palladium. pages 242–250, 1969. ISSN 00147672. doi: 10.1039/TF9706600242.
- [70] B. D. Morreale, M. V. Ciocco, B. H. Howard, R. P. Killmeyer, A. V. Cugini, and R. M. Enick. Effect of hydrogen-sulfide on the hydrogen permeance of palladium-copper alloys at elevated temperatures. *Journal of Membrane Science*, 241(2): 219–224, 2004. ISSN 03767388. doi: 10.1016/j.memsci.2004.04.033.
- [71] AM Tarditi, C Imhoff, and F Braun. PdCuAu ternary alloy membranes: Hydrogen permeation properties in the presence of H₂S. *Journal of Membrane science*, 479: 246–255, 2014.
- [72] Amanda E Lewis, Hongbin Zhao, Haseeba Syed, Colin A Wolden, and J Douglas Way. PdAu and PdAuAg composite membranes for hydrogen separation from synthetic water-gas shift streams containing hydrogen sulfide. *Journal of Membrane Science*, 465:167–176, 2014. doi: 10.1016/j.memsci.2014.04.022.
- [73] CO (US); Shane E. Roark, Boulder, CO (US); Richard MacKay, Lafayette, Michael V. Mundschau Longmont S, and s CO (US). DENSE, LAYERED MEMBRANES FOR HYDROGEN SEPARATION, 2006. ISSN 2004001828.
- [74] D.S dos Santos and P.E.V de Miranda. The use of electrochemical hydrogen permeation techniques to detect hydride phase separation in amorphous metallic alloys. *Journal of Non-Crystalline Solids*, 232-234:133–139, 1998. ISSN 00223093. doi: 10.1016/S0022-3093(98)00487-6. URL <http://linkinghub.elsevier.com/retrieve/pii/S0022309398004876>.
- [75] Hiroshi Yukawa, Daisuke Yamashita, Shigeyuki Ito, Masahiko Morinaga, and Shu Yamaguchi. Alloying effects on the phase stability of hydrides formed in vanadium alloys. *Materials Transactions*, 43(11):2757–2762, 2002. ISSN 1345-9678. doi: 10.2320/matertrans.43.2757. URL [\%5Cnpapers2://publication/uuid/3C0A7ADC-9BA8-471E-9CF3-40C116284411\%5Cnhttp://joi.jlc.jst.go.jp/JST.JSTAGE/matertrans/43.2757?from=CrossRef](http://www.jim.or.jp/journal/e/pdf3/43/11/2757.pdf).
- [76] Hiroshi Yukawa, Akira Teshima, Daisuke Yamashita, Shigeyuki Ito, Masahiko Morinaga, and Shu Yamaguchi. Alloying effects on the hydriding properties of vanadium at low hydrogen pressures. *Journal of Alloys and Compounds*, 337(1-2): 264–268, 2002. ISSN 09258388. doi: 10.1016/S0925-8388(01)01936-3.
- [77] Hiroshi Yukawa, Daisuke Yamashita, Shigeyuki Ito, Masahiko Morinaga, and Shu Yamaguchi. Compositional dependence of hydriding properties of vanadium alloys

at low hydrogen pressures. *Journal of Alloys and Compounds*, 356-357:45–49, 2003. ISSN 09258388. doi: 10.1016/S0925-8388(03)00099-9.

- [78] J. Xu, X. K. Sun, Q. Q. Liu, and W. X. Chen. Hydrogen permeation behavior in IN718 and GH761 superalloys. *Metallurgical and Materials Transactions A*, 25 (3):539–544, 1994. ISSN 10735623. doi: 10.1007/BF02651595.
- [79] S Hara, K Sakaki, N Itoh, H.-M. Kimura, K Asami, and A Inoue. An amorphous alloy membrane without noble metals for gaseous hydrogen separation. *Journal of Membrane Science*, 164:289–294, 2000.
- [80] Shin-ichi Yamaura, Yoichiro (Fukuda Metal Foil & Powder Co. Ltd.) Shimpo, Hitoshi (Fukuda Metal Foil & Powder Co. Ltd.) Okouchi, Motonori (Fukuda Metal Foil & Powder Co. Ltd.) Nishida, Osamu (Fukuda Metal Foil & Powder Co. Ltd.) Kajita, Hisamichi Kimura, and Akihisa Inoue. Hydrogen Permeation Characteristics of Melt-Spun Ni-Nb-Zr Amorphous Alloy Membranes. *Materials Transactions*, 42(9):1885–1890, 2001. ISSN 1345-9678. doi: 10.2320/matertrans.42.1885. URL <http://ci.nii.ac.jp/naid/130004451634/>.
- [81] S Hara, K Sakaki, N Itoh, H.-M. Kimura, K Asami, and A Inoue. An amorphous alloy membrane without noble metals for gaseous hydrogen separation. *Journal of Membrane Science*, 164:289–294, 2000.
- [82] Shin Ichi Yamaura, Yoichiro Shimpo, Hitoshi Okouchi, Motonori Nishida, Osamu Kajita, and Akihisa Inoue. The effect of additional elements on hydrogen permeation properties of melt-spun Ni-Nb-Zr amorphous alloys. *Nippon Kinzoku Gakkaishi/Journal of the Japan Institute of Metals*, 68(12):1039–1042, 2004. ISSN 00214876. doi: 10.2320/jinstmet.68.1039.
- [83] C Nishimura, M Komaki, S Hwang, and M Amano. V-Ni alloy membranes for hydrogen purification. *Journal of Alloys and Compounds*, 330-332:902–906, 2002.
- [84] Tetsuya Ozaki, Yi Zhang, Masao Komaki, and Chikashi Nishimura. Preparation of Palladium-coated V and V-15Ni membranes for hydrogen purification by electroless plating technique. *International Journal of Hydrogen Energy*, 28:297–302, 2003.
- [85] C. Nishimura, T. Ozaki, M. Komaki, and Y. Zhang. Hydrogen permeation and transmission electron microscope observations of V-Al alloys. *Journal of Alloys and Compounds*, 356-357:295–299, 2003. ISSN 09258388. doi: 10.1016/S0925-8388(02)01273-2.
- [86] T. Takano, K. Ishikawa, T. Matsuda, and K. Aoki. Hydrogen Permeation of Eutectic Nb-Zr-Ni Alloy Membranes Containing Primary Phases. *Materials Transactions*, 45(12):3360–3362, 2004. ISSN 13459678. doi: 10.2320/matertrans.45.3360.

- [87] Kunihiko Hashi, Kazuhiro Ishikawa, Takeshi Matsuda, and Kiyoshi Aoki. Microstructures and Hydrogen Permeability of Nb-Ti-Ni Alloys with High Resistance to Hydrogen Embrittlement. *Materials Transactions*, 46(5):1026–1031, 2005. ISSN 1345-9678. doi: 10.2320/matertrans.46.1026. URL https://www.jstage.jst.go.jp/article/matertrans/46/5/46{_}5{_}1026/{_}article.
- [88] H. Yukawa, T. Nambu, and Y. Matsumoto. Ta-W Alloy for Hydrogen Permeable Membranes. *Materials Transactions*, 52(4):610–613, 2011. ISSN 1347-5320. doi: 10.2320/matertrans.MA201007. URL <http://joi.jlc.jst.go.jp/JST.JSTAGE/matertrans/MA201007?from=CrossRef>.
- [89] Zetian Tao, Litao Yan, Jinli Qiao, Baolin Wang, Lei Zhang, and Jiujun Zhang. A review of advanced proton-conducting materials for hydrogen separation. *Progress in Materials Science*, 74:1–50, 2015. ISSN 00796425. doi: 10.1016/j.pmatsci.2015.04.002. URL <http://dx.doi.org/10.1016/j.pmatsci.2015.04.002>.
- [90] John W. Phair and Richard Donelson. Developments and design of novel (non-palladium-based) metal membranes for hydrogen separation. *Industrial and Engineering Chemistry Research*, 45(16):5657–5674, 2006. ISSN 08885885. doi: 10.1021/ie051333d.
- [91] Wen Hui Yuan, Ling Ling Mao, and Li Li. Novel SrCe0.75Zr0.20Tm0.05O3-alpha membrane for hydrogen separation. *Chinese Chemical Letters*, 21(3):369–372, 2010. ISSN 10018417. doi: 10.1016/j.cclet.2009.11.002.
- [92] Sonia Escolástico, Cecilia Solís, and José M. Serra. Hydrogen separation and stability study of ceramic membranes based on the system Nd₅LnWO₁₂. *International Journal of Hydrogen Energy*, 36(18):11946–11954, 2011. ISSN 03603199. doi: 10.1016/j.ijhydene.2011.06.026.
- [93] Sonia Escolástico, Cecilia Solís, Tobias Scherb, Gerhard Schumacher, and Jose M. Serra. Hydrogen separation in La_{5.5}WO_{11.25-δ} membranes. *Journal of Membrane Science*, 444:276–284, 2013. ISSN 03767388. doi: 10.1016/j.memsci.2013.05.005. URL <http://dx.doi.org/10.1016/j.memsci.2013.05.005>.
- [94] Sonia Escolástico, Vicente B. Vert, and José M. Serra. Preparation and characterization of nanocrystalline mixed proton-electronic conducting materials based on the system Ln₆WO₁₂. *Chemistry of Materials*, 21(14):3079–3089, 2009. ISSN 08974756. doi: 10.1021/cm900067k.
- [95] Sonia Escolastico, Janka Seeger, Stefan Roitsch, Mariya Ivanova, Wilhelm A. Meullenberg, and José M. Serra. Enhanced H₂ separation through mixed proton-electron conducting membranes based on La_{5.5}W_{0.8}M_{0.2}O_{11.25-δ}. *ChemSusChem*, 6(8):1523–1532, 2013. ISSN 18645631. doi: 10.1002/cssc.201300091.
- [96] Sonia Escolástico, Cecilia Solís, and José M. Serra. Study of hydrogen permeation in (La 5/6Nd 1/6) 5.5WO 12-δ membranes. *Solid State Ionics*, 216:31–35, 2012.

ISSN 01672738. doi: 10.1016/j.ssi.2011.11.004. URL <http://dx.doi.org/10.1016/j.ssi.2011.11.004>.

- [97] Einar Vøllestad, Camilla K. Vigen, Anna Magrasó, and Reidar Haugsrud. Hydrogen permeation characteristics of La₂₇Mo_{1.5}W_{3.5}O_{55.5}. *Journal of Membrane Science*, 461:81–88, 2014. ISSN 18733123. doi: 10.1016/j.memsci.2014.03.011. URL <http://dx.doi.org/10.1016/j.memsci.2014.03.011>.
- [98] Sonia Escolástico, Simona Somacescu, and José M. Serra. Tailoring mixed ionic–electronic conduction in H₂ permeable membranes based on the system Nd_{5.5}W₁xMo_xO_{11.25}δ. *J. Mater. Chem. A*, 3(2):719–731, 2015. ISSN 2050-7488. doi: 10.1039/C4TA03699A. URL <http://xlink.rsc.org/?DOI=C4TA03699A>.
- [99] Zhiwen Zhu, Wenping Sun, Yingchao Dong, Zhongtao Wang, Zhen Shi, Qingping Zhang, and Wei Liu. Evaluation of hydrogen permeation properties of Ni–Ba(Zr_{0.7}Pr_{0.1}Y_{0.2})O₃δ cermet membranes. *International Journal of Hydrogen Energy*, 39(22):11683–11689, 2014. ISSN 03603199. doi: 10.1016/j.ijhydene.2014.05.163. URL <http://linkinghub.elsevier.com/retrieve/pii/S0360319914015754>.
- [100] Zhiwen Zhu, Wenping Sun, Litao Yan, Weifeng Liu, and Wei Liu. Synthesis and hydrogen permeation of Ni–Ba(Zr_{0.1}Ce_{0.7}Y_{0.2})O₃δ metal–ceramic asymmetric membranes. *International Journal of Hydrogen Energy*, 36(10):6337–6342, 2011. ISSN 03603199. doi: 10.1016/j.ijhydene.2011.02.029. URL <http://linkinghub.elsevier.com/retrieve/pii/S0360319911003466>.
- [101] Jonathan M Polfus, Wen Xing, Marie-Laure Fontaine, Christelle Denonville, Partow P Henriksen, and Rune Bredesen. Hydrogen separation membranes based on dense ceramic composites in the La₂₇W₅O_{55.5}-LaCrO₃ system. *Journal of Membrane Science*, 479:39–45, 2015. ISSN 03767388. doi: 10.1016/j.memsci.2015.01.027. URL <http://dx.doi.org/10.1016/j.memsci.2015.01.027>.
- [102] S. Escolástico, C. Solís, C. Kjølseth, and J. M. Serra. Outstanding hydrogen permeation through CO₂-stable dual-phase ceramic membranes. *Energy Environ. Sci.*, 7(11):3736–3746, 2014. ISSN 1754-5692. doi: 10.1039/C4EE02066A. URL <http://xlink.rsc.org/?DOI=C4EE02066A>.
- [103] Zhiwen Zhu, Wenping Sun, Zhongtao Wang, Jiafeng Cao, Yingchao Dong, and Wei Liu. A high stability Ni-Lainf_{0.5}/infCeinf_{0.5}/infOinf_{2-δ}/inf asymmetrical metal–ceramic membrane for hydrogen separation and generation. *Journal of Power Sources*, 281:417–424, 2015. ISSN 03787753. doi: 10.1016/j.jpowsour.2015.02.005. URL <http://dx.doi.org/10.1016/j.jpowsour.2015.02.005>.
- [104] Shumin Fang, Lei Bi, Litao Yan, and Wenping Sun. CO₂ Resistant Hydrogen Permeation Membranes Based on Doped Ceria and Nickel. *Journal of Physical Chemistry C*, pages 10986–10991, 2010. ISSN 1932-7447. doi: 10.1021/jp102271v. URL <http://pubs.acs.org/doi/abs/10.1021/jp102271v>.

- [105] Litao Yan, Wenping Sun, Lei Bi, Shumin Fang, Zetian Tao, and Wei Liu. Effect of Sm-doping on the hydrogen permeation of Ni-La₂Ce₂O₇ mixed protonic-electronic conductor. *International Journal of Hydrogen Energy*, 35(10):4508–4511, 2010. ISSN 03603199. doi: 10.1016/j.ijhydene.2010.02.134. URL <http://dx.doi.org/10.1016/j.ijhydene.2010.02.134>.
- [106] Jay Kniep and Y. S. Lin. Effect of zirconium doping on hydrogen permeation through strontium cerate membranes. *Industrial and Engineering Chemistry Research*, 49(6):2768–2774, 2010. ISSN 08885885. doi: 10.1021/ie9015182.
- [107] Tak keun Oh, Heesung Yoon, and E. D. Wachsman. Effect of Eu dopant concentration in SrCe_{1 - x}EuxO_{3 - ??} on ambipolar conductivity. *Solid State Ionics*, 180 (23-25):1233–1239, 2009. ISSN 01672738. doi: 10.1016/j.ssi.2009.07.001.
- [108] Wei Liu, Victor G. Ruiz, Guo Xu Zhang, Biswajit Santra, Xinguo Ren, Matthias Scheffler, and Alexandre Tkatchenko. Structure and energetics of benzene adsorbed on transition-metal surfaces: Density-functional theory with van der Waals interactions including collective substrate response. *New Journal of Physics*, 15 (111), 2013. ISSN 13672630. doi: 10.1088/1367-2630/15/5/053046.
- [109] Jian Song, Liping Li, Xiaoyao Tan, and K. Li. BaCe_{0.85}Tb_{0.05}Co_{0.1}O_{3-??} perovskite hollow fibre membranes for hydrogen/oxygen permeation. *International Journal of Hydrogen Energy*, 38(19):7904–7912, 2013. ISSN 03603199. doi: 10.1016/j.ijhydene.2013.04.104.
- [110] Shumin Fang, Kyle Brinkman, and Fanglin Chen. Unprecedented CO₂-Promoted Hydrogen Permeation in Ni-BaZr_{0.1}Ce_{0.7}Y_{0.1}Yb_{0.1}O_{3-δ} Membrane. *ACS Applied Materials & Interfaces*, 6(1):725–730, 2014. ISSN 1944-8244. doi: 10.1021/am405169d. URL <http://pubs.acs.org/doi/abs/10.1021/am405169d>.
- [111] Shumin Fang, Kyle S. Brinkman, and Fanglin Chen. Hydrogen permeability and chemical stability of Ni-BaZr_{0.1}Ce_{0.7}Y_{0.1}Yb_{0.1}O_{3-δ} membrane in concentrated H₂O and CO₂. *Journal of Membrane Science*, 467:85–92, 2014. ISSN 18733123. doi: 10.1016/j.memsci.2014.05.008. URL <http://dx.doi.org/10.1016/j.memsci.2014.05.008>.
- [112] Xihan Tan, Xiaoyao Tan, Naitao Yang, Bo Meng, Kun Zhang, and Shaomin Liu. High performance BaCe_{0.8}Y_{0.2}O_{3-A} (BCY) hollow fibre membranes for hydrogen permeation. *Ceramics International*, 40(2):3131–3138, 2014. ISSN 02728842. doi: 10.1016/j.ceramint.2013.09.132.
- [113] Vanesa Gil, Jonas Gurauskis, Christian Kjølseth, Kjell Wiik, and Mari-Ann Einarsrud. Hydrogen permeation in asymmetric La_{28-x}W₄ + xO₅₄ + 3x/2 membranes. *International Journal of Hydrogen Energy*, 38(7):3087–3091, 2013.

ISSN 03603199. doi: 10.1016/j.ijhydene.2012.12.105. URL <http://linkinghub.elsevier.com/retrieve/pii/S0360319912028406>.

- [114] Camilla K. Vigen and Reidar Haugsrud. Hydrogen flux in La_{0.87}Sr_{0.13}CrO_{3- δ} . *Journal of Membrane Science*, 468:317–323, 2014. ISSN 18733123. doi: 10.1016/j.memsci.2014.06.012.
- [115] Jian Song, Bo Meng, Xiaoyao Tan, and Shaomin Liu. Surface-modified proton conducting perovskite hollow fibre membranes by Pd-coating for enhanced hydrogen permeation. *International Journal of Hydrogen Energy*, 40(18):6118–6127, 2015. ISSN 03603199. doi: 10.1016/j.ijhydene.2015.03.057. URL <http://dx.doi.org/10.1016/j.ijhydene.2015.03.057>.
- [116] Jian Song, Jian Kang, Xiaoyao Tan, Bo Meng, and Shaomin Liu. Proton conducting perovskite hollow fibre membranes with surface catalytic modification for enhanced hydrogen separation. *Journal of the European Ceramic Society*, 36(7): 1669–1677, 2015. ISSN 1873619X. doi: 10.1016/j.jeurceramsoc.2016.01.006. URL <http://dx.doi.org/10.1016/j.jeurceramsoc.2016.01.006>.

Chapter 3

Experimental methods

3.1 Simulations

Density functional theory calculations were performed using the Quantum Espresso (QE) ab initio simulation package using the generalized gradient approximation with the PW91 functional to describe electron-correlation effects. Ion-electron interactions were described using ultra-soft pseudopotentials. A plane-wave expansion with a cut-off of 233.73 eV was used in all calculations. Geometry relaxations were performed with a conjugate gradient method until the forces on all unconstrained atoms were less than 0.03 eV/A. A Monkhorst Pack mesh with 4x4x4 k-points was used for all calculations.

The supercell used contained 20 metal atoms and one gaseous molecule located on one of four available sites on the metal lattice. It was assumed that all palladium systems adopt the substitutional; random fcc structure. Metal atoms were randomly distributed among the fcc lattice in the supercell. All atoms were allowed to relax during the calculation, with the volume of the super cell fixed at the optimised volume of the super cell without adsorbed molecules.

Geometry optimization was performed to get the lattice constant and total energy of each alloy prior to adsorption of gaseous molecules. Python with scikit learn, pandas, numpy packages were used for scripting, data collection and analysis.

3.2 Membrane manufacture

3.2.1 Materials used

3.2.2 Support fabrication

The YSZ 3% hollow fibre substrates with a desired micro-structure were fabricated by a fingering induced phase-inversion process, followed by high temperature sintering. A uniform ceramic suspension, with 60 wt.% solid loading YSZ 3% powder (1 μ m, VWR), was prepared by ball milling. After degassing, the ceramic suspension was transferred into 200 mL stainless steel syringes and extruded through a tube-in-orifice spinneret

(outer diameter 3 mm, inner diameter 1.2 mm) into a coagulation bath with no air gap. An extrusion rate of 7 and 5 mL min⁻¹ was adopted for ceramic suspension and bore fluid (15 wt.% 1,4-dioxane in n-hexane) respectively. The formed precursor fibres were kept in deionized water for a minimum of 12 h, in order to remove the excess solvent. After being gently washed with deionized water, the precursor fibres were dried at room temperature and sintered at 1400°C in a tubular furnace (Elite, Model TSH 17/75/450).

3.2.3 Membrane deposition

Electroless Plating

Palladium silver, copper, gold, and ternary alloy compositions (expect for PdCuZr) were deposited onto the surface of the porous YSZ substrate through electroless plating. The process was performed in two steps; the first involves ‘activating’ the surface of the material intended for deposition by seeding the surface with particles of a metal with a higher electro positivity than the metal intended to be plated. Palladium was used due to its high electro positivity compared to other metals commonly plated through electroless deposition. This activation step is required for non-conductive supports such as ceramics and glass but is usually not required for conductive supports depending on the specific support material and intended plating layer. The ‘activation’ step is followed by the ‘plating’ step where a solution containing a metallic salt complexing agent, and stabilising agent is reduced through the use of a reducing agent, causing solid metal to be displaced from the solution, and due to the catalytic activity of the seeds placed in the prior step, forming a dense metal layer on the intended surface.

Electroless plating results in a strongly adhered, dense metallic layer which can be deposited easily on a large range of morphologies.

Prior to deposition, the outer surface of the fibre was cleaned by sequential washings with a 1:1 mixture of ethanol and water for 10 min in an ultrasonic bath, and were then dried overnight at 120°C.

Preceding electroless plating, the substrates were coated at one end with a gas tight glaze and sintered at 900°C for 1 hour. Prior to deposition, the outer surface of the fibre was cleaned by sequential washings with a 1:1 mixture of ethanol and water for 10 min in an ultrasonic bath, and were then dried overnight at 120 °C.

The substrates were then activated with Pd nuclei via sensitisation in an acidic SnCl₂ solution, followed by activation in an acidic PdCl₂ solution. The sensitisation/activation process was carried out by immersing the glazed hollow fibre substrates sequentially in five chemical baths, i.e. acidic SnCl₂ solution for 5 min; deionised water for 5 min, acidic PdCl₂ solution for 5 min; 0.01 M HCl solution for 2 min; and finally deionised water for 3 mins. All chemical baths were homogenised using compressed air. The sensitisation/activation process was repeated for 8 cycles. The composition of each bath is shown in Table 3.1.

The substrates were then immersed in a Pd electroless plating (ELP) solution, at 60°C, in order to deposit metallic Pd layers onto the activated surface. The Pd ELP solution was prepared according to the composition presented in Table 3.1 and left to

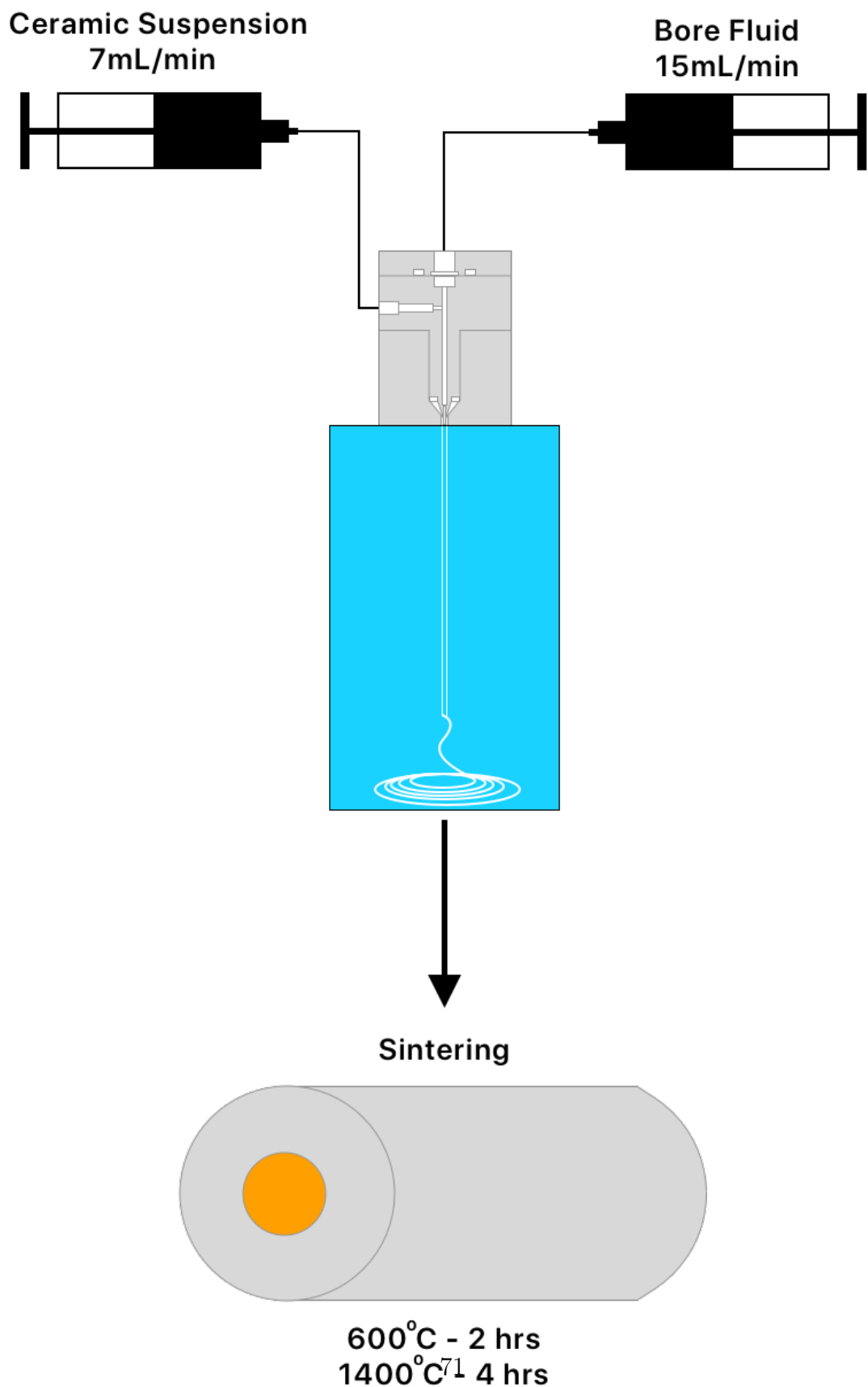


Figure 3.1: Schematic representation of the fabrication process of SZ hollow fibre.

Table 3.1: Compositions used for preparation of palladium based membranes on YSZ substrate through electroless plating and immersion plating

Compound	Deposited metal			
	Pd	Ag	Cu	Au
Metal Source (g/L)				
PdCl ₂	4	-	-	-
AgNO ₃	-	3.4	-	-
CuSO ₄	-	-	10	-
AuCl ₃	-	-	-	0.1
Stabilising agent				
NH ₃ -H ₂ O (mL/L)	198	200	-	-
NaOH (g/L)	-	-	8.63	1
Complexing Agent (g/L)				
Na ₂ EDTA-2H ₂ O	40	35	-	-
Persulfate	-	-	30	-
Reducing agent (mL/L)				
N ₂ H ₄	5.6	4.2	-	-
Formaldehyde	-	-	14	-

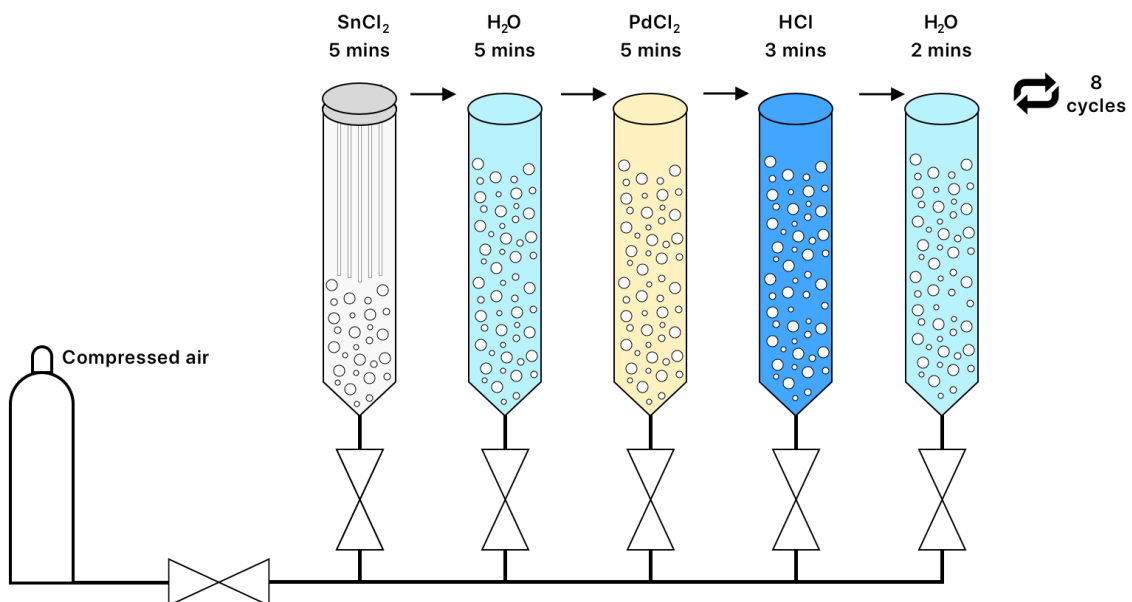


Figure 3.2: Schematic representation of the sequential baths for sensitisation/activation process.

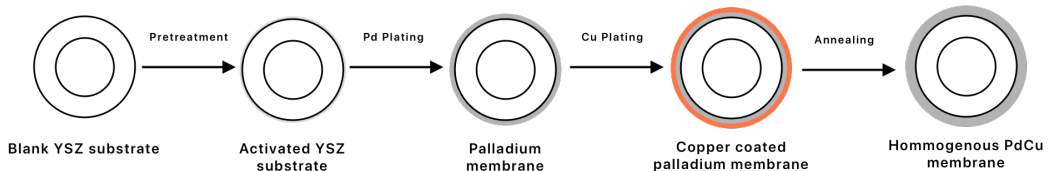


Figure 3.3: Example of ELP procedure when manufacturing a PdCu membrane on YSZ substrate

stabilize for 1 h in an ultrasonic bath prior to use. The volume of Pd ELP solution was fixed at 4 mL per cm² of substrate surface area. The electroless plating procedure was performed twice, with a total plating time of 60 mins.

After the palladium coating the membranes were then subjected to one, or multiple, other plating steps of silver, gold, or copper. The plating time for silver was 30 minutes for one cycle and the volume of plating solution to substrate was the same as the palladium steps.

It should be noted that the deposition of gold is through immersion plating rather than electroless plating. Immersion plating is the process of applying adhering layers of nobler metals to another metal's surface by dipping the material in a heated nobler metal solution ion to produce a replacement reaction. This causes the deposition of a metallic coating on a base metal from solutions that contain coating metal. One metal is typically displaced by metal ions that have lower levels of oxidation potential, relative to the metal ion being displaced. The plating time for gold was 3 hours and the volume of plating solution to substrate was 4mL per cm³.

The resulting composite membranes consisting of multiple metal layers stacked were then heat treated at 500°C under an environment containing 25% H₂ in Ar balance for 24 hours in order to alloy the layers into a homogenous membrane and reduce any oxides that were present on the surface.

Magnetron Sputtering

Membranes were deposited using a closed field unbalanced magnetron sputter ion plating system produced by Teer Coatings Ltd. The thin film membranes were deposited onto the YSZ 3% hollow fibres by mounting them vertically inside the sputtering system. The system was then evacuated to 1x10⁻⁶ mBar and subjected to an ion cleaning process with Ar plasma prior to sputtering. Pd, Cu, and Zr targets (99.9% purity) were used to sputter the chosen alloy composition onto the membranes at the target currents shown in. A bias voltage of 50 V was applied to the magnetron during deposition runs. Samples were deposited using pulsed DC, with a constant target to substrate distance and a sample rotation speed of 16 rpm. An Ar flux of 25 (SCC/m) was used during deposition. PdCu membranes in both BCC and FCC phase were manufactured through magnetron sputtering along with PdCuZr ternary alloys.

Table 3.2: Conditions used during magnetron sputtering of palladium membranes on YSZ tubular substrate

Alloy	Target current (A)		
	Pd	Cu	Zr
PdCuZr	1.25	0.65	0.4
PdCu (fcc)	1.25	0.8	-
PdCu (bcc)	1.2	1.0	-

3.2.4 Materials testing

The thickness of the plated layers was characterised by first using a Focused Ion Beam (FIB) to mill through a section of the hollow fibre to provide a flat, cross sectional surface for analysis. The thickness of the metal later was then measured using high resolution Scanning Electron Microscopy (SEM) and composition analysed using Energy Dispersive x-ray Spectrometry (EDS) on the same sample.

The surface composition of the membrane was further characterised using X-ray Photoelectron Spectroscopy to provide a more accurate compositional analysis for the top 10 nm of the membrane, the depth which is most relevant for catalytic dissociation of hydrogen and adsorption of impurities.

Prior to the H₂ permeation tests, the integrity of the hollow fibre membranes was evaluated by testing the gas-tightness of the membrane under N₂ atmosphere, up to 10 bar and room temperature and using a gas-tightness apparatus developed in house. [1]

3.3 Membrane testing

3.3.1 Preparation of gas standards

Gas standards of hydrogen were prepared gravimetrically in 10 litre cylinders (BOC, UK) in accordance with ISO 6142-1 from pure hydrogen (Air Products, UK), nitrogen (Air Products), carbon monoxide (Scott Speciality Gases, UK), methane (CK Gases, UK) and krypton (BOC, UK). Any impurities that were detected in these pure gases were quantified and these values were then incorporated into the final determination of the gas mixture compositions and uncertainties. For the purpose of this paper the gas standards that were used to perform the permeation tests will be referred to as gas mixtures, and the gas standards that were used to calibrate the analytical instruments will be referred to as calibration gas standards. Before use, the gas mixtures were verified against traceable primary reference materials using Gas Chromatography with either a pulsed helium discharge ionisation detector (PDHID) for samples not containing sulphur, and sulphur chemiluminescence detector (SCD) for sulphur containing samples. The compositions of the non-sulphur, and sulphur containing gas standards created for the purposes of this thesis are shown in tables 3.3 and 3.4

Table 3.3: Gas mixture composition of the non-sulphur sample used during impurity tests

Impurity	Concentration ($\mu\text{mol/mol}$)
O ₂	10.06
N ₂	10.04
CH ₄	10.01
CO ₂	10
CO	9.98
H ₂	Balance

Table 3.4: Gas mixture composition of the sulphur sample used during impurity tests

Impurity	Concentration ($\mu\text{mol/mol}$)
Kr	1.1
H ₂ S	0.41
OCS	0.42
CS ₂	0.362
t-BuSH	0.391
THT	0.409
H ₂	Balance

3.3.2 Membrane testing rig

After the membranes were ensured to be gas tight, hydrogen permeation measurements were performed using the experimental apparatus shown in Figure 1. The palladium alloy composite hollow fibre membranes were sealed on to a stainless steel $\frac{1}{4}$ " NPT fitting. The membrane was then placed in a Sulfinert®-treated sample vessel (Thames Restek, UK) with nominal volume of 300 cm^3 . The vessel was then heated using heavy insulated heating tape (OMEGA STH051-020). The heating was controlled using the temperature of the membrane using a PID temperature controller (OMRON). The feed was supplied from a cylinder either containing BIP+ hydrogen (Air Products) for pure hydrogen permeability tests or one of two gravimetrically prepared gas mixtures for impurity testing shown in tables 3.3 and 3.4. Prior to introducing gas to the membrane the system was evacuated down to $1 \times 10^{-6}\text{ mbar}$.

The flux and permeability of the membrane were automatically calculated using software developed in house. Each membrane sample was made using the same batch of substrate and cut to the same length prior to deposition. The permeability (P) of a dense metal membrane is given by Eqn (1) and is a function of the hydrogen flux through the membrane (J), the concentration and pressure gradient across the membrane ($P_{ret}^{0.5} - P_{perm}^{0.5}$), and the thickness of the metallic membrane (l).

$$P = \frac{Jl}{P_{ret}^{0.5} - P_{perm}^{0.5}} \quad (3.1)$$

3.4 Hydrogen impurity enrichment

3.4.1 Device design

References

- [1] Ana Gouveia Gil, Miria Hespanhol M Reis, David Chadwick, Zhentao Wu, and K Li. A highly permeable hollow fibre substrate for Pd/Al₂O₃ composite membranes in hydrogen permeation. *International Journal of Hydrogen Energy*, 40(8):3249–3258, 2015. ISSN 0360-3199. doi: <https://doi.org/10.1016/j.ijhydene.2015.01.021>. URL <http://www.sciencedirect.com/science/article/pii/S0360319915000580>.

Chapter 4

Density functional theory as a screening method for dense metal membranes

4.1 Abstract

4.2 Introduction

High impurity resistant dense metal membranes are being developed for hydrogen impurity enrichments of HRS samples with hydrogen derived from biomass, hydrocarbon or electrolysis. Metal membranes operate by selectively dissociating hydrogen, which then allows the hydrogen atoms to solubilize and subsequently permeate through the bulk of the separation layer. The problem is that many hydrogen impurities are also capable of adsorbing onto and interacting with the surface of many of the metals which comprise dense metal membranes. The impact of this adsorption can vary depending the molecule, Carbon monoxide for example will simply adsorb onto the surface and result in competitive adsorption between the hydrogen and impurity. Sulphur containing impurities which are commonly found in hydrocarbon sources and therefore are potentially present in any hydrogen produced from these methods. Sulphur containing impurities present more of a problem since they can potentially react with many metals used for hydrogen separation membranes. The impact of these contaminants can be minimized by designing alloy compositions that have a weaker attraction to the membrane, and therefore will have less of an affect at higher temperatures where these membranes operate.

Physically testing each potential membrane composition would be time consuming and costly due to the high price of palladium, the time required to synthesise specific membrane compositions, and performing the tests. Simulations provide a solution to this, allowing potential alloys to be screened for their interaction strength with each individual ISO 14687-2 impurity quickly, avoiding the cost of manufacturing each alloy composition.

This chapter will calculate the behaviour of 56 palladium alloy composition under

Table 4.1: Simulated total energy values of ISO 14687-2 impurities

Gas	Total Energy (kJ × 10 ⁻²¹)
H	-2.01
N ₂	-123.91
O ₂	-180.86
CO	-130.93
CO ₂	-221.95
NH ₃	-1933.22
Ar	-208.10
CH ₄	-50.73
Formaldehyde	-136.13
Formic Acid	-227.08
H ₂ S	-150.36
He	-12.62
H ₂ O	-95.99

13 ISO 14687-2 impurities. This is done by comparing the total energy of different configurations after relaxation of internal forces in the system. The close packed surfaces of palladium alloys were simulated as

The pure metals and alloy slabs were modelled as slabs with periodic boundary conditions in the two directions parallel to the surface and separated by at 10Å thick vacuum region.

4.3 Results and discussion

The adsorption energy, $E_{i,ads}$, for the adsorption of a gaseous impurity on the surface is calculated using:

$$E_{i,ads} = E_{slab} + E_i - E_{slab+i} \quad (4.1)$$

Where E_{slab+i} is the total energy of the relaxed gas-surface system where i is the simulated gas, E_{slab} and E_i are the total energy of relaxed bare surface and gas molecule respectively. Since a system will always tend towards it's lowest energy state, if the total energy of the $E_{i,ads}$ is lower than the sum of it's component energies, it indicates an affinity for the target impurity to adsorb onto the surface of the membrane.

Table 4.2: Simulated total energy values of alloy slabs

Alloy/Metal Composition	Space group	Calculated lattice parameter (A)	Total Energy (ry)	Total Energy kJ
Pd	-	-6653.38	-	-1.45x10-17
PdAg23	-	-6774.37	-	-1.48 x10-17
PdAu10	-	-7545.53	-	-1.64x10-17
PdAu20	-	-8437.613	-	-1.84x10-17
Pd60Cu40	-	-5703.15	-	-1.24x10-17
Pd80Cu20	-	-6178.29	-	-1.35x10-17
Pd70Au20Zr10	-	-8389.61	-	-1.83x10-17
Pd70Cu20Zr10	-	-6130.29	-	-1.34x10-17
Pd70Ag10Zr20	-	-6605.75	-	-1.44x10-17
PdZr10	-	-6605.45	-	-1.44x10-17
PdZr20	-	-6557.46	-	-1.43x10-17
Pd70Au20Ag10	-	-8485.99	-	-1.84x10-17
Pd70Au20Cu10	-	-8200.05	-	-1.79x10-17
Pd70Cu20Ag10	-	-6226.71	-	-1.36x10-17

4.3.1 Stability of palladium alloy compositions

4.3.2 Hydrogen and Impurity adsorption on palladium alloy membranes

Hydrogen

Helium, Nitrogen and Argon

Carbon Monoxide

Carbon Dioxide

Ammonia

Oxygen

Water

Methane

Formaldehyde

Formic Acid

Hydrogen sulphide

4.4 Conclusion

References

Chapter 5

Impurity resistance of dense metal membranes under hydrogen impurities

5.1 Abstract

In order to further develop hydrogen impurity enrichment as a suitable technique for hydrogen quality assurance more research is required on a suitable membrane material for use within such a device. In this chapter a number of dense palladium alloy membranes were synthesised on a YSZ substrate using a combination of electroless plating and magnetron sputtering.

The permeation of the synthesised membranes, in addition to a commercial membrane were tested under a variety of ISO 14687-2 impurities in order to determine which alloy composition was most suitable for use as a membrane material for hydrogen impurity enrichment, where low reactivity with impurities present in hydrogen samples are required. Of the tested membranes the best performing compositions were PdAuAg, PdAuCu and PdCuZr which only showed a 27%, 25% and 26% drop in permeability under atmospheres containing 10 ppm of non-sulphurous, and 2 ppm of sulphurous impurities typically expected to be found in hydrogen derived from steam methane reforming. This indicates that these alloys are most suitable for metrology purposes due to their low reactivity.

5.2 Introduction

In order to improve the accuracy and the cost of hydrogen impurity enrichment a suitable membrane composition must be found. In addition to this all previous studies used a commercial palladium-based membrane and in all cases it was noted that certain impurities reacted with the membrane. This interaction had the result of changing the composition of the enriched gas mixture and therefore reducing the final accuracy of the measurement. [1, 2] The self-supported commercial membranes used in both studies are

also generally between 20-100 μm in order to provide sufficient mechanical strength for a membrane. However, for palladium membranes to be economical this thickness must be reduced to about 1-5 μm giving the added benefit of greater flux and therefore lower enrichment times.

Palladium alloy membranes are generally created by forming an alloy with silver, copper or gold. By doing this the hydrogen embrittlement effect can be effectively mitigated. Using alloys has the added benefits of decreasing the overall amount of palladium required in the film, driving up their cost effectiveness, and in some cases increasing the flux of the membrane to higher levels achievable than a pure palladium membrane. The addition of extra metallic elements however will affect the membranes catalytic properties with impurities within the hydrogen sample. If the membrane catalyses reactions such as water gas shift, methanation, or CO oxidation, the composition of the gas sample could change, which would lead to inaccurate results during analysis of the enriched sample. In addition to this, it is possible that hydrogen samples contain sulphurous impurities such as H₂S or OCS, if produced from hydrocarbons (steam methane reforming etc.). Sulphurous impurities are known to chemisorb onto the surface of palladium membranes through a permanent reaction, not only changing the composition of the gas mixture and compromising analysis, but also severely reducing flux through the membrane, and potentially leading to membrane failure due to crack formation in the palladium layer.

This study aims to apply recent advances in palladium membrane manufacturing to improve impurity enrichment. Palladium alloy membranes will be deposited onto porous YSZ supports using both electroless plating and closed field unbalanced magnetron sputter ion plating. This will have the combined effect of reducing the amount of palladium used, driving down their cost, and increasing the flux, and therefore reducing the time taken to enrich a hydrogen sample. This work aims to quantify the degree of interaction of impurities with palladium alloy membranes in a three-step experimental procedure. The pure hydrogen flux of each membrane composition will be measured and the membranes hydrogen permeability calculated as a base line. The following two permeation tests will measure the change in permeability resulting from introducing part-per-million level impurities into the gas sample. The change in permeability which results from this will act as a measure for the membranes tendency to interact with different impurity types. Additionally, at all three testing stages, X-ray photoelectron spectroscopy (XPS) will be performed on the surface of the membranes to investigate how the composition on the surface of the membrane changes when exposed to each impurity environment. This will allow the alloy segregation behaviour to be observed, and more importantly, quantify the amount of sulphur which has reacted with the surface of the membrane.

Table 5.1: Membrane compositions analysed by EDS and their thickness measured using FIB-SEM

Membrane ID	Manufacturing technique	Composition (wt%) (+- 1% Relative)					Thickness (um)
		Pd	Cu	Ag	Au	Zr	
PdCu (Fcc)	Magnetron Sputtering	76.24	23.76	-	-	-	1.679
PdCu (Bcc)	Magnetron Sputtering	43.24	56.64	-	-	-	1.664
PdCuZr	Magnetron Sputtering	72.10	14.46	-	-	13.54	1.541
PdAg	Electroless Plating	65.55	-	34.45	-	-	0.573
PdAu	Electroless Plating	74.7	-	-	25.3	-	1.172
PdCuAg	Electroless Plating	72.1	-	8.27	19.58	-	0.867
PdCuAu	Electroless Plating	63.90	13.6	-	22.1	-	1.545
PdAuAg	Electroless Plating	60	-	11.2	28.3	-	0.736

5.3 Results and Discussion

5.3.1 Membrane characterisation

Figure 5.1 (a)-(g) shows the cross-sectional SEM images of the manufactured membranes. Through both electroless plating and magnetron sputtering dense and defect-free separation layers were able to be fabricated for all compositions. Thickness of the fabricated membranes are shown in 5.1 and ranged from 573 nm to 1.579 μm . In general thinner layers were achieved using electroless plating although theoretically sub-micron layers are possible through magnetron sputtering, examples of this being SINTEF's patented sputtering process.[3] The integrity of the manufactured membranes was measured using the procedure laid out in section 3.2.4. All membranes showed no leakage when pressurised to 10 bar indicating that all membranes were uniform, pinhole free and therefore suitable for hydrogen separation. [4]

The surface composition of each membrane was measured by XPS and is shown in Table 5.1. A wide range of compositions were fabricated. From phase data on the PdCu system [5, 6] both varieties of PdCu membranes (bcc phase and fcc phase) were successfully fabricated. In addition to this PdCuZr ternary alloy was fabricated through magnetron sputtering as there is evidence in literature that this alloy composition shows high resistance to impurities and Zr cannot be deposited through electroless plating. [6]

Silver is the most popular dopant for palladium membranes and forms a stable alloy with palladium at concentrations greater than 20 wt%, with the optimal composition occurring at 23 wt%. On top of mitigating the effects of hydrogen embrittlement, a 60% increase in permeability is observed when compared to pure Pd membranes. Despite having enhanced permeation properties, PdAg is still susceptible to poisoning, in particular from sulphurous compounds which can form both Pd_4S and $\text{Ag}_5\text{Pd}_{10}\text{S}_5$. A composition of $\text{Pd}_{64.9}\text{Ag}_{35.1}$ wt% was achieved, which, while higher than the desired composition of $\text{Pd}_{77}\text{Ag}_{23}$ wt%, was determined adequate for the purposes of this study.

Copper is another widely studied binary alloy which is known to suppress hydrogen embrittlement. Alloying with copper also has the advantage that it reduces the cost

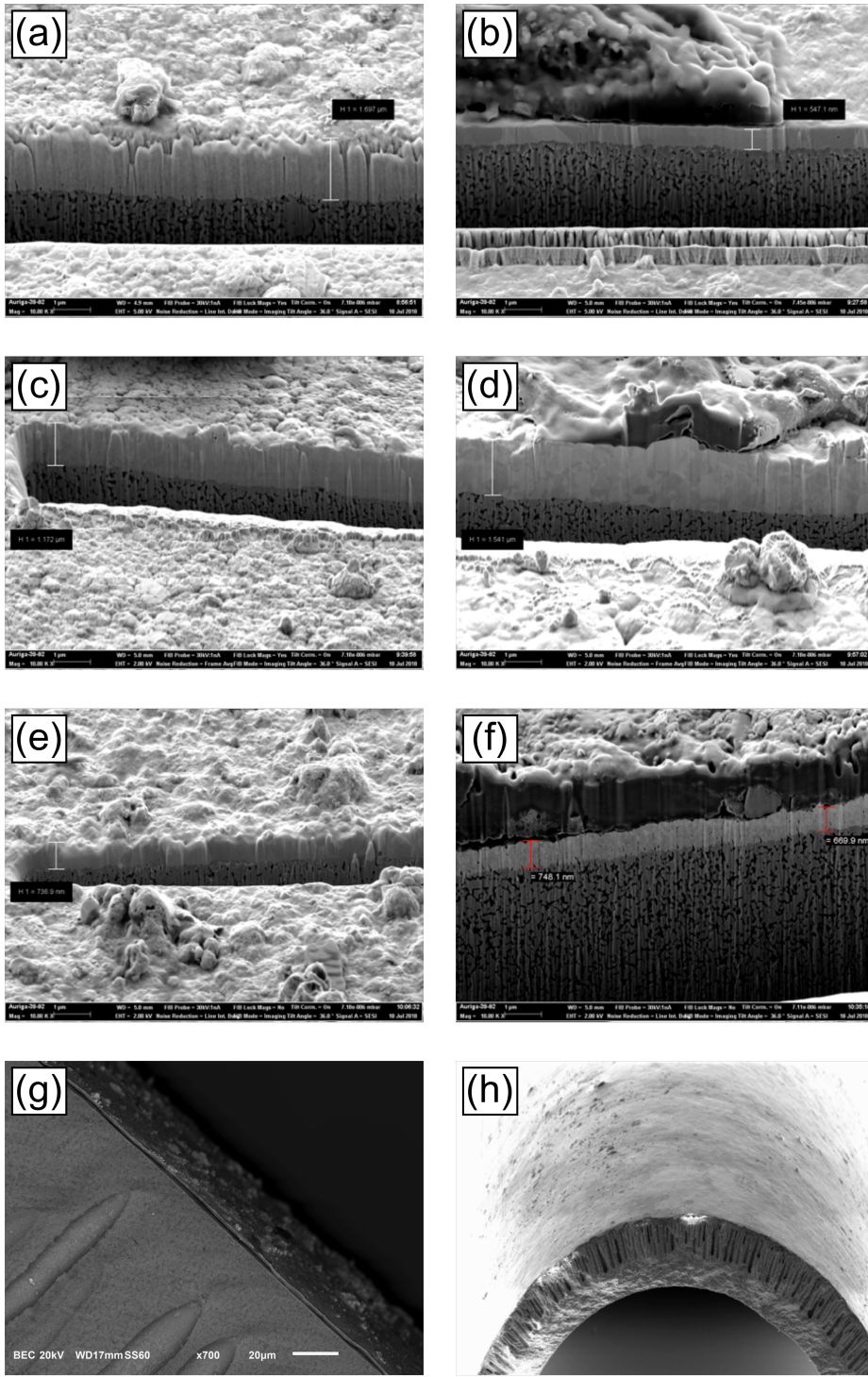


Figure 5.1: SEM images of fabricated membranes (a) PdCu (fcc) (Sputtering) (b) PdAg (ELP) (c) PdAu (ELP) (d) PdCuZr (Sputtering) (e) PdAgAu (ELP) (f) PdCuAg (ELP) (g) PdCu (bcc) (Sputtering) (h) typical cross section

of the membrane by a larger amount than most other metals and through improving the membranes sulphur resistance. The maximum permeability of a palladium copper membrane occurs at the composition $Pd_{60}Cu_{40}$ wt% and this is due to the formation of a bcc lattice rather than the fcc lattice commonly seen in pure palladium and most binary alloys. [7] Temperature cycling has previously been performed on this alloy composition and it has been found that the bcc crystalline configuration has a higher permeability than the fcc phase. [8] This behaviour is due to the increased number of hcp adsorption sites which hydrogen has a slight preference for, and the bcc structure allowing faster diffusion through the bulk of the membrane. [9] Conversely the fcc structure has a higher impurity resistance than the bcc structure, particularly for H_2S . [7, 10] $Pd_{44}Cu_{66}$ and $Pd_{65.5}Cu_{34.5}$ wt % membranes were manufactured using magnetron sputtering which were in the range for bcc and fcc phases respectively.

$PdAu$ alloys see a slight increase in permeability, up to 30% more than pure Pd [11], with gold additions up to 20%, after which the permeability rapidly decreases. While alloying with gold does not improve the permeability much compared to silver or copper, gold alloys show greatly improved sulphur resistance. [12] The synthesised membrane was found to have the composition $Pd_{74.7}Au_{25.3}$ which, while containing a high amount of gold resulting in lower permeation, will have a higher impurity resistance.

5.3.2 Hydrogen permeation

Table 6 shows the hydrogen permeation through the 9 tested membranes at steady state after 12 hours of operation. As expected, hydrogen permeation flux increases with the elevated temperatures. Moreover, the mass transfer resistance of the substrate will not represent major limitations since its gas transport resistance is negligible compared to that of the dense palladium alloy layer¹⁰. Deposited layers were all on the scale of 0.5-2 μm which from previous research indicates the main rate limiting step in hydrogen permeation being the thickness of the membrane layer. [13] The palladium copper alloy which was in the bcc phase showed the highest hydrogen permeability of all the synthesised membranes which was expected as discussed in **section 3.1**. The membrane which showed the lowest hydrogen permeability was the $PdCuZr$ membrane, this is likely due to the combined effects of the alloy having an fcc structure, and the alloy having the lowest concentration of palladium compared to the other synthesised membrane, resulting in the lowest number of sites for hydrogen dissociation and subsequent permeation. The $PdAu$ and $PdAuAg$ membranes both showed low permeabilities. Gold as an alloying material traditionally does not show much increase in permeability [12] but is instead used to suppress the effects of impurities on the membrane, [12] which is the main goal of this study. Despite the fact that the commercial membrane is also based on $PdA-gAu$, the membrane manufactured through electroless plating has a lower permeability due to the high gold concentration. It is likely that the concentration of silver in the commercial membrane is closer to 23%, which is the optimal value for hydrogen permeation, and it's gold concentration is much lower than the electroless plated membrane. Both $PdCuAg$ and $PdCuAu$ had reasonably high hydrogen permeabilities. While none of these membranes showed a hydrogen permeability as high as the commercial alloy, it

Table 5.2: Pure hydrogen permeability of studied alloy membranes under pure hydrogen at 300°C and 1 bar pressure differential

Membrane ID	Permeability ($mol\ m^{-1}s^{-1}pa^{1/2} \times 10^{-8}$)
PdCu (Fcc)	1.30
PdCu (Bcc)	1.68
PdCuZr	0.14
PdAg	0.94
PdAu	0.33
PdCuAg	1.22
PdCuAu	1.43
PdAuAg	0.19
Commercial (REB)	5.71

Table 5.3: Permeability results for all membranes under both impurity conditions

Membrane ID	Permeability ($mol\ m^{-1}s^{-1}pa^{1/2} \times 10^{-8}$)			% Drop	
	Pure H ₂	Non-Sulphur	Sulphur	Non-sulphur	Sulphur
PdCu (Fcc)	1.30	0.22	0.185	80%	86%
PdCu (Bcc)	1.68	0.721	2.47	55%	85%
PdCuZr	0.14	0.12	0.101	12%	26%
PdAg	0.94	0.117	0.007	88%	92%
PdAu	0.33	0.165	0.215	51%	35%
PdCuAg	1.22	0.48	0.299	61%	75%
PdCuAu	1.43	0.789	1.07	45%	25%
PdAuAg	0.19	0.163	0.142	16%	27%

should be noted that the commercial membrane had a much larger thickness resulting in a much higher cost and lower flux values than the composite membranes.

5.3.3 Impurity reactivity

Table 5.3 shows the results of hydrogen permeation under the presence of the two different impurity conditions discussed in Table 5.3 compared to the pure hydrogen permeability values shown in Table 5.2. The permeability data was taken once the flux had reached steady state after 12 hours of operation. For all membranes there was a reduction in permeability when the membranes were exposed to impurities. The magnitude of this reduction compared to the pure hydrogen permeability is used as an indication of the degree of interaction between the membrane and the impurities. Table 5.4 shows the composition of each membrane in between each test in order to measure permanent

surface reactions and segregation behaviour of the alloys under the chosen impurities.

Binary alloys

In non-sulphur tests the PdAg binary alloy was the worst performing, with the permeability dropping by 88% of its original value. This was expected as the addition of silver to a palladium system, while effective at increasing the permeability, does not contribute much to impurity resistance. [14] This was further supported by the results of the sulphur tests where the permeability dropped by 92% and composition analysis in Table 5.4 showing that sulphur was present in 42% of the surface. The PdAg alloy also showed a large degree of segregation behaviour under non-sulphur impurities which likely contributed to the large reduction in flux, with silver concentration increasing to 75% at the top 10 nm of the sample, resulting in a large drop in permeability.

Interestingly the PdCu membrane with a composition in the bcc phase showed higher resistance to non-sulphurous impurities than the fcc phase, with the former only experiencing a 55% drop in permeability compared to an 80% drop in permeability in the latter. This again seems to be a result of the segregation behaviour of the alloy, with the PdCu alloy in the fcc phase experiencing a large amount of segregation, with the palladium concentration increasing to around 90% on the retentate side. Conversely the PdCu composition in the BCC phase membrane only changed slightly. The XPS analysis showed that while the reactivity of sulphur on the surface of both copper based binary membranes was of a similar magnitude, the BCC phase had a slightly lower resistance, with 29% of the surface containing sulphur after exposure to sulphurous impurities as opposed to the 25% shown by the fcc phase alloy.

The PdAu alloy showed the best impurity resistance out of the binary alloys tested under both impurity conditions, with only a 51% and 35% drop in permeability under non-sulphur and sulphur conditions respectively and only a 12% concentration of sulphur was observed on the surface after XPS analysis. The alloy showed slight segregation of gold away from the permeate surface under non-sulphur impurity conditions likely due to the fact the difference in interaction strength between gold and palladium with the components of the gas mixture varies widely, with many gases preferentially adsorbing on palladium [15].

Ternary alloys

Five ternary alloy compositions were tested including the commercial alloy. The commercial alloy had the highest permeability of all ternary alloys with a value of $5.71 \text{ mol m}^{-1} \text{ s}^{-1} \text{ pa}^{-0.5} \times 10^{-8}$ under pure hydrogen and $4.28 \text{ mol m}^{-1} \text{ s}^{-1} \text{ pa}^{-0.5} \times 10^{-8}$ under non-sulphur conditions, a drop in permeability of 25%. However, the commercial membrane nearly lost all of its permeability under sulphurous conditions. The PdAuAg membrane manufactured through electroless plating performed better under both impurity conditions than the commercial alloy despite being based on the same composition, only seeing a 16% and 27% drop in hydrogen permeability under non-sulphur and sulphur conditions respectively compared to a 25% and 96% drop shown by the commercial alloy.

Table 5.4: XPS composition analysis of the palladium alloy membrane surfaces after impurity tests

Membrane ID	Pure Hydrogen Exposure					Non-Sulphur Exposure					Sulphur Exposure					
	Pd	Ag	Au	Cu	Zr	Pd	Ag	Au	Cu	Zr	Pd	Ag	Au	Cu	Zr	S
PdCu (Fcc)	65.5	-	-	35.5	-	92.5	-	-	7.5	-	67.5	-	-	7.5	-	25
PdCu (Bcc)	44	-	-	66	-	54.85	-	-	45.15	-	40	-	-	31	-	29
PdCuZr	63.6	-	-	22.6	13.8	64.4	-	-	27.5	8.5	54.2	-	-	27	8	10.8
PdAg	65.5	34.5	-	-	-	25	75	-	-	-	29	29	-	-	-	42
PdAu	75	-	25	-	-	82.9	-	17.1	-	-	71	-	16	-	-	13
PdCuAg	64.6	9.1	-	26.3	-	8.6	8.9	-	82.5	-	6	5	-	64	-	25
PdCuAu	63.9	-	22.5	13.6	-	84.9	-	1.46	13.6	-	65.3	-	1	18.5	-	15.2
PdAuAg	60	11.7	28.3	-	-	47.2	49.8	3	-	-	52	35	1	-	-	12

The high levels of gold likely contributed to the low levels of sulphur on the surface of the electroless plated PdAuAg membrane. These results indicate that the composition of the commercial membrane, while ideal for separation, does not contain enough gold to withstand the levels of sulphur impurities expected for analytical purposes.

The worst performing ternary alloy was the PdCuAg alloy which showed large permeability drops under all conditions, 61% under non-sulphur and 75% under sulphurous conditions. In addition to these, large degrees of segregation were observed under non-sulphur impurities, with the palladium concentration at the surface dropping to 8.5 wt%, showing that the alloy is not completely stable under the varying conditions expected during analytical purposes.

Both gold containing ternary alloys, PdAuAg and PdCuAu, performed well under sulphur conditions, with the PdCuAu alloy only reducing in permeability by 25% and the PdAgAu membrane by 27%. The PdCuAu membrane however had a stronger interaction with non-sulphur impurities, indicated by the permeability drop of 45% when exposed to the non-sulphur containing gas sample. This drop is likely due to the segregation of palladium to the surface with the XPS data indicating an increase of palladium to the surface to 84.9 wt% from 63.9%. The best performing ternary membrane was the PdCuZr membrane which showed the smallest drop in permeability of only 12% non-sulphur conditions, and a permeability percentage drop of 26% under sulphur conditions which on a similar magnitude to that of the gold containing alloys.

Segregation behaviour

All membranes tested showed some degree of segregation with the two thinnest membrane samples, PdAg (0.573 micron), PdAuAg (0.736 micron) and PdCuAg (0.873 micron) all showing the highest degrees of segregation. While this may still be a property of the alloy compositions it may also indicate that sub-micron palladium alloys layers are unstable and there may be a minimum thickness for alloys, below which the membrane layer is unstable and frequently varies during operation.

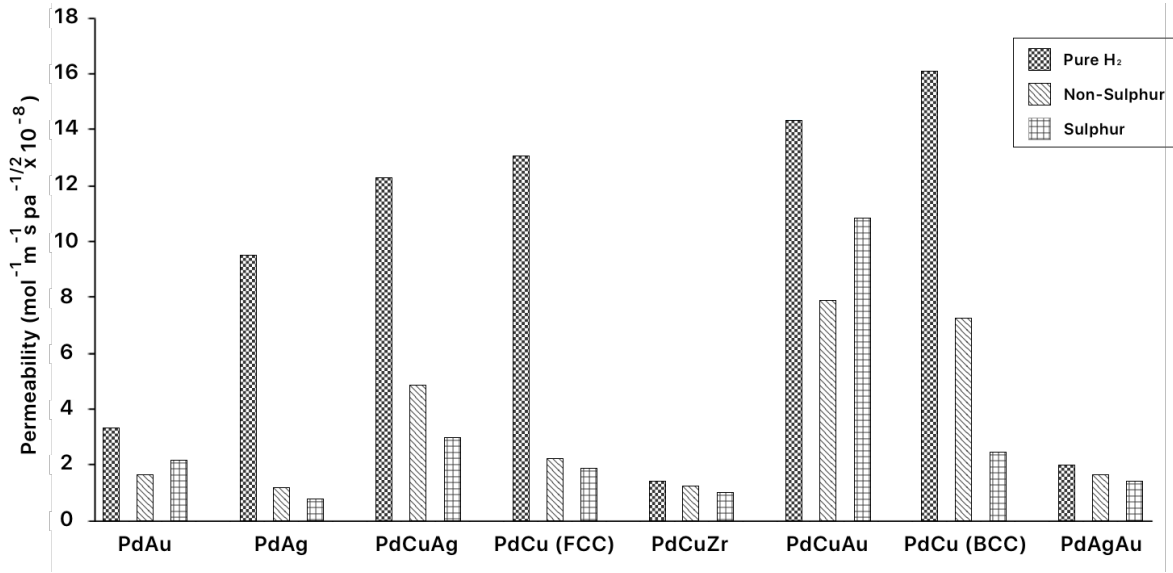


Figure 5.2: Permeability data for pure hydrogen, non-sulphur, and sulphur permeation tests

5.4 Conclusion

In order to identify a suitable palladium alloy composition for hydrogen impurity enrichment, eight different membrane compositions were manufactured and tested under three different hydrogen conditions against a commercial palladium membrane. Two different measures were used to compare the membrane compositions suitability for hydrogen impurity enrichment, the permeability deviation from the pure hydrogen permeability was used as an initial indicator of interaction between the alloy and impurities, and the surface composition was measured to detect any impurities which had permanently reacted with the membrane. The best performing membrane, and therefore the most suitable for hydrogen impurity enrichment was the PdCuZr alloy, which only showed a 12% and 26% drop in permeability under non-sulphur, and sulphur conditions, and low levels of sulphur on the surface. The permeability of this alloy was low, however, surface areas could easily be scaled up to increase the speed of hydrogen enrichment.

References

- [1] Arul Murugan and Andrew S Brown. Advancing the analysis of impurities in hydrogen by use of a novel tracer enrichment method. *Analytical Methods*, 6(15):5472, 2014. doi: 10.1039/c3ay42174k.
- [2] Shabbir Ahmed, Sheldon H D Lee, and Dionissios D Papadias. Analysis of trace impurities in hydrogen: Enrichment of impurities using a H₂ selective permeation membrane . *International Journal of Hydrogen Energy*, 35(22):12480–12490, 2010. doi: 10.1016/j.ijhydene.2010.08.042.
- [3] T. A. Peters, T. Kaleta, M. Stange, and R. Bredesen. Development of thin binary and ternary Pd-based alloy membranes for use in hydrogen production. *Journal of Membrane Science*, 383(1-2):124–134, 2011. ISSN 03767388. doi: 10.1016/j.memsci.2011.08.050. URL <http://dx.doi.org/10.1016/j.memsci.2011.08.050>.
- [4] Ana Gouveia Gil, Miria Hespanhol M Reis, David Chadwick, Zhentao Wu, and K Li. A highly permeable hollow fibre substrate for Pd/Al₂O₃ composite membranes in hydrogen permeation. *International Journal of Hydrogen Energy*, 40(8):3249–3258, 2015. ISSN 0360-3199. doi: <https://doi.org/10.1016/j.ijhydene.2015.01.021>. URL <http://www.sciencedirect.com/science/article/pii/S0360319915000580>.
- [5] Fernando Roa and J Douglas Way. Influence of Alloy Composition and Membrane Fabrication on the Pressure Dependence of the Hydrogen Flux of Palladium-Copper Membranes. *Ind. Eng. Chem. Res*, 42(23):5827–5835, 2003. ISSN 08885885. doi: 10.1021/ie030426x.
- [6] Shahrouz Nayebossadri, John Speight, and David Book. Development of Pd – Cu Membranes for Hydrogen Separation Why Hydrogen Separation ? 2013.
- [7] Ying She, Sean C Emerson, Neal J Magdefrau, Susanne M Opalka, Catherine Thibaud-Erkey, and Thomas H Vanderspurt. Hydrogen permeability of sulfur tolerant Pd–Cu alloy membranes. *Journal of Membrane Science*, 452:203–211, 2014. doi: 10.1016/j.memsci.2013.09.025.
- [8] M D Dolan. Non-Pd BCC alloy membranes for industrial hydrogen separation. *Journal of Membrane Science*, 362(1-2):12–28, 2010. doi: 10.1016/j.memsci.2010.06.068.

- [9] Ekin Ozdogan Wilcox and Jennifer. Investigation of H₂ and H₂S Adsorption on Niobium- and Copper-Doped Palladium Surfaces. *J. Phys. Chem. B*, pages 12851–12585, 2010. doi: 10.1021/acs.energyfuels.5b01294.
- [10] I R Harris D.T. Hughes. A comparative study of hydrogen permeabilities and solubilities in some palladium solid solution alloys. *Journal of Less Common Metals*, 61:9–21, 1978.
- [11] K Atsonios, K D Panopoulos, A Doukelis, A K Koumanakos, E Kakaras, T A Peters, and Y C van Delft. Introduction to palladium membrane technology. In A Doukelis, K Panopoulos, A Koumanakos, and E Kakaras, editors, *Palladium Membrane Technology for Hydrogen Production, Carbon Capture and Other Application*, pages 1–21. Woodhead Publishing, 2015. doi: 10.1533/9781782422419.1.
- [12] Chao-Huang Chen and Yi Hua Ma. The effect of H₂S on the performance of Pd and Pd/Au composite membrane. *Journal of Membrane Science*, 362(1-2):535–544, 2010. doi: 10.1016/j.memsci.2010.07.002.
- [13] Tina M Nenoff Nathan W. Ockwig. Membranes for Hydrogen Separation. *Chemical Reviews*, 107:4078–4110, 2007.
- [14] T A Peters, J M Polfus, M Stange, P Veenstra, A Nijmeijer, and R Bredesen. H₂ flux inhibition and stability of Pd-Ag membranes under exposure to trace amounts of NH₃. *Fuel Processing Technology*, 152:259–265, 2016. doi: 10.1016/j.fuproc.2016.06.012.
- [15] Sabina K. Gade, Sarah J. DeVoss, Kent E. Coulter, Stephen N. Paglieri, Gökhan O. Alptekin, and J. Douglas Way. Palladium-gold membranes in mixed gas streams with hydrogen sulfide: Effect of alloy content and fabrication technique. *Journal of Membrane Science*, 378(1-2):35–41, 2011. ISSN 03767388. doi: 10.1016/j.memsci.2010.11.044. URL <http://dx.doi.org/10.1016/j.memsci.2010.11.044>.

Chapter 6

A hydrogen impurity measurement device for measuring ISO 14687 impurities

6.1 Abstract

In this chapter a device capable of performing hydrogen impurity enrichment is designed and tested under a number of conditions using a commercial membrane compared against the best performing fabricated membranes in chapter 5. The aim of this chapter is to improve upon the designs in literature to provide a more efficient, and safe device which could be sold as a commercial product. A sample was taken from a commercial hydrogen refuelling station, spiked with krypton, and enriched using the device in order to validate the krypton tracer enrichment method using real world conditions, and to quantify the impurity concentrations present in commercial hydrogen fuel.

6.2 Introduction

6.3 Results and discussion

6.4 Conclusion

Chapter 7

Conclusion and future work

7.1 Impurity enrichment devices

7.1.1 Further research

7.1.2 Additional use cases

7.1.3 Commercialisation

7.2 Closing remarks